

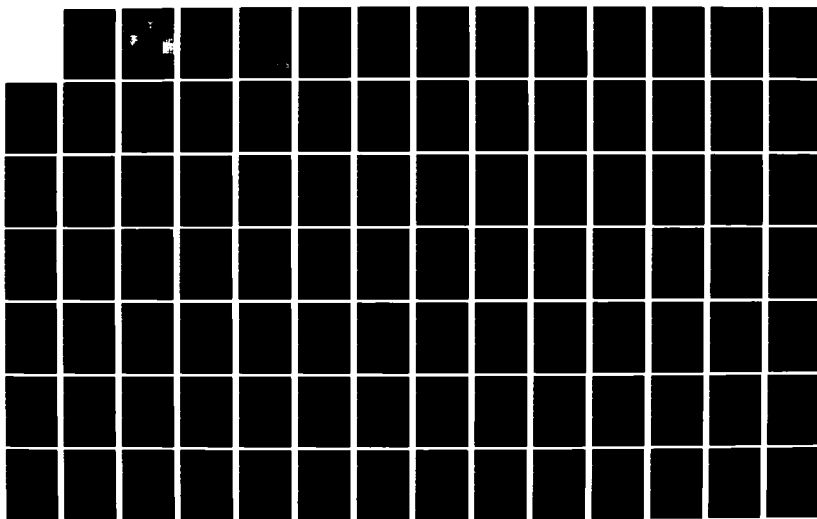
AD-A125 646

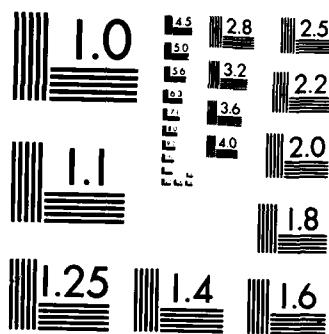
ANALYSIS OF THE INDUCED CURRENTS ON A SECTION OF  
PARALLEL WIRES IN FRONT OF (U) AIR FORCE INST OF TECH  
WRIGHT-PATTERSON AFB OH SCHOOL OF ENGI... T W GODOWSKY  
DEC 82 AFIT/GE/EE/82D-35 F/G 9/1

1/2

UNCLASSIFIED

NL





MICROCOPY RESOLUTION TEST CHART  
NATIONAL BUREAU OF STANDARDS-1963-A

# AIR FORCE INSTITUTE OF TECHNOLOGY



AIR UNIVERSITY  
UNITED STATES AIR FORCE

AD A125046



Copy available to DTIC does not  
permit fully legible reproduction

SCHOOL OF ENGINEERING

DTIC  
ELECTE

MAR 14 1983

B

WRIGHT-PATTERSON AIR FORCE BASE, OHIO

DISTRIBUTION STATEMENT A

Approved for public release  
Distribution Unlimited

DTIC FILE COPY

## **DISCLAIMER NOTICE**

**THIS DOCUMENT IS BEST QUALITY  
PRACTICABLE. THE COPY FURNISHED  
TO DTIC CONTAINED A SIGNIFICANT  
NUMBER OF PAGES WHICH DO NOT  
REPRODUCE LEGIBLY.**

ANALYSIS OF THE INDUCED CURRENTS ON A  
SECTION OF PARALLEL WIRES IN  
FRONT OF A GROUND PLANE

THESIS

AFIT/GE/EE/82D-35

Thomas W. Godowsky  
2d Lt USAF

DTIC  
ELECTE  
MAR 14 1983

B

DISTRIBUTION STATEMENT A

Approved for public release;  
Distribution Unlimited

# ANALYSIS OF THE INDUCED CURRENTS ON A SECTION OF PARALLEL WIRES IN FRONT OF A GROUND PLANE

THIS IS

Presented to the Faculty of the School of Engineering  
of the Air Force Institute of Technology

Air University

in Partial Fulfillment of the  
Requirements for the Degree of  
Master of Science

Thomas W. Godowsky, B.S.E.E.

2d Lt USAF

Graduate Electrical Engineering

December 1982

### Acknowledgements

I wish to express my appreciation to my thesis committee readers, Captain Pedro Rustan and Professor Raymond Potter, for their helpful suggestions during the final revision of this thesis. I also wish to thank my thesis advisor, Captain Thomas Johnson, for the topic suggestion and for his continual guidance and encouragement throughout the entire development of this thesis. Without his help, this thesis would have been much more difficult to complete. Thanks is also due for the outstanding efforts of the typist, Mrs. Babiarz.

Finally, and most importantly, I am indebted the most to my fiancée, Miss Nancy Hendrickson, for her emotional support and encouragement. Only by allowing me to sacrifice much of my personal time with her was I able to complete this thesis and my other work at AFIT.

Thomas W. Godowsky



DTIC	
COPY	
INSPECTED	
2	
A	CP

## Contents

	Page
Acknowledgements . . . . .	ii
List of Figures . . . . .	iv
Notation . . . . .	vii
Abstract . . . . .	x
I. Introduction . . . . .	1
Background . . . . .	1
Review of Literature . . . . .	4
Problem . . . . .	16
Scope/Assumptions . . . . .	16
Approach . . . . .	17
II. Development of Theory . . . . .	19
Wire Geometry . . . . .	19
Free Space Geometry . . . . .	19
Ground Plane Case Geometry . . . . .	21
Distance Between Two Arbitrary Segments . . . . .	22
Fields At An Arbitrary Wire Segment . . . . .	23
Method of Moments . . . . .	28
Induced Voltage by Incident Plane Wave . . . . .	38
III. Results . . . . .	40
Wire Spacings . . . . .	41
Number of Segments per Wire . . . . .	45
Wire Length . . . . .	48
Varying Incidence Angle Effects . . . . .	51
Array $0.25\lambda$ Above a Ground Plane . . . . .	64
IV. Conclusions and Recommendations . . . . .	71
Conclusions . . . . .	71
Recommendations . . . . .	74
Bibliography . . . . .	75
Appendix A: Computer Program . . . . .	76
VITA . . . . .	107



## List of Figures

Figure	Page
1 Side view of a Cassegrainian Antenna with wire reflector surfaces . . . . .	2
2 Conducting plans approximation for a parallel wire array . . . . .	5
3 Wait's planar wire grid with incident plane wave . . . . .	10
4 Richmond's wire grid model . . . . .	12
5 Free space wire array geometry . . . . .	20
6 Image Theory model for an array near a ground plane . . . . .	21
7 Representation of separation between segments . . . . .	23
8 A typical segment in free space . . . . .	26
9 Staircase approximation to an actual current distribution . . . . .	31
10 Piecewise sinusoidal expansion function . . . . .	32
11 Five segment piecewise sinusoidal current approximation . . . . .	33
12 Current on a horizontal cut of a $1\lambda^2$ array with various wire spacings for a normally incident plane wave . . . . .	42
13 Current on a vertical cut of a $1\lambda^2$ array with various wire spacings for a normally incident plane wave . . . . .	43
14 Current on a horizontal cut of a $1\lambda^2$ array with various wire segment divisions for a normally incident plane wave . . . . .	46
15 Current on a vertical cut of a $1\lambda^2$ array with various wire segment divisions for a normally incident plane wave . . . . .	47
16 Current on a horizontal cut of a $1\lambda$ wide array with various wire lengths for a normally incident plane wave . . . . .	49

Figure		Page
17	Current on a vertical cut of a $1\lambda$ wide array with various wire lengths for a normally incident plane wave . . . . .	50
18	Current on a horizontal cut of a 26 wire, 5 segment array for $\theta$ varying, $\phi = 0$ . . . . .	52
19	Current on a horizontal cut of a 26 wire, 5 segment array for $\phi$ varying, $\theta = \pi/2$ . . . . .	53
20	Current on a vertical cut of a 26 wire, 5 segment array for $\theta$ varying, $\phi = 0$ . . . . .	54
21	Current on a vertical cut of a 26 wire, 5 segment array for $\phi$ varying, $\theta = \pi/2$ . . . . .	55
22	Horizontal cut of current phase on a 26 wire, 5 segment array for various incidence angles . . . . .	56
23	Vertical cut of current phase on a 26 wire, 5 segment array for various incidence angles . . . . .	57
24	Current on a horizontal cut of a 13 wire, 10 segment ( $2\lambda$ long) array for $\phi$ varying, $\theta = \pi/2$ . . . . .	59
25	Current on a vertical cut of a 13 wire, 10 segment ( $2\lambda$ long) array for $\theta$ varying, $\phi = 0$ . . . . .	61
26	Horizontal cut of current phase one 13 wire, 10 segment ( $2\lambda$ long) array for various incidence angles . . . . .	62
27	Vertical cut of current phase on a 13 wire, 10 segment ( $2\lambda$ long) array for various incidence angles . . . . .	63
28	Horizontal cut of current density on an 18 wire, 5 segment array $\frac{1}{2}\lambda$ above a ground plane for $\phi$ varying, $\theta = \pi/2$ . . . . .	65
29	Vertical cut of current density on an 18 wire, 5 segment array $\frac{1}{2}\lambda$ above a ground plane for $\theta$ varying, $\phi = 0$ . . . . .	66
30	Horizontal cut of current phase on an 18 wire, 5 segment array $\frac{1}{2}\lambda$ above a ground plane for various incidence angles . . . . .	67

Figure		Page
31	Vertical cut of current phase on an 18 wire, 5 segment array $\frac{1}{2}\lambda$ above a ground plane for various incidence angles . . . . .	68
32	Top view of geometry illustrating reflection effects . . . . .	70
A-1	Computer program flowchart . . . . .	80
A-2	Computer program . . . . .	85

## Notation

### GREEK LETTER SYMBOLS

$\epsilon'$	Relative permittivity
$\epsilon$	Free space permittivity
$\mu$	Relative permeability
$\mu_0$	Free space permeability
$\sigma$	Conductivity (of wires and ground plane)
$\Phi$	Scalar potential
$\lambda$	Wavelength
$\omega$	Angular frequency
$\theta$	Angular separation between $\hat{z}$ and incident field
$\phi$	Angular separation between $\hat{x}$ and incident field
$\beta$	Propagation constant

## Notation

### ROMAN LETTER SYMBOLS

$a$	Radius of wire
$\hat{n}$	Unit normal vector to scattering surface
$\hat{e}$	Unit vector parallel to wire axis
$\bar{r}$	Radius vector from origin
$\bar{n}$	Propagation vector
$\bar{H}^i$	Incident magnetic field vector
$\bar{H}^r$	Reflected magnetic field vector
$\bar{E}^i$	Incident electric field vector
$\bar{E}^r$	Reflected electric field vector
$E_{\text{tan}}^s$	Scattered tangential electric field component
$E_{\text{tan}}^i$	Incident tangential electric field component
$E_{\text{tan}}^{\text{res}}$	Residual tangential electric field component
$\bar{A}$	Magnetic vector potential
$\psi( )$	Scalar Green's function
$F_n( )$	Expansion function
$W_n( )$	Weighting function
$\bar{I}_n$	Complex expansion coefficient
$\bar{J}_s$	Surface current density
$N$	Number of segments per wire
$M$	Number of wires
$wsy$	Wire spacing in y direction

wsx	Wire spacing in x direction
WL	Wire length
L	Segment length
Q	Total number of segments
R	Distance between observation and source segments
DZ	Length of $\frac{1}{2}$ of the expansion function, $F_n( )$

NOTE: PRIMED coordinates and distances refer to SOURCE segments.

UNPRIMED coordinates refer to OBSERVATION segments.

Abstract

This investigation determines the induced currents on a finite sized array of parallel wires when illuminated by a plane wave with varying incidence angles by the method of moments. The arrays considered are of various spacings, lengths, and widths, ranging from 5 to 36 wires per wavelength, and one to two wavelengths in length. The effects of a ground plane parallel to the array, and located one quarter wavelength away, is also studied.

The analysis is accomplished by the method of moments using piecewise sinusoidal expansion functions and Galerkin's method. An algorithm is developed to accomplish the integration and matrix inversion. It was written general enough for the user to specify: number of wires, number of segments, wire length, wire diameter, wire spacing, spacing above the ground plane, frequency, and magnitude of incident electric field. The results illustrate the various effects that changing the wire spacing, wire length, number of segments, and incidence angle have upon the induced current. The results are also compared to the modified physical optics approximation. The results of this investigation indicate that the moment method is accurate enough to produce very reasonable approximations of the induced current for most applications.

# ANALYSIS OF THE INDUCED CURRENTS ON A SECTION OF PARALLEL WIRES IN FRONT OF A GROUND PLANE

## I. Introduction

### 1.1 Background

Considerable work has been accomplished by many authors in the analysis of the induced currents on wires. In many problems of this nature, the boundary condition that the tangential electric field equal zero along the wire surface must be satisfied. This approach will yield a complex integral equation (Pocklington's Integral Equation). Classical solutions to this integral equation, and therefore for the induced currents, are tedious and solvable for only a few simple wire geometries. Any wire geometries whose surfaces are not easily describable in a conventional coordinate system are generally unsolvable by classical methods.

Because of the difficulty in obtaining completely accurate solutions for arbitrary wire geometries, justifiable approximations are often made which yield good, approximate solutions. One commonly used approximation is a physical optics technique. Even the physical optics technique, however, is limited to a few basic wire geometries. Most of the previous studies are limited to four basic cases: (1) a single dipole, (2) an array of parallel dipoles, (3) single wires of both finite and infinite length, and (4) an array of parallel wires of infinite length. Approximate solutions have been found for the induced currents for the above cases when the wires are assumed to be in free space. A review of the articles relevant to this thesis is given in the following section.



This thesis will be an extension of case (4) above; the problem to be considered is an array of this, infinitely conducting, parallel wires of finite length. Approximate solutions will be found for the induced current when the array is completely in free space and in the proximity of a ground plane. At present, no detailed analysis of this problem exists.

The need to determine the induced currents on an array of parallel wires has arisen in several situations, particularly when a wire array antenna is being studied. A problem of this nature of interest to the Air Force is a type of Cassegrainian antenna with wire reflector surfaces. The general antenna geometry may be represented as in Figure 1.

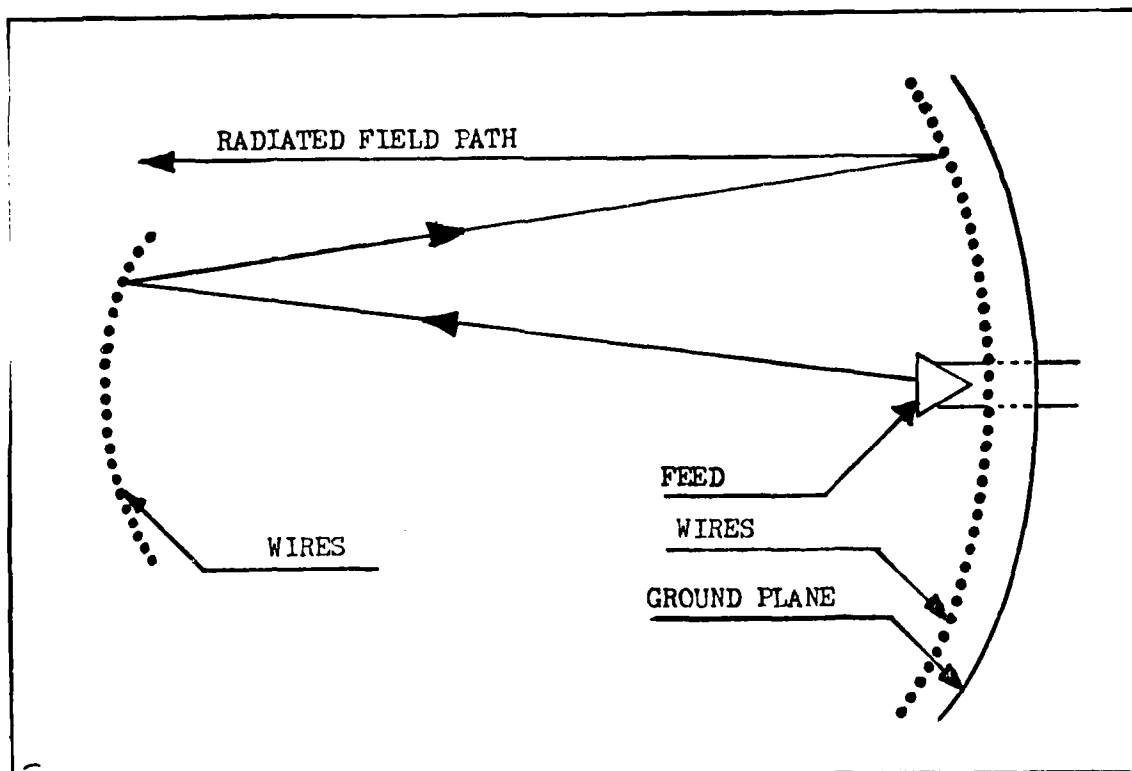


Figure 1. Side view of a Cassegrainian Antenna with wire reflector surfaces.

In order to determine the (far field) radiation pattern, the induced currents on each of the wires must be found. Because of the complicated geometry, completely accurate results are realistically impossible to obtain. By making some justifiable approximations, the problem can be reduced to a workable complexity, and approximate solutions for the induced current can be obtained.

A fundamental approximation to be made concerns the geometry of the wires and the ground plane. Working with the curved ground plane and wire surfaces of the antenna is obviously undesirable; approximating these surfaces as flat, rather than curved, considerably simplifies the problem. This approximation can be justified by considering the entire curved rear reflector to be subdivided into a large number of perfectly flat sections. The approximation will approach the true condition as the number of divisions increases. Therefore, the accuracy of the approximate solution can be increased as desired by simply dividing the reflector into a greater number of sections. If the induced current can be found for any arbitrary flat section, then by superposition, the approximate currents on the entire reflector will be known to any desired accuracy.

The problem, then, has been reduced to determining the induced currents on the wires of an arbitrary, flat section. In order to remain general, the solution must be valid for an arbitrary section which lies on the edge of the reflector. To account for this possibility, the currents may be forced to zero on at least one end of the array. However, a more general problem will be considered where the current is forced to zero at both ends of the array.

While no exact analytical solution for wires of finite length exists, the currents are often assumed to be represented by a modified physical optics approximation. The usual physical optics approximation is

$$\bar{J}_s = 2\hat{n} \times \bar{H}^i \quad (1)$$

where  $\hat{n}$  is a unit normal vector to the scattering surface

$\bar{H}^i$  is the incident magnetic field vector

$\bar{J}_s$  is the surface current density

The physical optics approximation is actually an approximate solution to the surface current density  $\bar{J}_s$  on a large, flat conducting plate. It seems reasonable, then, that an array of closely spaced, parallel thin wires can be approximated by a conducting plane, as in Figure 2. The approximation will become increasingly better as the radius and the spacing of the wires approach zero.

In order to account for the fact that the current may only flow along the wire axis, the actual physical optics approximation is modified as

$$\bar{J}_s = \hat{e} \cdot (2\hat{n} \times \bar{H}^i) \quad (2)$$

where  $\hat{e}$  is a unit vector parallel to the wire axis as in Figure 2.

## 1.2 Review of Literature

As stated in the previous section, considerable work in obtaining the induced currents on wire structures has been accomplished by various authors. This section will briefly review those works which are most relevant to this thesis.

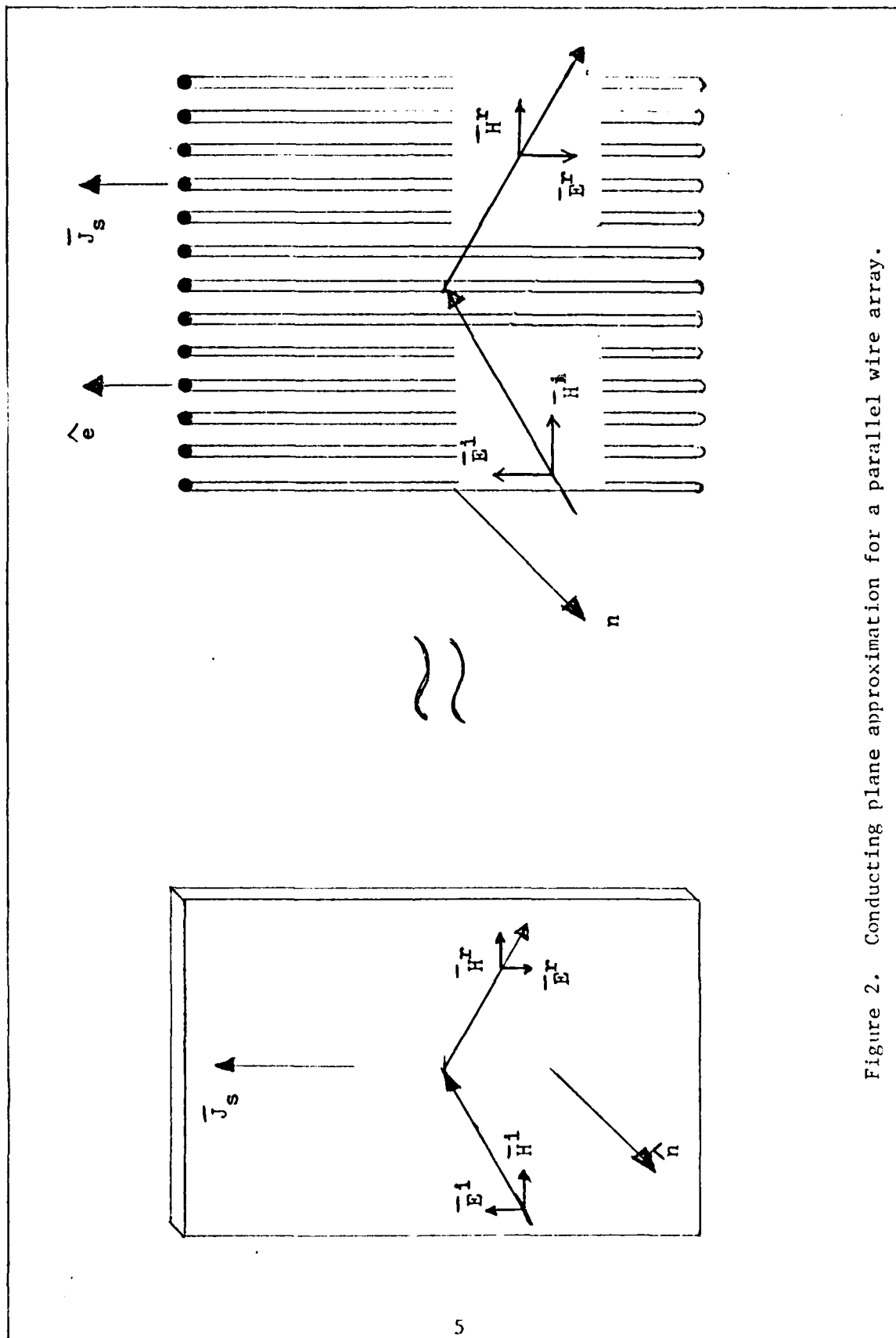


Figure 2. Conducting plane approximation for a parallel wire array.

The first article to be reviewed was written by Jack H. Richmond (Ref 1). It was one of the first articles written discussing digital computer solutions of scattering problems. The paper introduced a new technique for solving for the induced currents on perfectly conducting and dielectric bodies. Before the paper was published in 1965, high speed digital computers were relatively unavailable. The accepted technique for solving problems of this nature prior to 1965 were variational and quasi-static methods.

Richmond states that considerable success for scatterers of various shapes has been established; however, these techniques (variational and quasi-static methods) are limited to bodies which are small in comparison to the wavelength, or at most are on the order of one wavelength in maximum diameter. Larger scatterers are handled with the aid of physical optics, geometrical optics, and the theory of diffraction.

Richmond's paper introduced a technique which generated a system of linear equations by enforcing the boundary conditions at many points within the scatterer or upon its surface. Then, with the aid of a digital computer, this system of equations was solved to determine the current distribution of the surface, or the coefficients in the mode expansion for the scattered field. The distant radiated pattern was then found using the approximated currents.

This technique is impractical without a computer, because a large system of equations must be solved to provide a reasonably accurate solution. Richmond expects the linear equation solution to be accurate for bodies of arbitrary material, size, and shape. His paper briefly reviews recent progress of the technique, discusses methods for reducing

the computational effort, and illustrates an example by considering a plane wave to be incident upon a single straight wire or dielectric rod of finite length.

Richmond begins by stating that the electric field intensity is the sum of the incident and scattered intensities. Since it is known that the tangential electric field at the wire surface must be zero (the wire was assumed to be infinitely conducting), the scattered field equals the negative incident field. He writes the scattered field as integral of the current density multiplied by an expansion function over the length of the wire. The expansion function used here is a Fourier Series.

Richmond states that even if the true current distribution were actually known, the integral describing the radiated electric field could not be evaluated analytically, except in the form of an infinite series. He claims, though, that numerical integration is both possible and feasible with a digital computer. It should be noted that any solution employing this technique will only be approximate, because only a finite number of terms may be realistically considered.

Results are given for the Fourier coefficients of the current expansion on a wire illuminated by an incident plane wave. The length of the wire is varied from 0.1 to 0.7 wavelengths; the diameter of the wire is 0.01 wavelengths. The results show good agreement with the experimental results (within 10%) when the integrals are evaluated with fifth order Newton-Cotes formulas (which are exact for fifth order polynomials) using 1000 terms.

Richmond also applied this linear equation technique to a dielectric rod of 0.0625 inches in radius, 0.5 inches in length. Results include a graph of the rod length versus the echo area per square wavelength. His results show that the field scattered from the rod differ significantly from that of the physical optics approximation (by about 10%), but agree well with experimental data (within 10%).

Therefore, it can be concluded that (1) the physical optics approximation is probably not applicable to single dielectric rods and wires of small radius, and (2) that this linear equation technique using infinite series expansions will not be practical when arrays of wires are considered, because Richmond used 1000 terms to obtain good results for a single wire.

The second article to be reviewed was written by K. K. Mei; numerical solutions of a dipole antenna are considered (Ref 2). Mei begins by citing the integral equation used by Pocklington for  $\hat{z}$  directed dipoles

$$\int_L \bar{J}(z) \left[ -\frac{\partial^2}{\partial z^2} G(z, z') + \beta^2 G(z, z') \right] dz' = -j\omega\epsilon \bar{E}_z^i \quad (3)$$

where  $\bar{J}(z)$  is the current density

$G(z, z')$  is the free space Green's function,  $\frac{e^{-j\beta R}}{4\pi R}$

A numerical solution of the integral equation is then obtained by approximating the integration at a finite sum of N points. A matrix equation is therefore generated. In effect, Mei has simply "relaxed" the boundary condition that the tangential electric field must be everywhere zero to only be zero at N discrete points. This is known as the point matching

solution of the moment method. Although the point matching technique is only an approximation, good results were obtained.

In a separate article, Richmond considered scattering by an arbitrary array of parallel wires (Ref 3). He considered three wires not in the same plane, 30 parallel wires in a semicircle, and 15 parallel wires in an I beam configuration. Each wire is infinitely long. The radius and spacing was 0.03 and 0.2 wavelengths, respectively.

A set of  $N$  linear equations is generated by representing the current on each wire as the unknown quantity. This is not a point matching technique since only one equation is generated for each wire, along the center of each wire. Because each wire is infinitely long, Richmond writes the current on each wire as an expansion of a Hankel function. Thus, the electric field is defined as the product of a constant, a current magnitude, and a Hankel function expansion.

This technique, then, is to represent the current on each of the infinitely long wires in the form of Hankel functions. A linear equation is then written for each of the  $N$  wires. These linear equations are then solved using matrix algebra.

Results were obtained for each of the above wire configurations. A graph of electric field vs. incidence angle is presented which compares Richmond's results with the physical optics approximation for conducting strips of similar geometry. Richmond's results compare favorably. Thus, it is evident that solutions for the currents on an array of wires can be obtained by assuming that the current is uniform along each wire. However, this necessitates the wires to be infinitely long. Therefore, this technique is not applicable to the problem of finitely sized arrays.



In the fourth article under review, Wait investigates a similar problem to that of Richmond, i.e., reflection from a parallel wire grid (Ref 4). Wait outlines a solution for the problem of a plane wave which is obliquely incident upon an infinitely long parallel wire array. He assumes that the wires are small compared with the separation and the wavelength.

The plane wave has an electric field which can be given by

$$\vec{E}(x,y,z) = A \exp\{j\beta(x \cos \psi_0 \cos \theta + y \sin \psi_0 \cos \theta - z \sin \theta)\} \quad (4)$$

as shown in Figure 3.

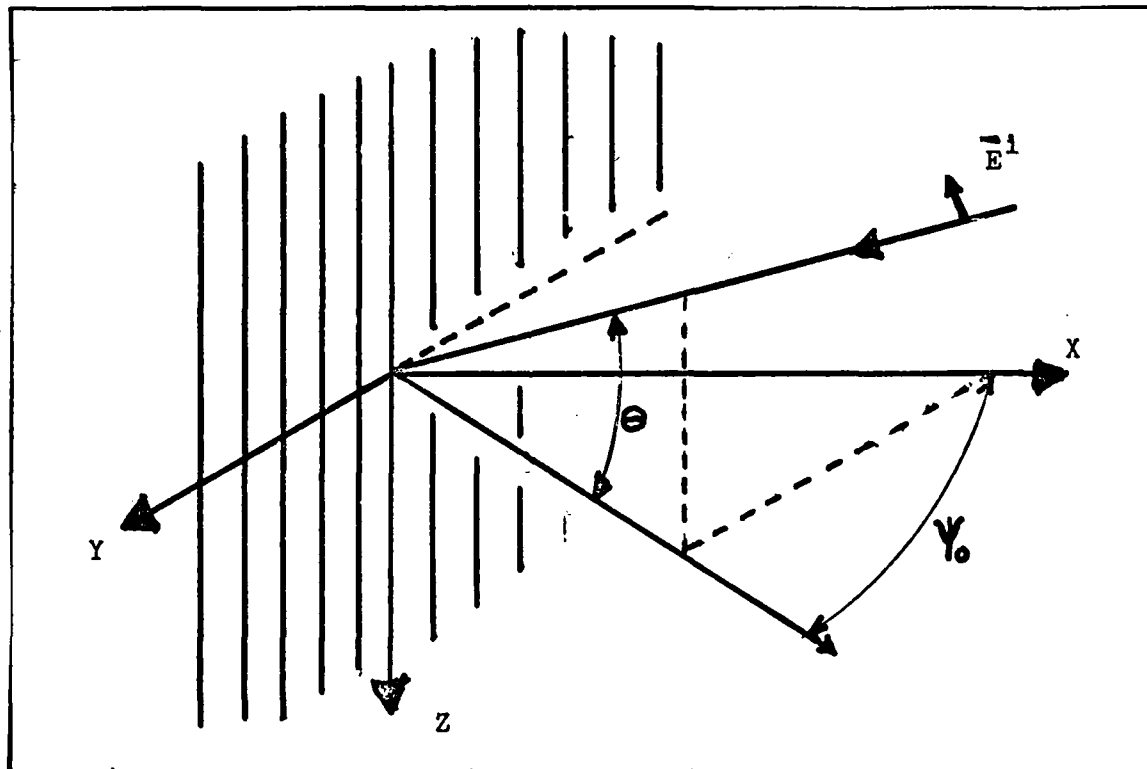


Figure 3. Wait's planar wire grid with incident plane wave.

With this assumption, the radius of the wires must be small compared to the wavelength, since axial symmetry is assumed. Because the wires are infinitely long, the solution can be found by using Hankel functions, in a similar manner to Richmond. Although Wait gives no concrete examples or experimental data, his theory agrees with results obtained by Richmond.

Scattering by an array of infinitely long parallel wires is also the subject of the fifth paper reviewed. Michel, Pauchard, and Vidal describe a mathematical solution to the scattering problem by an infinitely long array (Ref 5). They claim that their technique applies to conductors which are (1) continuous, (2) loaded with localized impedances, or (3) cut in equal length segments and equally spaced in a colinear alignment of dipoles. The continuous case is most similar to this thesis.

They assume the wires to be parallel and infinitely long. Equations are generated using Hankel functions which are very similar to those found by Richmond and Wait. The current on each of the conductors is represented by the product of constants, a current magnitude, and a Hankel function expansion. Their paper, however, is more general than Wait's or Richmond's, since theory accounting for the possibility that localized impedances may lie on the conductors is included.

As an example, they give a double planar array of conductors which is alternately continuous with no impedances, and also continuous with impedances. These results are compared to the experimental radiation pattern of a double planar array illuminated by a uniform, equi-phase plane wave. Their theoretical results agree quite well with experimental data.

Thus, to this point, the only geometries of wires which have been analyzed in detail are (1) single wires of infinite length, (2) dipoles, or (3) wire arrays of infinite length. No author has considered the problem of a finite sized array of closely spaced, parallel wires. Richmond, however, in a subsequent article, did consider a wire grid model, where the wires are finite length (Ref 6).

Richmond shows that a point matching solution can be developed for scattering by conductors of arbitrary shape. In his paper, he describes a practical technique for calculating scattered fields of wire loops, conducting plates, and bodies of arbitrary shape. He models a conducting plate with intersecting wire arrays as shown in Figure 4.

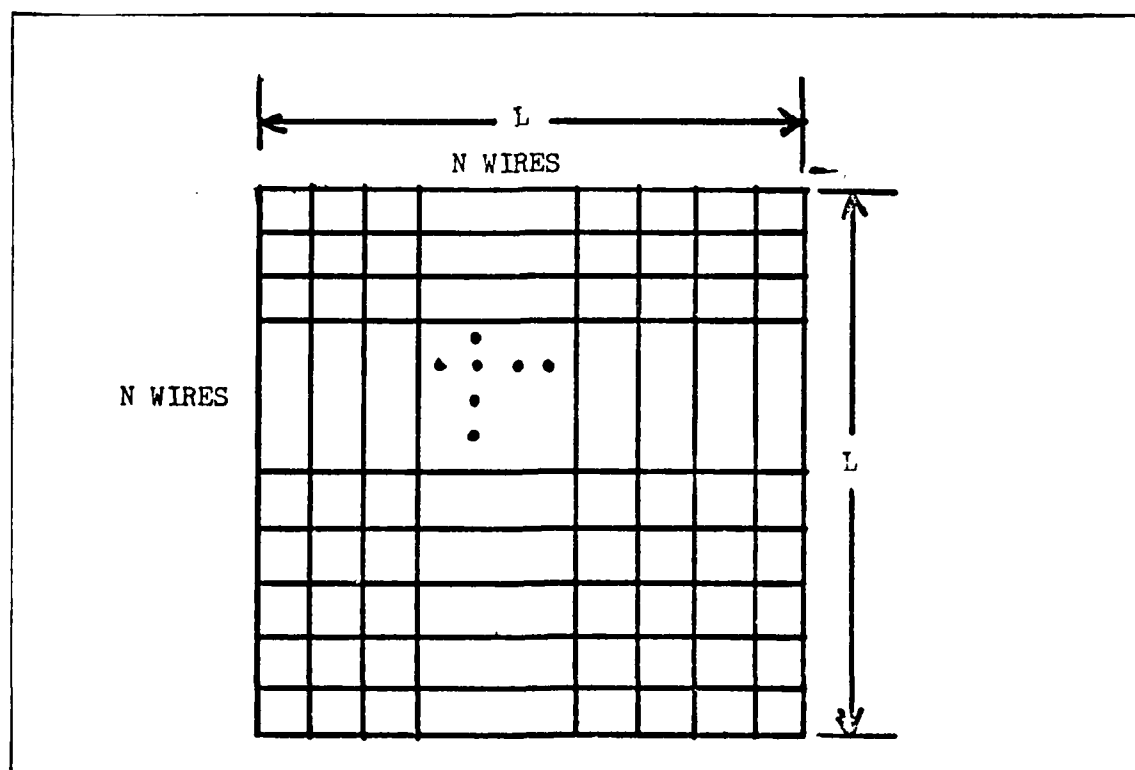


Figure 4. Richmond's wire grid model.

Richmond's wire grid model is not like the problem under consideration, since it contains two intersecting wire arrays. His case does assume, however, that the wires are of finite length. The major distinction is that the current is modeled to flow along either wire axis or any combination thereof. This thesis is not considering a finite conducting plate but rather a finite array of wires, where the current is allowed to flow only along the wire axis.

Richmond solves for the induced currents on his wire grid model by a point matching technique. Each of the finite length wires in the wire grid model is divided into an equal number of segments of lengths. Then, the tangential electric field is forced to zero only at a single point at the midpoint of each segment. Therefore, a system of linear equations is generated which can be solved by the aid of a digital computer.

In a later paper, which is on the same topic, Richmond gives a computer program for solving thin wire scatterers using sinusoidal bases and Galerkin method (Ref 7). As examples to illustrate the validity of this point matching technique, Richmond gives results comparing experimental data with point matching solutions for circular wire loops, square wire loops, square wire grid models, conducting hemispheres, and conducting spheres. Each shows good agreement (5 to 10% difference) with experimental results.

The work which presented much of the basic moment method theory used in this thesis also merits a brief review. Stutzman and Thiele presented a good, fundamental explanation of the moment method in their text, Antenna Theory and Design (Ref 8:306-332). Although they omit much

detail, a derivation of Pocklington's Integral Equation for a single wire case using the Lorentz gauge condition and free space scalar Green's function is presented. They include a section explaining how Pocklington's Integral Equation resembles Kirchoff's Network Equations when expansion functions are used. Two examples with results are included: they are (1) point matching on a short dipole, and (2) a pulse-pulse Galerkin solution for a short dipole. Although no examples are included for the piecewise sinusoidal expansions, a brief description of their efficiency is given. Included in the Appendix is a program for calculating the currents on a single array of parallel dipoles. Because their matrix is block Toeplitz, it cannot be applied to this thesis, i.e., an array over a ground plane, since this case does not produce a block Toeplitz matrix.

The final article reviewed was recently written (July '82) by Kastner and Mittra (Ref 9:673-679). The paper is an analysis of a corrugated surface twist reflector by a spectral iteration technique. It is included in this review to illustrate that alternative techniques for analyzing twist reflectors do exist. Although their corrugated surface twist polarizer is not exactly the same as the Cassegrainian Antenna reflector (Figure 1) of this study, both antennas are functionally similar, i.e., they are designed to rotate the incident wave  $90^\circ$ . Instead of using a wire array over a ground plane, their corrugated surface twist reflector uses a set of thin metallic strips on top of a dielectric substrate which is  $\lambda/4$  thick and is backed by a ground plane, thus forming a series of troughs which are  $\lambda/4$  deep.

They claim their spectral iteration approach is more efficient than the conventional moment method or mode-matching techniques, since

the spectral iteration approach requires no matrix inversion. Without including all the details, the spectral iteration approach for this problem is based on the fact that Green's function for both the regions interior and exterior to the trough is expressible in terms of a Fourier type series. Because of this, the authors indicate that in each of these regions the integral operator that relates the  $\bar{E}$  and  $\bar{H}$  fields is exactly invertible.

There are two different iteration sequences, depending upon whether the incident wave is TE or TM. The general sequence, however, is to (1) evaluate the outer region operator via two-step fast Fourier transform (FFT), (2) obtain H or E, (3) evaluate the inner region operator and estimate  $\bar{E}$  of  $\bar{H}$ , and (4) repeat as desired for accuracy. The reflection coefficient is computed at each step of the iteration, and convergence is attained with three or four iterations.

The authors claim that the use of the FFT procedure, combined with the small number of iterations needed to attain convergence, result in a considerable amount of saved computation time as compared to the moment method and mode-matching techniques which require a large matrix inversion. Results are included for a sample twist reflector, and the authors cite the results to be "very good".

Thus, the existing situation is that a general technique (the moment method) exists for approximating the induced currents on finite sized arrays. Richmond has demonstrated that the moment method produces accurate results for his finite sized wire grid model and other geometries. The problem of determining the induced currents on an array of finite sized wires, though, has not been solved to date. The most similar

geometries to the problem of this thesis which have previously been solved are (1) an array of parallel wires of infinite length, and (2) wires of finite length arranged in two intersecting, perpendicular arrays as in Richmond's wire grid model, Figure 4.

### 1.3 Problem

The problem under consideration is to determine the induced currents on an array of parallel wires of finite length, both in free space and in front of a ground plane. This thesis will compare these results with those of the modified physical optics approximation.

### 1.4 Scope/Assumptions

This thesis will determine the induced currents on an arbitrary section (array of parallel wires in front of a ground plane). The wires will be of finite length, and will have a small but finite diameter. Length, diameter, and spacing will be varied in order to gain some insight of their effect on the currents. As initial values, the diameter will be approximately 0.1 of the wire spacing; the spacing will be 25 wires per wavelength.

To make the problem solvable under given constants, several assumptions must be made. This thesis will assume the following:

- (1) Ground plane is perfectly flat and perfectly conducting ( $\sigma = \infty$ ).
- (2) Wires are perfectly conducting ( $\sigma = \infty$ ).
- (3) Wires are 0.25 wavelength in front of the ground plane.
- (4) The incident plane wave is at an arbitrary angle of incident with matched polarization.

- (5) The wires have a small enough diameter and are far enough apart so that there is no variation of current around the circumference, only along the length.

### 1.5 Approach

The analysis will be broken down into two cases. The first case will be the analysis of the currents on a section of wire with no ground plane present. The second case will be the analysis of a section of wires with a ground plane present. Image theory will be used to model the wires and ground plane as two rows of parallel wires separated by 0.5 wavelengths. In both cases, the polarization will be assumed to be parallel to the wire axis ( $TM_z$  mode).

The actual analysis of the currents in each case will be accomplished by using the method of moments, as described by Stutzman and Thiele. The method of moments is a technique for solving an integral equation which can be readily implemented on a computer. This will be done by approximating an integral equation by a set of linear algebraic equations with the induced current being the unknown.

Each wire will be divided into N segments, with each segment having an unknown current function. This current function can be any type of continuous functions, i.e., pulse, triangle, etc. If pulse functions are used, the technique is known as point matching, since only the center point of each segment is forced to obey the equation. For this study, sinusoidal functions will be assumed. By also assuming that both the source segments and testing functions are sinusoidal, the procedure is referred to as Galerkin Method. The reason for using sinusoidal bases (rather than other functions) is that the current is assumed to be



sinusoidal in nature, and therefore more accurate solutions should be obtainable with fewer of segments, thus reducing the size of the matrix to be inverted. In this way, the numerical computational effort by the computer is reduced.

Since the incident field is assumed to be known, we have a matrix equation with one unknown of the form  $\bar{V} = \bar{Z} \bar{I}$ , where

$\bar{V}_\alpha$  is the known Incident Field.

$\bar{Z}_\alpha$  is an impedance matrix representing the array of wires, each of which is divided into N segments.

$\bar{I}_\alpha$  is the unknown current distribution.

$\bar{I}$  can then be found by using the computer to perform a matrix inversion of  $\bar{Z}$ . Finally, these results will be compared to the modified physical optics approximation.

## II. Development of Theory

### 2.1 Wire Geometry

As stated in Chapter I, this thesis will be a study of an array of parallel wires, both in free space and in the proximity of a ground plane. In both cases, the relative distance between any two arbitrary segments must be known, because the integral equation is a function of this distance. In order to determine this distance, it is necessary to define an orientation of the array on a coordinate system. Although any coordinate system may be used, a rectangular coordinate system is chosen here for convenience.

#### 2.1.1 Free Space Geometry

For this case, the array of wires is considered planar, and can be expressed in two dimensions (temporarily ignoring the wire radius). The array will be defined as in Figure 5, where

N = number of segments per wire

M = number of wires

WSY = spacing between adjacent wires

WL = wire length

L = segment length

In this manner, any arbitrary segment can be specified by an array coordinate (n,m). Because there are M wires, each with N segments, there will be a total of

$$Q \triangleq MN \quad (5)$$

segments.

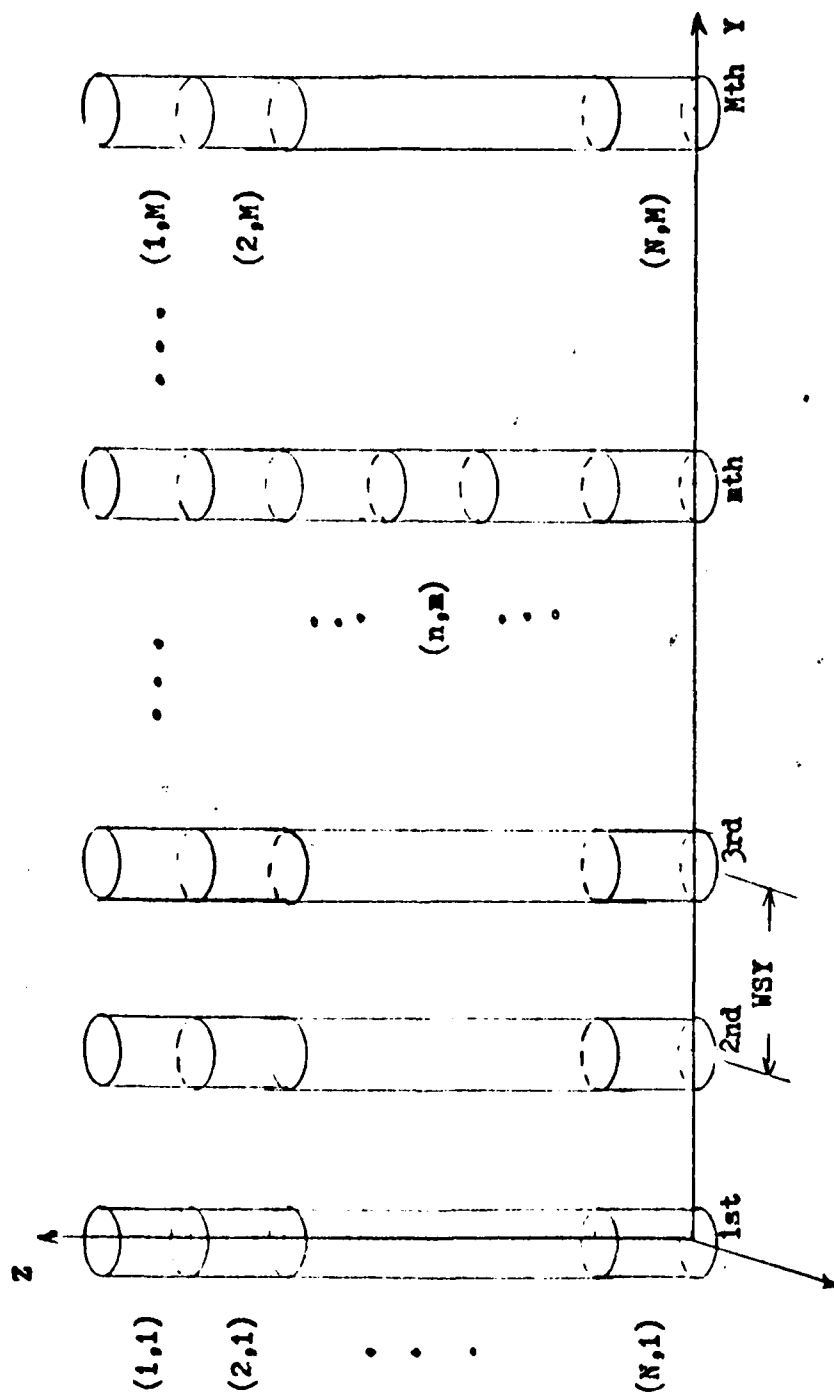


Figure 5. Free space wire array geometry.

### 2.1.2 Ground Plane Case Geometry

The ground plane is assumed to be perfectly conducting. When the array is located near the ground plane, the total electric field at a point P will be the sum of two components: (1) the direct field, and (2) the reflected field. Using Image Theory, the array and ground plane can be modelled as two parallel arrays separated by twice the original separation, as in Figure 6.

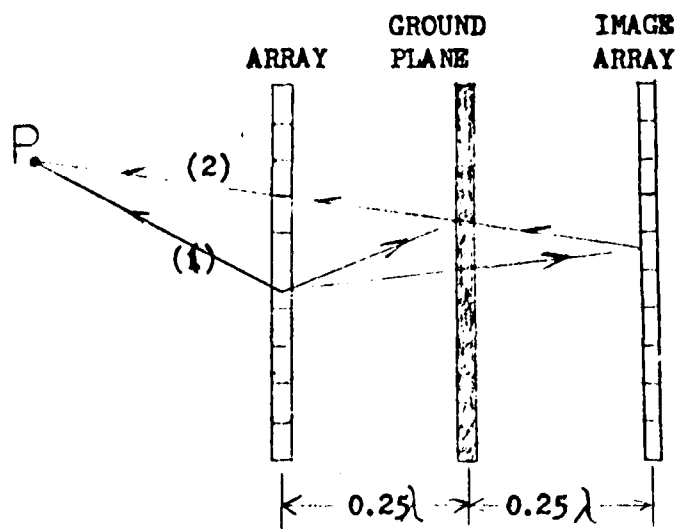


Figure 6. Image Theory model for an array near a ground plane.

Therefore, since the array is  $0.25$  wavelengths above the ground plane, the equivalent geometry is two parallel arrays separated by  $0.5$  wavelengths. The orientation for this case will be similar to that in Figure 5, except that the image array will exist in the  $X = -0.5\lambda$  plane.

For this case, the segments are relabelled so that the total number of segments

$$Q \triangleq 2MN \quad (6)$$

for easier implementation to the computer program (see Appendix A).

### 2.1.3 Distance Between Two Arbitrary Segments

The purpose of this section is to define the geometry for calculating the distance between two segments. For purpose of identification, one segment is labelled "observation" segment (obs), with its location with reference to the origin given by

$$\bar{r}_{\text{obs}} = x\hat{x} + y\hat{y} + z\hat{z} \quad (7)$$

Similarly, the other segment is labelled "source", with its location with reference to the origin given by

$$\bar{r}_{\text{source}} = x'\hat{x} + y'\hat{y} + z'\hat{z} \quad (8)$$

For notational purposes, primed variables will refer to source segments, and unprimed variables will refer to observation segments.

The distance between obs and source segments, then, is the magnitude of the difference between these two vectors, hence

$$R \triangleq |\bar{r}_{\text{source}} - \bar{r}_{\text{obs}}| = \sqrt{(x'-x)^2 + (y'-y)^2 + (z'-z)^2} \quad (9)$$

as in Figure 7.

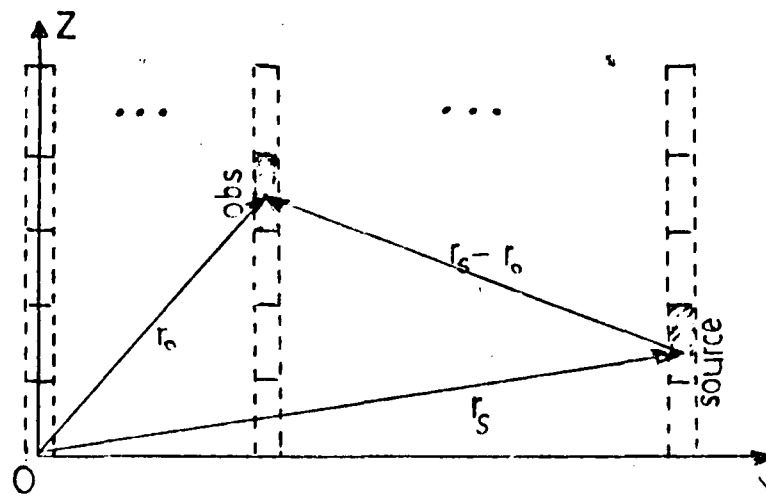


Figure 7. Representation of separation between segments.

## 2.2 Fields At An Arbitrary Wire Segment

This section develops the theory for the electric field at an arbitrary observation segment caused by a current on an arbitrary source segment. Beginning with the time-harmonic form of Maxwell's Equations

$$\nabla \times \vec{E} = -j\omega\mu\vec{H} \quad (10)$$

$$\nabla \times \vec{H} = j\omega\epsilon\vec{E} + \vec{J} \quad (11)$$

and using the definition for the magnetic vector potential  $\vec{A}$ ,

$$\vec{H} = \nabla \times \vec{A} \quad (12)$$

Eq (11) can be written as:

$$\nabla \times \vec{H} = \nabla \times \nabla \times \vec{A} = j\omega\epsilon\vec{E} + \vec{J} \quad (13)$$

Using the vector identity

$$\nabla \times \nabla \times \bar{A} \triangleq \nabla(\nabla \cdot \bar{A}) - \nabla^2 \bar{A} \quad (14)$$

Eq (13) is also equal to

$$\nabla(\nabla \cdot \bar{A}) - \nabla^2 \bar{A} \triangleq j\omega\epsilon'(-j\omega\mu\bar{A} - \nabla\Phi) + \bar{J} \quad (15)$$

because the scalar potential  $\Phi$  is defined from:

$$\bar{E} \triangleq -j\omega\mu\bar{A} - \nabla\Phi \quad (16)$$

Rewriting Eq (15) as

$$\nabla^2 \bar{A} + \omega^2\mu\epsilon'\bar{A} - \nabla(j\omega\epsilon'\Phi + \nabla \cdot \bar{A}) = -\bar{J} \quad (17)$$

and employing the Lorentz condition (Ref 8:10) to specify the divergence of the vector potential

$$\nabla \cdot \bar{A} = -j\omega\epsilon'\Phi \quad (18)$$

then Eq (17) reduces to:

$$\nabla^2 \bar{A} + \omega^2\mu\epsilon'\bar{A} = -\bar{J} \quad (19)$$

which is known as the "vector wave equation".

A solution to this vector wave equation is (Ref 8:13)

$$\bar{A} = \underset{\text{volume}}{\iint\!\!\!\int}_{\text{source}} \bar{J} \frac{e^{-jkR}}{4\pi R} dv' \quad (20)$$

or in terms of the scalar Green's function

$$\bar{A} = \iiint_{\substack{\text{source} \\ \text{volume}}} \bar{J} \psi(R) dv' \quad (21)$$

where  $\psi(R) = \frac{e^{-jkR}}{4\pi R}$ , Green's function.

From the definition of the scalar potential, Eq (16),  $\bar{E}$  can be expressed in terms of  $\bar{A}$ . This can be done by taking the divergence of Eq (18)

$$\nabla(\nabla \cdot \bar{A}) = -j\omega\epsilon' \nabla\phi \quad (22)$$

and solving for  $\nabla\phi$ , yielding

$$\nabla\phi = -\frac{1}{j\omega\epsilon'} \nabla(\nabla \cdot \bar{A}) \quad (23)$$

Substituting Eq (23) into Eq (16) leaves

$$\begin{aligned} \bar{E} &= -j\omega\mu_0 \bar{A} + \frac{1}{j\omega\epsilon'} \nabla(\nabla \cdot \bar{A}) \\ &= \frac{1}{j\omega\epsilon'} (A\omega^2\mu\epsilon' + \nabla^2 \bar{A}) \end{aligned} \quad (24)$$

or, because the propagation constant  $\beta^2 = \omega^2\mu\epsilon'$ , then

$$\bar{E} = \frac{1}{j\omega\epsilon'} (\beta^2 \bar{A} + \nabla^2 \bar{A}) \quad (25)$$

By finally inserting the Green's function wave equation solution Eq (20) into Eq (25), the desired result is obtained:

$$\bar{E} = \frac{1}{j\omega\epsilon'} \iiint_{\substack{\text{source} \\ \text{volume}}} [\nabla^2 \psi(R) + \beta^2 \psi(R)] \bar{J} dv' \quad (26)$$



Some clarification is needed, however, on what is meant by "source volume". If a typical source segment is defined in cylindrical coordinates as in Figure 8,

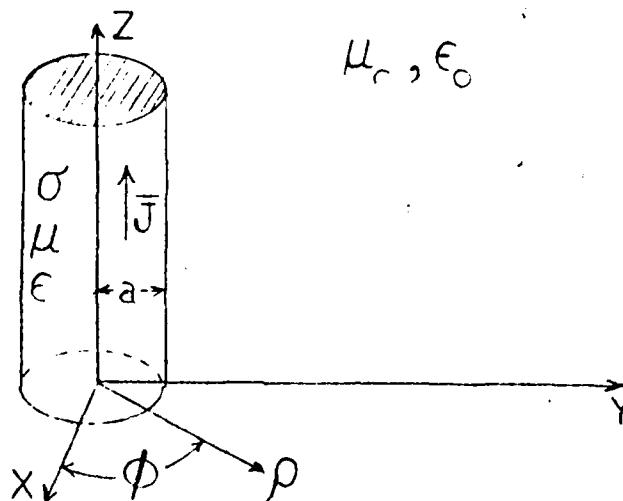


Figure 8. A typical segment in free space.

then:

$$\bar{E} = \frac{1}{j\omega\epsilon} \int_0^L \int_0^{2\pi} \int_0^a [\nabla^2 \psi(R) + \beta^2 \psi(R)] \bar{J} \rho' d\rho' d\phi' dz' \quad (27)$$

It will be assumed here that the conductivity of air approximately equals the conductivity of free space, so that  $\epsilon' = \epsilon$ . Because it was assumed that the conductivity of the wire was infinite ( $\sigma = \infty$ ), all of the current density is assumed to exist only upon the wire surface (at  $\rho = a$ ), not on the interior region. Hence,

$$\bar{E} = \frac{a}{j\omega\epsilon} \int_0^L \int_0^{2\pi} [\nabla^2 \psi(R) + \beta^2 \psi(R)] \bar{J} d\phi' dz' \quad (28)$$

Since it was stipulated that the wire must be very small in diameter, it can be assumed that the current only flows along the wire axis, not transverse to it. Therefore, this assumption implies that only a  $\hat{z}$  electric field will exist; the  $\hat{z}$  component of the electric field expressed in Eq (28) is then:

$$E_z = \frac{a}{j\omega\epsilon_0} \int_0^L \int_0^{2\pi} \left[ \frac{\partial^2}{\partial z^2} \psi(R) + \beta^2 \psi(R) \right] \bar{J} d\phi' dz' \quad (29)$$

Also because the wires are of small diameter, it can be assumed that the current density is equally distributed on the circumference of the wire surface in an infinitely thin shell (only at  $\rho = a$ ), so

$$\bar{I}(z') = \bar{J}(z') 2\pi a \quad (30)$$

Then, substituting Eq (30) into Eq (29) and integrating yields the final desired result:

$$E_z = \frac{1}{j\omega\epsilon_0} \int_0^L \left[ \frac{\partial^2}{\partial z^2} \psi(R) + \beta^2 \psi(R) \right] I(z') dz' \quad (31)$$

Before continuing, it should be noted that the assumption of the current existing only upon the wire surface will necessitate a modification to Eq (9). The observation points of each segment are along the wire axis; with the above assumption, the source points are on the wire surface. This difference, the wire radius  $a$ , must be taken into consideration. If the radius were not included, it would be possible for  $R$  to equal zero when the source and observation segments were the same. If  $R$  did equal zero, Green's function would become infinite, which would require consideration of the shape of the principle volume and the

principle value of the integral. Fortunately, this is not necessary in this case. Eq (9) should therefore be modified to include the radius as:

$$R = \sqrt{a^2 + (x' - x)^2 + (y' - y)^2 + (z' - z)^2} \quad (32)$$

### 2.3 Method of Moments

The method of moments is a technique for numerically approximating a solution to an integral equation of the first kind, like Eq (31). Schelkunoff demonstrated that this technique is analogous to solving Kirchhoff's network equation (Ref 8):

$$\sum_{q'=1}^Q Z_{qq'} I_{q'} = V_q \quad (33)$$

where

$Q$  = total number of segments

$q = q^{\text{th}}$  source segment

$q' = q^{\text{th}}$  observation segment

By defining a function  $K(R)$  as

$$K(R) = \frac{1}{j\omega\epsilon} \left[ \frac{\partial}{\partial z^2} \psi(R) + \beta^2 \psi(R) \right] \quad (34)$$

then Eq (31) can be expressed as:

$$E_z = \int_0^L K(R) I(z') dz' \quad (35)$$

Furthermore, the current on a wire can be approximated by a series of orthogonal expansion functions  $F_n$  such that

$$\bar{I}(z') \approx \sum_{n=1}^N \bar{I}_n F_n(z') \quad (36)$$

where

$\bar{I}_n$  is the  $n^{\text{th}}$  complex expansion coefficient

$F_n$  is the  $n^{\text{th}}$  expansion function (yet to be described)

$n$  is the number of segments per wire

Then, using Eq (36) in Eq (35) yields

$$E_z = \sum_{n=1}^N \int_0^L \bar{I}_n F_n(z') K(R) dz' \quad (37)$$

Since  $\bar{I}_n$  is not a function of source segment length  $z'$ , it can be removed from the integrand:

$$E_z = \sum_{n=1}^N \bar{I}_n \int_0^L F_n(z') K(R) dz \quad (38)$$

Eq (38) is now in the form of Kirchhoff's voltage equation if:

$$V_q = E_z \quad (39a)$$

$$I_q = \bar{I}_n \quad (39b)$$

$$Z_{qq} = \int_0^L F_n(z') K(R) dz' \quad (39c)$$

For notational simplification,

$$Z_{qq} = \int_0^L F_n(z') K(R) dz' = f(z, z') \quad (40)$$

For a single wire with  $N$  segments, there will be  $N$  independent equations. For an array of wires, however, with  $Q$  total segments, there

will be a system of Q equations

$$\begin{aligned}
 E_z(z_1) &\approx I_1 f(z_1, z_1') + I_2 f(z_1, z_2') + \dots + I_Q f(z_1, z_Q') \\
 E_z(z_2) &\approx I_1 f(z_2, z_1') + I_2 f(z_2, z_2') + \dots + I_Q f(z_2, z_Q') \\
 &\vdots \\
 E_z(z_Q) &\approx I_1 f(z_Q, z_1') + I_2 f(z_Q, z_2') + \dots + I_Q f(z_Q, z_Q')
 \end{aligned} \tag{41}$$

which can be more conveniently expressed in matrix notation as:

$$[V_q] = [Z_{qq}] [I_q] \tag{42}$$

The  $I_q$ 's can then be found by simply premultiplying Eq (42) by  $[Z_{qq}]^{-1}$ , obtaining:

$$[I_q] = [Z_{qq}]^{-1} [V_q] \tag{43}$$

The previous few paragraphs are an explanation of the general form of the method of moments (Ref 8:310-312). Specific forms of the method of moments are obtained by choosing different expansion functions  $F_n$  in Eq (36).

Although any set of orthogonal functions may be used for expansion functions, the simplest and most intuitively obvious choice may be a pulse function:

$$F_n(z') = \begin{cases} 1 & \text{for } z' \text{ in } L \\ 0 & \text{else} \end{cases} \tag{44}$$

where L is a segment of the wire length  $WL/N$ .

This choice of expansion functions is commonly used with the "point matching solution". It is so labelled because the boundary condition (tangential electric field equals zero) is only enforced at  $N$  discrete points. A physical interpretation of this is shown in Figure 9 (Ref 8:311).

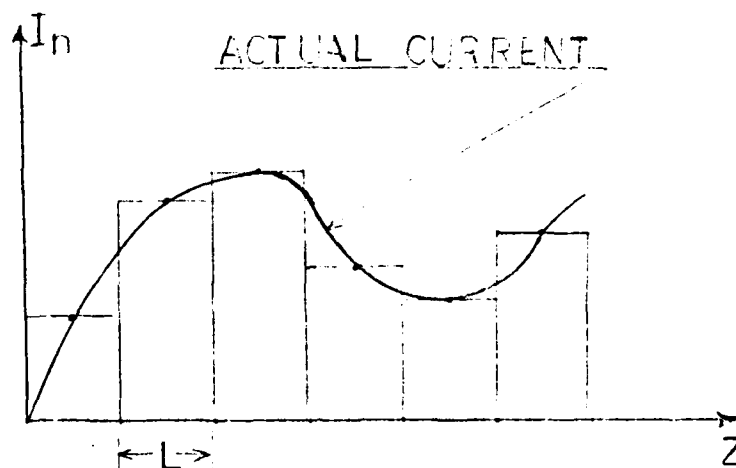


Figure 9. Staircase approximation to an actual current distribution.

Exactly accurate solutions are obtained using this method if  $N$  equals infinity. In practice, however, good approximations are obtained by making  $N$  sufficiently large.  $N$  cannot be made arbitrarily large, however, due to difficulties encountered with the large computational effort.

Stutzman and Thiele state that approximately fifty segments per wavelength are needed to obtain reasonable results (Ref 8:324). For a single wire as they studied, the point matching approach is adequate. However, when a large array is encountered (as in this thesis of 25 wires

per wavelength), it becomes evident that the point matching approach will become computationally unfeasible. For example, if this thesis were to attempt a point matching approach, the size of the array to be inverted would be (50 segments times 25 wires implies) a 1250 by 1250 array; this is clearly an unreasonable task for all but the most advanced computer systems. Obviously, a different expansion function must be chosen.

This thesis will use piecewise sinusoidal expansion functions (PWSEF) defined as

$$\hat{z} \frac{\sin\beta(z-z_{n-1})}{\sin\beta(z_n-z_{n-1})} \quad z_{n-1} \leq z < z_n \quad (45a)$$

$$F_n(z) \triangleq \hat{z} \frac{\sin\beta(z_n-z)}{\sin\beta(z_{n+1}-z_n)} \quad z_n \leq z < z_{n+1} \quad (45b)$$

which are pictured in Figure 10 (Ref 8:324).

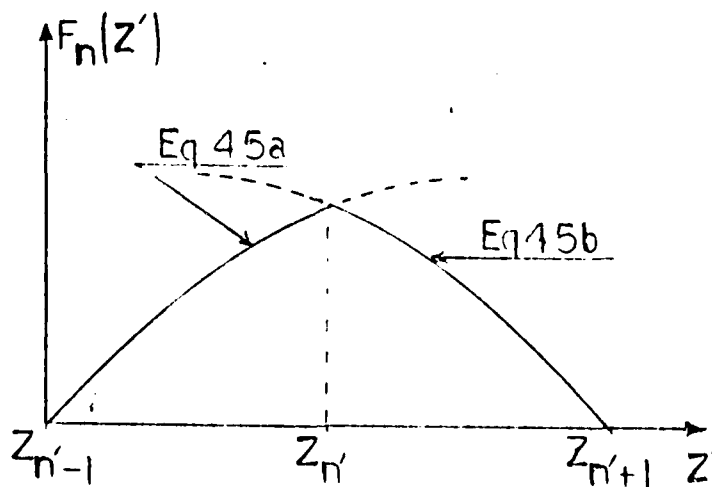


Figure 10. Piecewise sinusoidal expansion function.

Each segment will overlap with adjacent segments to approximate the current on the entire wire, as shown in Figure 11.

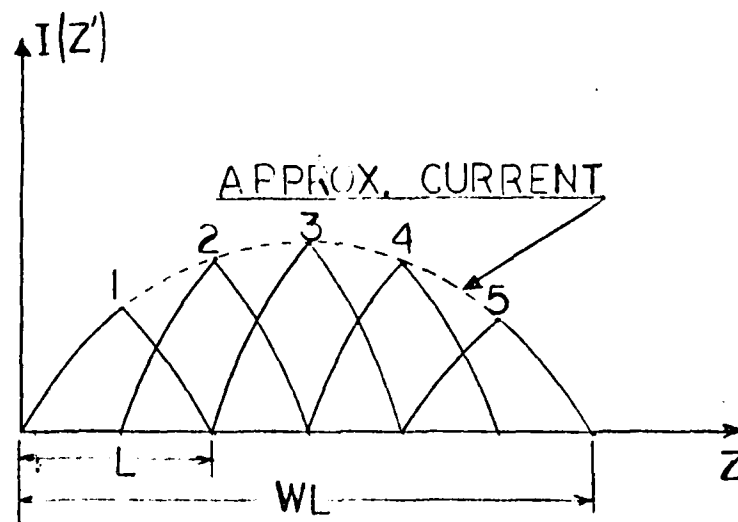


Figure 11. Five segment piecewise sinusoidal current approximation.

PWSEF are chosen because the actual current is anticipated to be sinusoidal, and therefore the closest approximation should be PWSEF. The greatest advantage in using PWSEF instead of pulse functions is the inherent reduction in segments. To obtain the same degree of accuracy, Stutzman and Thiele find that "almost ten times fewer segments are required for the PWSEF as for the pulse expansion function" (Ref 8:325).

Therefore, using PWSEF, only about five segments per wavelength are needed. This reduction, then, makes the study of a 25 wire per wavelength array feasible using the moment method with PWSEF. Now, only a 125 by 125 array (250 by 250 for ground plane case because of image array) need be inverted. This is possible for many computer systems.



In order to obtain the best possible approximation, the boundary condition (tangential electric field equal zero) must be enforced as "closely" as possible. The point matching technique is not an exceptionally good approximation because the boundary condition is only enforced at one point in each segment. Instead, a better technique is to attempt to enforce the boundary condition in an "average" sense (as many points as possible) over the segment. This is what is done in an approach known as the method of weighted residuals (Ref 10).

A residual field  $E_{tan}^{res}$  can be defined as

$$E_{tan}^{res} = E_{tan}^s + E_{tan}^i \quad (46)$$

Clearly, the exact solution occurs when  $E_{tan}^{res} = 0$ . In any approximate solution,  $E_{tan}^{res} \neq 0$ ; however, the best approximation would be to make  $E_{tan}^{res}$  approach zero in some "average" sense. This can be done by defining a Weighting Function  $W_n(z)$  such that:

$$\int_0^L W_n(z) E_{tan}^{res}(z) dz = 0 \quad n=1,2,\dots,N \quad (47)$$

The weighting function  $W_n(z)$  is similar to the expansion function  $F_n(z)$ ; it can be any set of orthogonal functions. If the weighting and expansion functions are chosen to be the same (in this case, piece-wise sinusoidal), then the technique is known as the Galerkin method. As previously stated, this thesis is using the Galerkin method; therefore,  $W_n(z) = F_n(z)$ . Then using Eq (46), Eq (47) is equivalent to:

$$\int_0^L W_n(z) E_{tan}^s(z) dz + \int_0^L W_n(z) E_{tan}^i(z) dz = 0 \quad (48)$$

Since a current on a wire will produce a scattered field  $\bar{E}^s$ , and because there are only  $\hat{z}$  directed wires, Eq (31) can be interpreted to represent the scattered field which was caused by the induced current. Eq (31) can then be substituted into Eq (48) for  $E_{\tan}^s$ , yielding:

$$\int_L W_n(z) \left[ \frac{1}{j\omega\epsilon_0} \int_0^L \left[ \frac{\partial}{\partial z^2} \psi(R) + \beta^2 \psi(R) \right] I(z') dz' \right] dz = - \int_L W_n(z) E_{\tan}^i dz \quad (49)$$

The right side of Eq (49) is recognized to be the "average" induced voltage,  $V_q$ ; it will be discussed in the following section. The left side is equal to the induced current multiplied by the cross impedance  $Z_{qq}$  between the source and observation segments. It can be simplified by realizing that:

$$\frac{\partial}{\partial z} \psi(R) = - \frac{\partial}{\partial z'} \psi(R) \quad (50a)$$

$$\frac{\partial}{\partial z} \psi(R) = \frac{\partial}{\partial z'^2} \psi(R) \quad (50b)$$

Using Eqs (50a) and (50b) in Eq (31) and integrating twice by parts yields (Ref 8:329):

$$E_z = \frac{j}{\omega\epsilon_0} \left[ \psi(R) \frac{\partial}{\partial z'} I(z') + I(z') \frac{\partial}{\partial z} \psi(R) \right] + \frac{1}{j\omega\epsilon_0} \int_0^L \left[ \frac{\partial}{\partial z'^2} I(z') + \beta^2 I(z') \right] \psi(R) dz' \quad (51)$$

Since the current is being approximated by PWSEF, for a single  $q^{\text{th}}$  source segment, Eq (51) becomes:

$$E_z = \frac{j}{\omega \epsilon_0} \left[ \psi(R) \frac{\partial}{\partial z} F_q(z') + F_q(z') \frac{\partial}{\partial z} \psi(R) \right] + \frac{1}{j\omega \epsilon_0} \int_L \frac{\partial^2}{\partial z'^2} F_q(z') + \beta^2 F_q(z') \psi(R) dz' \quad (52)$$

An interesting simplification occurs because PWSEF were chosen. Using Eq (44) and twice differentiating, it is discovered that:

$$\frac{\partial^2}{\partial z'^2} F_q(z') = -\beta^2 F_q(z') \quad (53)$$

This indicates that the bracketed expression in the integrand of Eq (52) is zero (Ref 9:370). Eq (52) then reduces to:

$$E_z = \frac{j}{\omega \epsilon_0} \left[ \psi(R) \frac{\partial}{\partial z} F_q(z') + F_q(z') \frac{\partial}{\partial z} \psi(R) \right] \quad (54)$$

source  
segment

Evaluating Eq (54) over a typical source segment (pictured in Figure 10), and denoting the distance from the obs point to  $z_{q-1}'$ ,  $z_q'$ , and  $z_{q+1}'$  as  $R_{q-1}$ ,  $R_q$ , and  $R_{q+1}$ , respectively, Eq (54) equals:

$$E_z = \frac{j}{\omega \epsilon_0} \left[ \psi(R_q) \frac{\partial}{\partial z} F_q(z_q') + F_q(z_q') \frac{\partial}{\partial z} \psi(R_q) - \psi(R_{q-1}) \frac{\partial}{\partial z} F_q(z_{q-1}') - F_q(z_{q-1}') \frac{\partial}{\partial z} \psi(R_{q-1}) + \psi(R_{q+1}) \frac{\partial}{\partial z} F_q(z_{q+1}') + F_q(z_{q+1}') \frac{\partial}{\partial z} \psi(R_{q+1}) - \psi(R_q) \frac{\partial}{\partial z} F_q(z_q') - F_q(z_q') \frac{\partial}{\partial z} \psi(R_q) \right] \quad (55)$$

The first and seventh bracketed terms cancel, and  $F_{q'}(z_{q'-1}) =$

$F_{q'}(z_{q'+1}) = 0$ , leaving

$$E_z = \frac{j}{\omega \epsilon_0} \{ \psi(R_q) \left[ \frac{\beta \cos \beta (z_{q'} - z_{q'-1})}{\sin \beta (z_{q'} + z_{q'-1})} - \frac{\beta \cos \beta (z_{q'+1} - z_{q'})}{\sin \beta (z_{q'+1} - z_{q'})} \right] \right. \\ \left. - \psi(R_{q'-1}) \frac{\beta}{\sin \beta (z_{q'} - z_{q'-1})} \right. \\ \left. - \psi(R_{q'+1}) \frac{\beta}{\sin \beta (z_{q'+1} - z_{q'})} \right\} \quad (56)$$

which, using the trigonometric identity

$$\sin (\alpha + \beta) = \cos \alpha \sin \beta + \sin \alpha \cos \beta \quad (57)$$

can finally be expressed as:

$$E_z^s = -j30 \left\{ \frac{e^{-j\beta R_{q'-1}}}{R_{q'-1} \sin \beta (z_{q'} - z_{q'-1})} \right. \\ \left. - \frac{e^{-j\beta R_{q'}} \sin \beta (z_{q'+1} - z_{q'-1})}{R_{q'} \sin \beta (z_{q'} - z_{q'-1}) \sin \beta (z_{q'+1} - z_{q'})} \right. \\ \left. + \frac{e^{-j\beta R_{q'+1}}}{R_{q'+1} \sin \beta (z_{q'+1} - z_{q'})} \right\} \quad (58)$$

Then, the expression for  $Z_{qq'}$  can be given using Eq (58):

$$\begin{aligned}
 Z_{qq'} &= \int_{\text{seq}}^{\text{obs}} I_q E_z^s dz \\
 &= \left[ \int_{z_{q-1}}^{z_q} \frac{\sin\beta(z - z_{q-1})}{\sin\beta(z_q - z_{q-1})} + \int_{z_q}^{z_{q+1}} \frac{\sin\beta(z_{q+1} - z)}{\sin\beta(z_{q+1} - z_q)} \right] \\
 &\quad \cdot \left[ j30 \left( \frac{e^{-j\beta R_{q'-1}}}{R_{q'-1} \sin\beta(z_{q'} - z_{q'-1})} - 2 \frac{\cos\beta(z_{q'+1} - z_{q'})}{\sin\beta(z_{q'+1} - z_{q'})} \frac{e^{-j\beta R_{q'}}}{R_{q'}} \right. \right. \\
 &\quad \left. \left. + \frac{e^{-j\beta R_{q'+1}}}{R_{q'+1} \sin\beta(z_{q'+1} - z_{q'})} \right) \right] dz \quad (59)
 \end{aligned}$$

Stutzman and Thiele present a similar but less detailed derivation for their simpler case of a single wire. Eq (59) agrees with their result if appropriately simplified (Ref 8:331).

#### 2.4 Induced Voltage by Incident Plane Wave

This section describes the  $q^{\text{th}}$  voltage matrix element,  $V_q$ . From Eq (49), the "average" weighted voltage is:

$$V_q = \int_L W_q(z) E_{\text{tan}}^i dz \quad (60)$$

$\bar{E}_{\text{tan}}^i$  must be determined for a plane wave of arbitrary incidence angle with matched polarization, as stated in the initial assumptions. An arbitrary plane wave can be specified by the "plane wave solution" to the vector wave equation as:

$$\bar{E} = \bar{E}_0 e^{+j\beta \bar{n} \cdot \bar{r}} \quad (61)$$

where

$\bar{E}_0$  is a constant vector, to be specified

$\beta$  is the propagation constant

$\bar{n}$  is the propagation vector

$\bar{r}$  is the radius vector from the origin

Since matched polarization is assumed, then  $\bar{E}_0 = E_0 \hat{z}$ , because the wires are  $\hat{z}$  directed. By expressing the radius vector  $\hat{r}$  in terms of rectangular coordinates, then

$$\bar{E} = E_0 \hat{z} e^{+j\beta((\sin\theta\cos\phi)x + (\sin\theta\sin\phi)y + (\cos\theta)z)} \quad (62)$$

so that:

$$V_q = - \left[ \int_{z_{q-1}}^{z_q} \frac{\sin\beta(z - z_{q-1})}{\sin\beta(z_q - z_{q-1})} + \int_{z_q}^{z_{q+1}} \frac{\sin\beta(z_{q+1} - z)}{\sin\beta(z_{q+1} - z_q)} \right] \\ \cdot E_0 \hat{z} e^{+j\beta((\sin\theta\cos\phi)x + (\sin\theta\sin\phi)y + (\cos\theta)z)} dz \quad (63)$$

Now, both  $Z_{qq}$  and  $V_q$  have been expressed in a form suitable for computer implementation (see Appendix A). Results for different wire spacings, lengths, and incidence angles are given in the following chapter.

### III. Results

This chapter presents the results of the computer program and compares them with the physical optics approximation. The parameters investigated include: (1) wire spacings, (2) number of segments per wire, (3) wire lengths, and (4) varying incidence angles. Unless otherwise indicated, all results were obtained with the same set of input values. These are:

Number of wires = as indicated

Segments per wire = as indicated

Wire length = 1.0 meters

Wire radius = 0.005 meters

X wire spacing = 0.50 meters

Y wire spacing = determined by  $\frac{\# \text{ wires}}{\text{width of array}}$

Frequency =  $300.0\text{MH}_z$

Propagation constant  $\beta = 2\pi/\lambda$

$|E_o| = 1.0 \text{ volts}$

Width of array =  $1.0 \lambda = 1.0 \text{ meters}$

The current is in units of AMPS, voltage in VOLTS, and length in METERS.

For each of the different cases studied, both current density magnitude and phase is presented in either a "horizontal cut" or a "vertical cut". These terms need to be properly defined for accurate interpretation. A horizontal cut is the current on the center segment of each wire across the width of the array. For example, with 5 segments per wire, a horizontal cut presents the 3rd, 8th, 13th,...(Q-2)th segments. Conversely, a vertical cut presents the current of the center of

the wire array for the length of the wire. For example, with  $N=5$  and  $M=7$ , a vertical cut presents the current on the center wire, segments 16, 17, 18, 19, and 20.

### 3.1 Wire Spacings

A fundamental question to be considered is for what range of wire spacings is this moment method technique applicable. It is known that the technique can be used successfully for a single wire case, as demonstrated by Stutzman and Thiele (Ref 8). However, an objective of this thesis was to determine if a parallel wire array could sufficiently model a flat, conducting plane. This involves using "enough" wires to achieve a "reasonable" approximation.

As was stated in Chapter I, it is expected that the moment method results should become more accurate as the number of wires/wavelength is increased. Results in Figures 12 and 13 verify this expectation to a certain extent. The purpose of establishing these results is to determine if a trend exists as the number of wires is increased.

For a normally incident plane wave upon a flat, conducting sheet, the physical optics approximation would yield a current density of:

$$\begin{aligned}\bar{E}^i &= \hat{z}e^{+jkx} \\ \therefore \bar{H}^i &= \frac{\hat{y}e^{+jkx}}{376.7} \\ \therefore \bar{J}_s &= \hat{e} \cdot 2\hat{n} \times \bar{H} = \frac{2}{376.7} \approx 5.31 \text{mA/m}\end{aligned}$$

This does not totally agree, however, with what the actual distribution is expected to be. One would expect the actual current to be basically uniform (flat) across the center of the sheet, with perhaps a perturbation



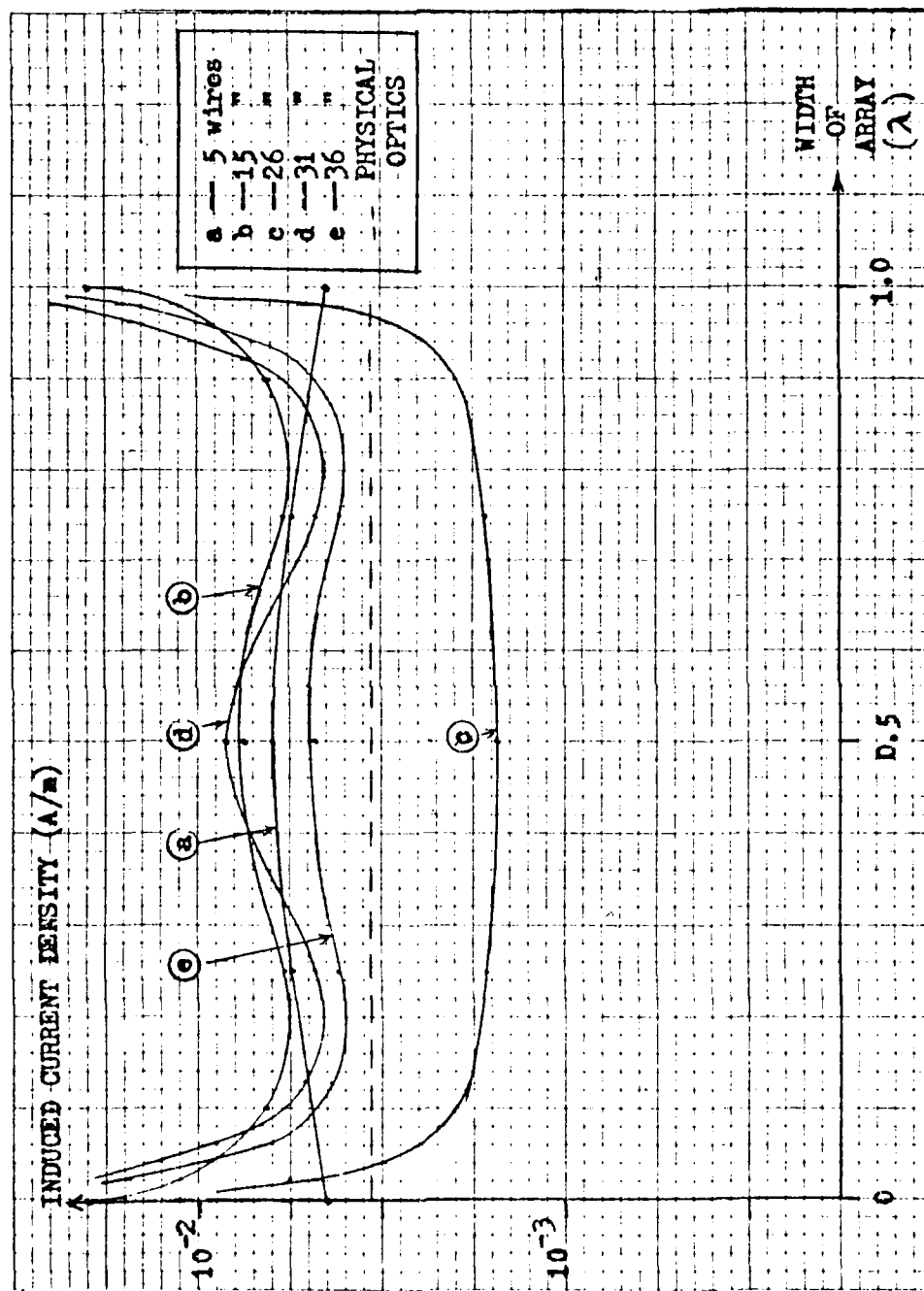


Figure 12. Current on a horizontal cut of a  $1\lambda^2$  array with various wire spacings for a normally incident plane wave.

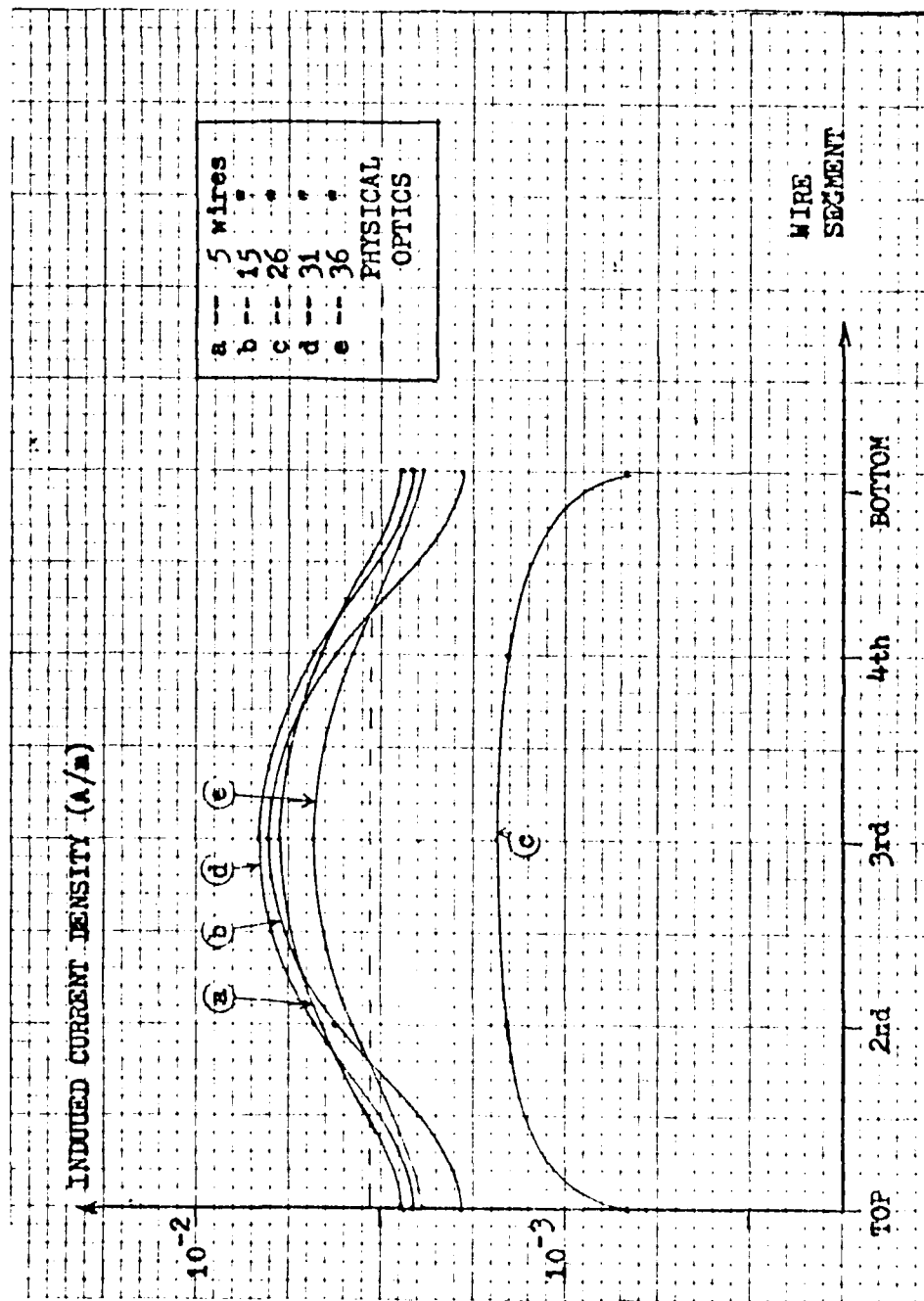


Figure 13. Current on a vertical cut of a  $1\lambda^2$  array with various wire spacings for a normally incident plane wave.

near the edge caused by the abrupt boundary change. The current along each wire (vertical cut) should be sinusoidal, with the endpoints of each wire equal to zero.

It is evident from Figures 12 and 13 that the moment method seems to be more accurate than the physical optics approximation. The horizontal cut indicates a basically flat distribution across the center with a perturbation at the edge, as is physically expected. The physical optics approximation is flat and of the correct order of magnitude, but does not represent any effects caused by the edges. The vertical cut is symmetric and sinusoidal, as expected. The current is zero at the ends of the wire, but Figure 14 does not apparently indicate this because the current at the center of each sinusoidal piece was plotted, not the current at the exact endpoint of the wire. Note that the physical optics approximation does not show the currents approaching zero at the ends of the wire.

The current distributions also tend to "flatten out" in the center region as the number of wires is increased, as expected. A word of caution is in order, however. Although this flattening trend is present through 36 wires/wavelength (which should be enough for most applications), it may not continue to exist for arbitrarily large numbers of wires/wavelength. It was initially assumed that the wire diameter was "small enough" so that there was no circumferential current variation on the wires. If the spacing/diameter ratio becomes too small, this assumption may become invalid. Although the lower limit of this ratio has not been identified by this thesis, good results are achievable as low as  $(1/36)/0.005 = 5.55:1$ . This point may be an aspect of future study.

### 3.2 Number of Segments per Wire

As presented in the theory, more accurate results should be obtained by using a greater number of segments/wire. Theoretically, there is no upper limit; there is an upper limit imposed, however, by the increased computational effort incurred and the available computer resources. The question this section investigates is whether increasing the number of segments (beyond five) is worth the additional effort.

Figures 14 and 15 display the induced current (horizontal and vertical cuts, respectively) for a  $1\lambda^2$  array with five wires. By increasing the number of segments, one would expect a more accurate distribution of the current along the length of the wire, with little or no change across the array (in the horizontal cut). Note that the physical optics approximation is unchanged for each case, since changing the number of segments has no meaning with this approximation.

Results show good agreement with actual expected behavior. The horizontal current distribution changes little in both general shape and magnitude for all five cases. This is reasonable, since one would not expect the current across the wires to be appreciably affected by changing the sampling increment along the length of the wire. The vertical current also changes as expected. The midpoint current remains relatively constant while the endpoints decrease nearly in order of magnitude.

This sixfold increase in the number of segments shows no significant change in the horizontal current or the center region of the vertical current, but does indicate the expected decrease near the endpoints of the wire. Since it is known that the current must be zero at the ends of each

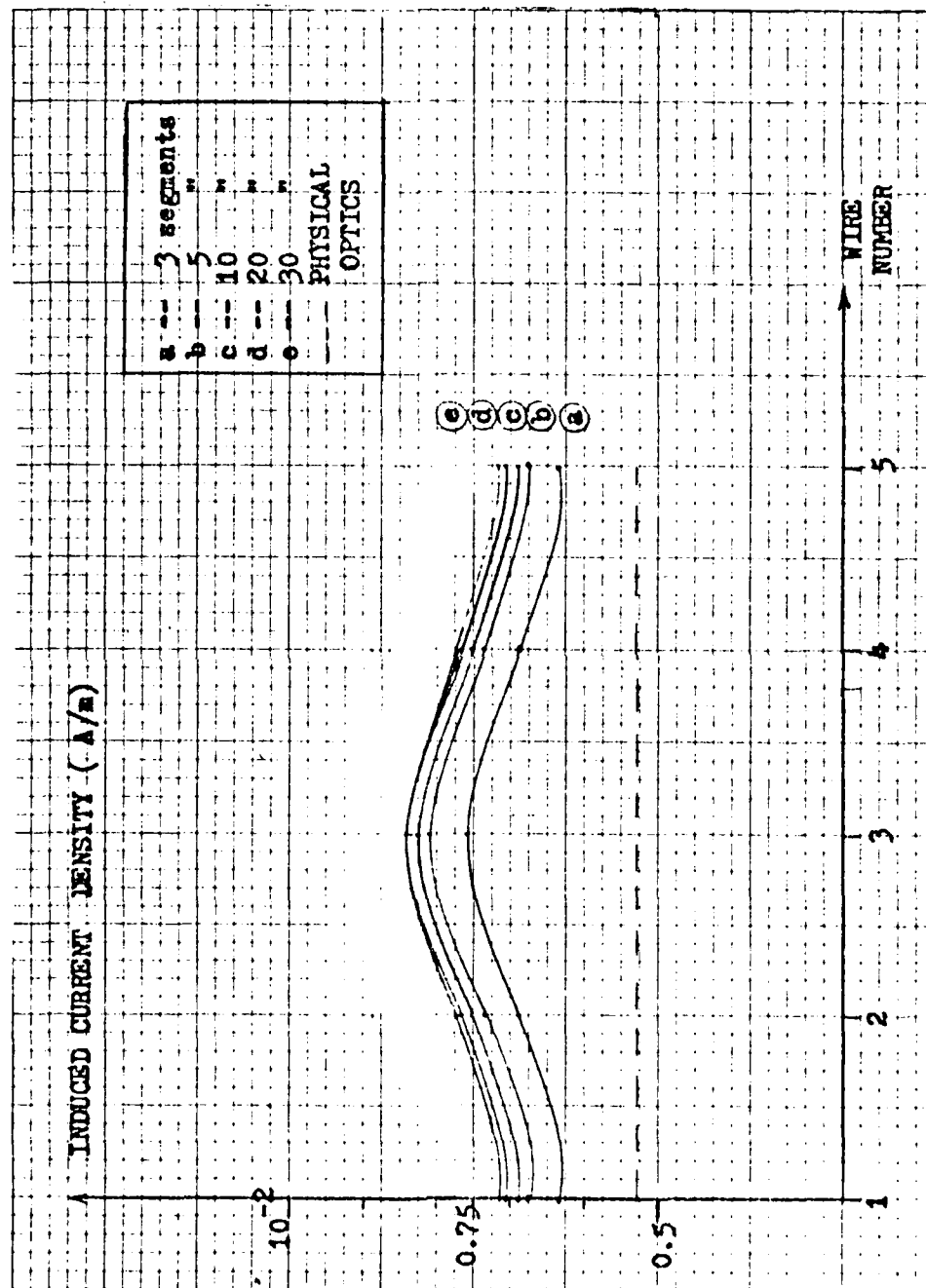


Figure 14. Current on a horizontal cut of a  $1\lambda^2$  array with various wire segment divisions for a normally incident plane wave.

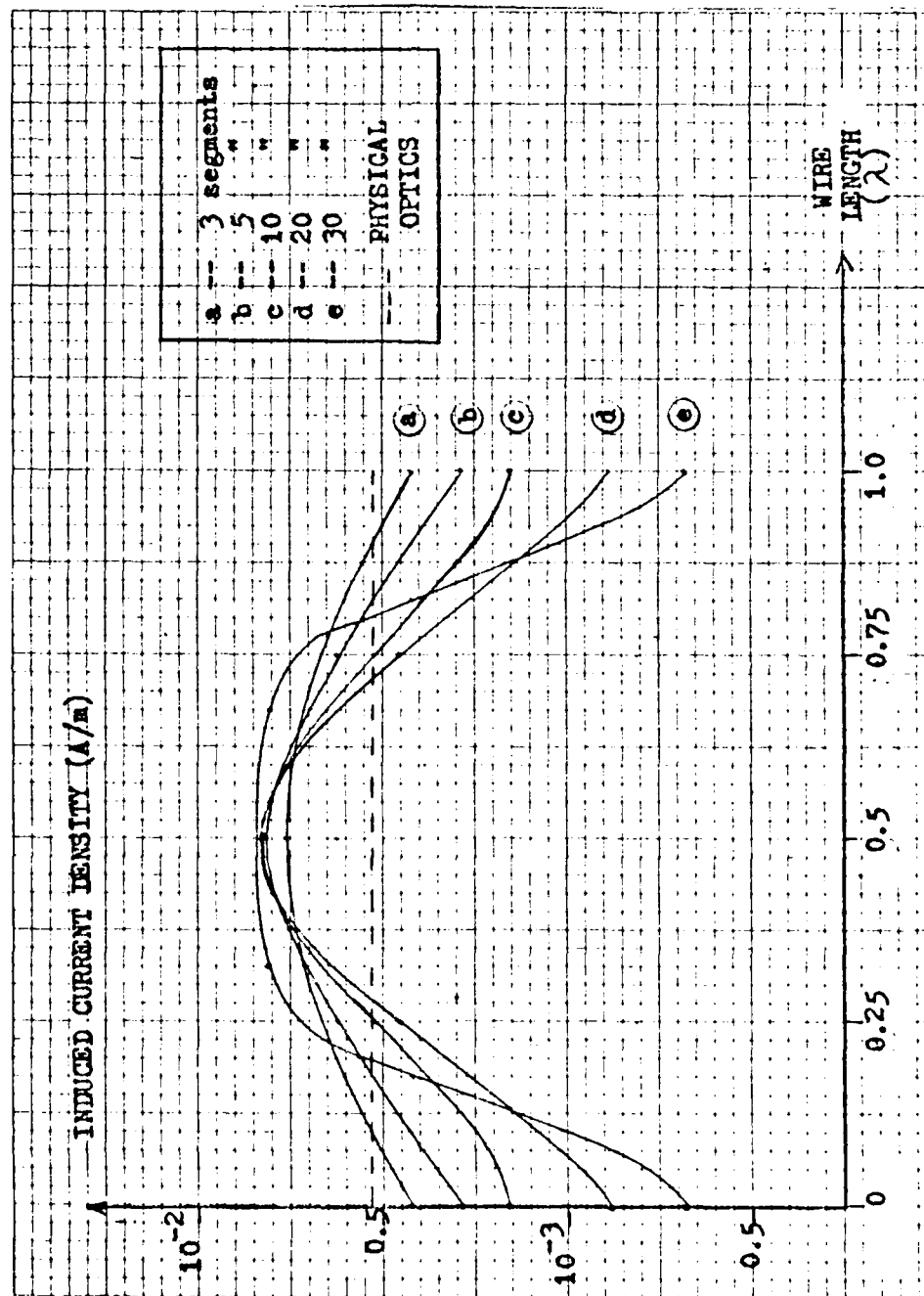


Figure 15. Current on a vertical cut of a  $1\lambda^2$  array with various wire segment divisions for a normally incident plane wave.

wire, the region of interest is the relatively uniform center region. Because increasing the number of segments/wavelength beyond five contributes little additional information, it can be concluded that five segments/wavelength is sufficient to obtain reasonably accurate results.

### 3.3 Wire Length

Figures 16 and 17 present the horizontal and vertical current distributions on a  $1\lambda$  wide array for four values of wire lengths. The purpose of this section is to determine if the moment method will reflect the expected changes along the wire length.

Results for the horizontal cut are reasonable. All four curves are symmetrical with respect to the center wire, and tend to flatten out as the wire length is increased. This is reasonable, since as the array size is increased, one would expect the edges to have less of a distorting effect upon the center region, thus allowing the current to become more uniform. The decreasing trend is explained by considering the vertical cut, Figure 17.

Currents on the vertical cut also change appropriately as the wire length is increased. Figure 17 indicates a trend to form two main lobes (d) as the length is increased to  $2.0\lambda$ , which seems quite acceptable. As these two lobes are formed, the center segment (#10) value must be decreased accordingly; this in turn causes the decrease in the horizontal cut, Figure 16. Therefore, the primary effect of increasing the wire length is to cause the appropriate number of lobes to form along the length of the wire, and to cause the horizontal current to shift accordingly. Note that the physical optics approximation reflects no change in either cut as the wire length is increased.

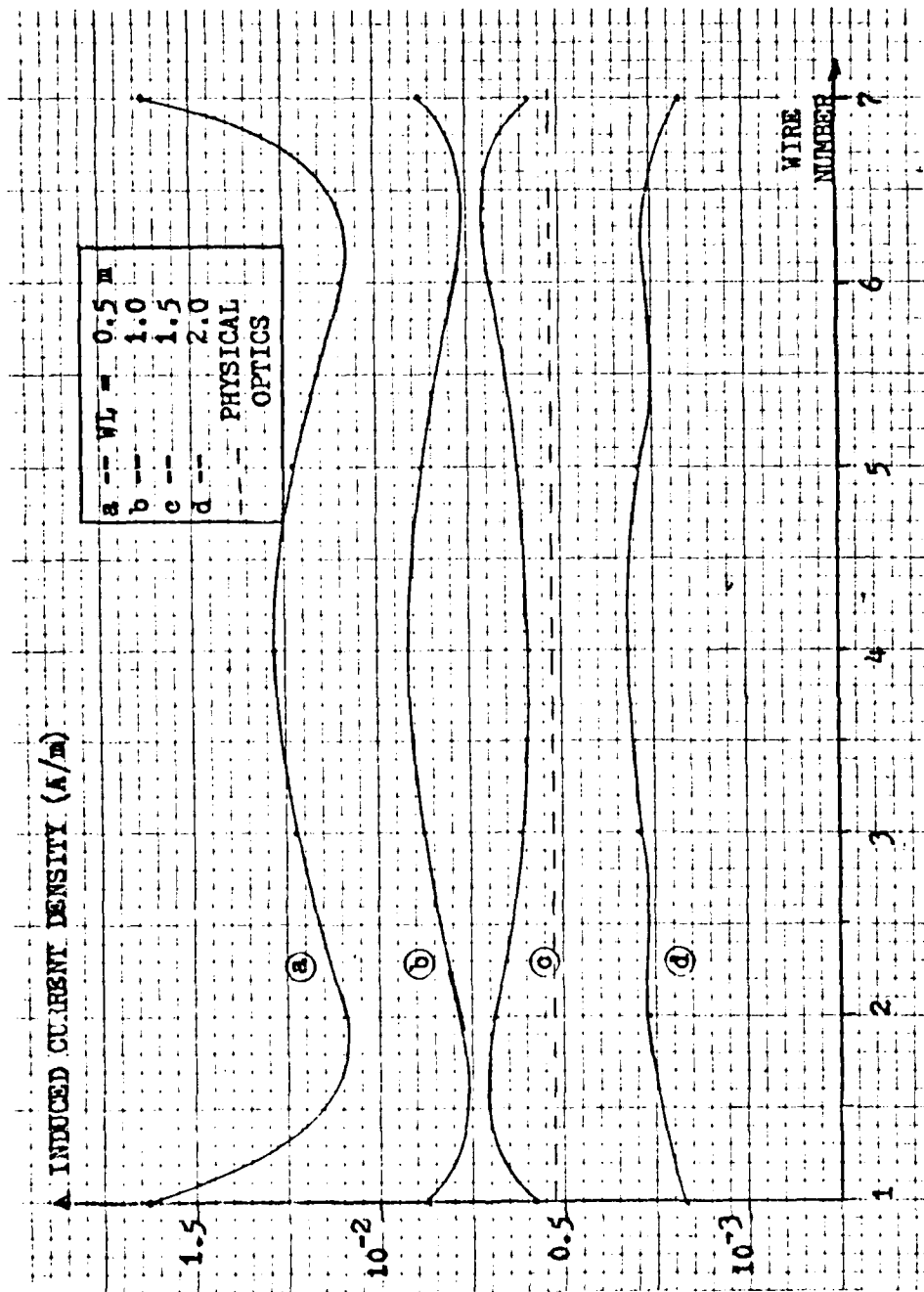


Figure 16. Current on a horizontal cut of a  $1\lambda$  wide array with various wire lengths for a normally wide plane wave.



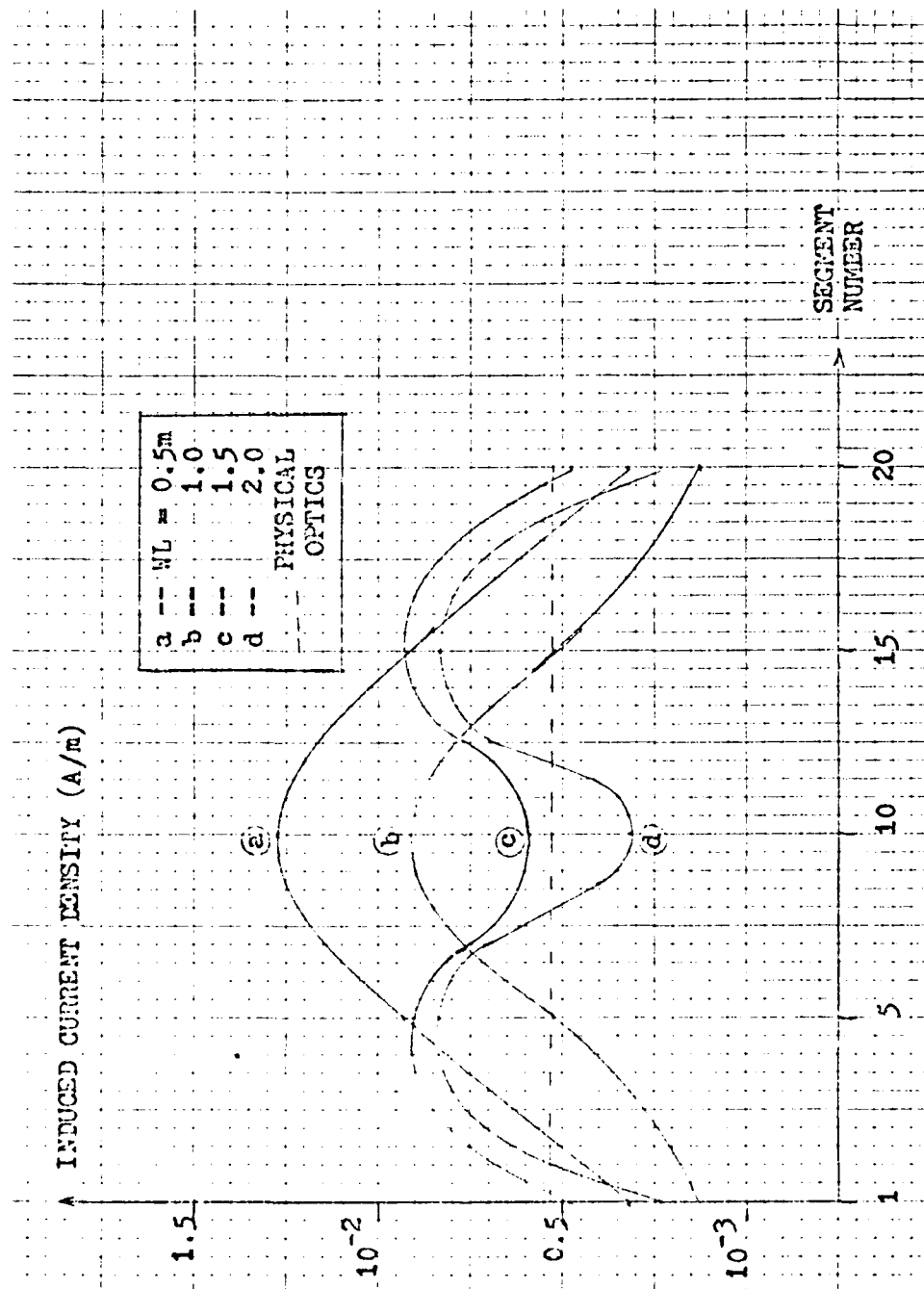


Figure 17. Current on a vertical cut of a  $1\lambda$  wide array with various wire lengths for a normally incident plane wave.

### 3.4 Varying Incidence Angle Effects

The horizontal and vertical current distributions are determined for different sized arrays when the plane wave incidence angles ( $\theta$ ,  $\phi$ ) are varied along their major axis, i.e., when  $\theta$  is varied and  $\phi=0$ , and when  $\phi$  is varied and when  $\theta=\pi/2$ . Phase plots of each are also included in this section, since there will be phase variations in both cuts.

The first array considered is  $1\lambda^2$ , using 26 wires of five segments each. Results for this example are presented in Figures 18 through 23. For  $\theta$  variations, Figures 18 and 20 present the horizontal and vertical currents, respectively. Physically, one would expect little change in shape for the horizontal cut as  $\theta$  is varied, since all segments will still lie on the same phase front for all  $\theta$ 's. This is exactly what is shown by Figure 18. For this and all other examples, the physical optics approximation of the current and phase is calculated by:

$$\text{with } \vec{E}^i = (\sin\theta)E_o \hat{z} e^{j\beta((\sin\theta\cos\phi)x + (\sin\theta\sin\phi)y + (\cos\theta)z)} \quad (64)$$

$$\text{then } |\vec{J}_s| = \frac{2E_o(\sin\theta)(\cos\phi)}{376.7} \quad (65)$$

$$\text{and } \vec{J}_s = \frac{2\pi}{\lambda} (x\sin\theta\cos\phi + y\sin\theta\sin\phi + z\cos\theta) \quad (66)$$

For each  $\theta$ , the physical optics approximation is of correct order of magnitude, but does not represent the distortion of the current near the edges.

The currents for the  $\phi$  variations, Figures 19 and 21, are also in agreement with expected results. The horizontal current is symmetric at normal incidence, and varies as  $\phi$  is varied. Note that the physical optics approximation shows only a shift in magnitude, which does not

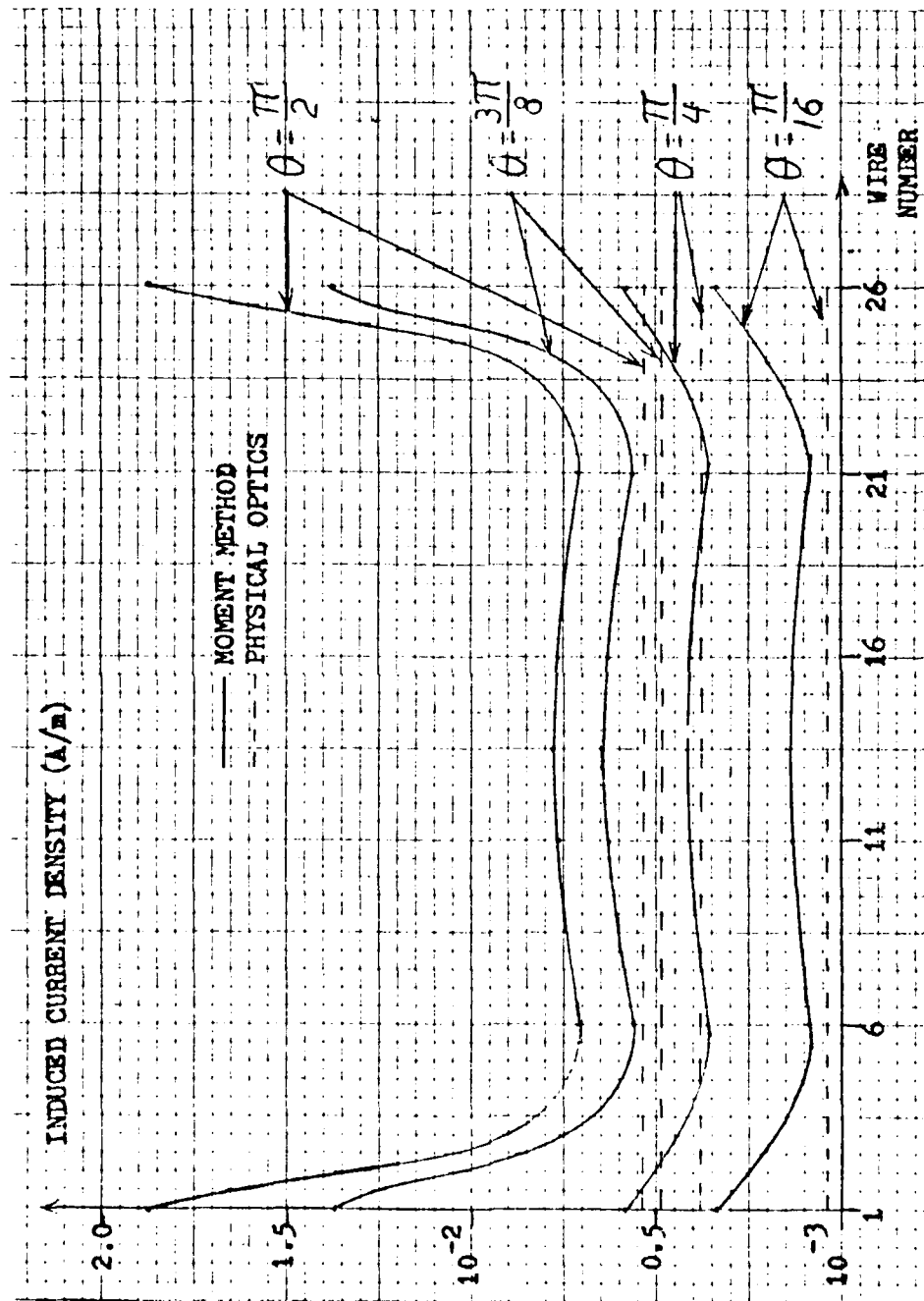


Figure 18. Current on a horizontal cut of a 26 wire, 5 segment array for  $\theta$  varying,  $\phi = 0$ .

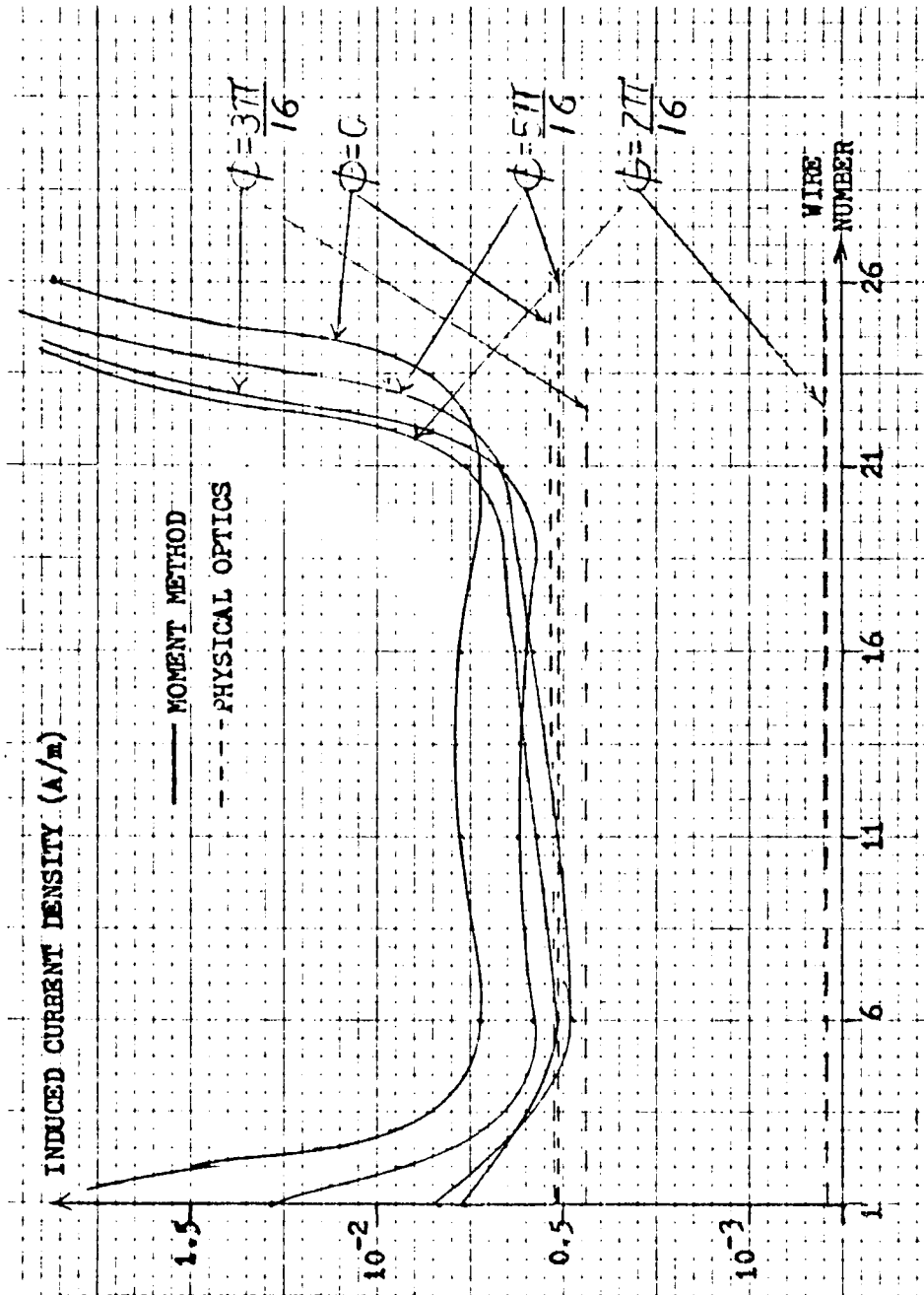


Figure 19. Current on a horizontal cut of a 26 wire, 5 segment array for  $\phi$  varying,  $\theta = \pi/2$ .

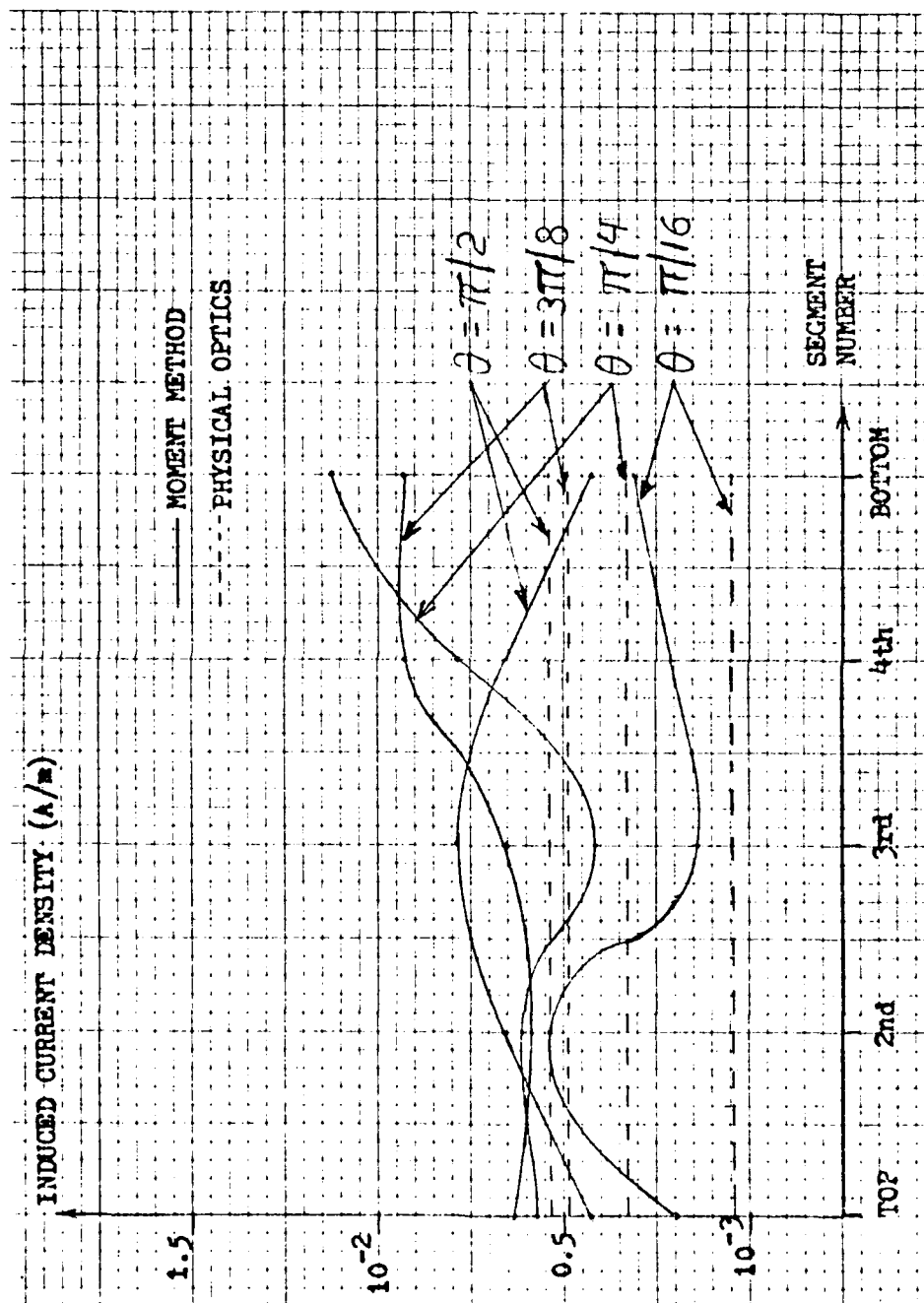


Figure 20. Current on a vertical cut of a 26 wire, 5 segment array for  $\theta$  varying,  $\phi = 0$ .

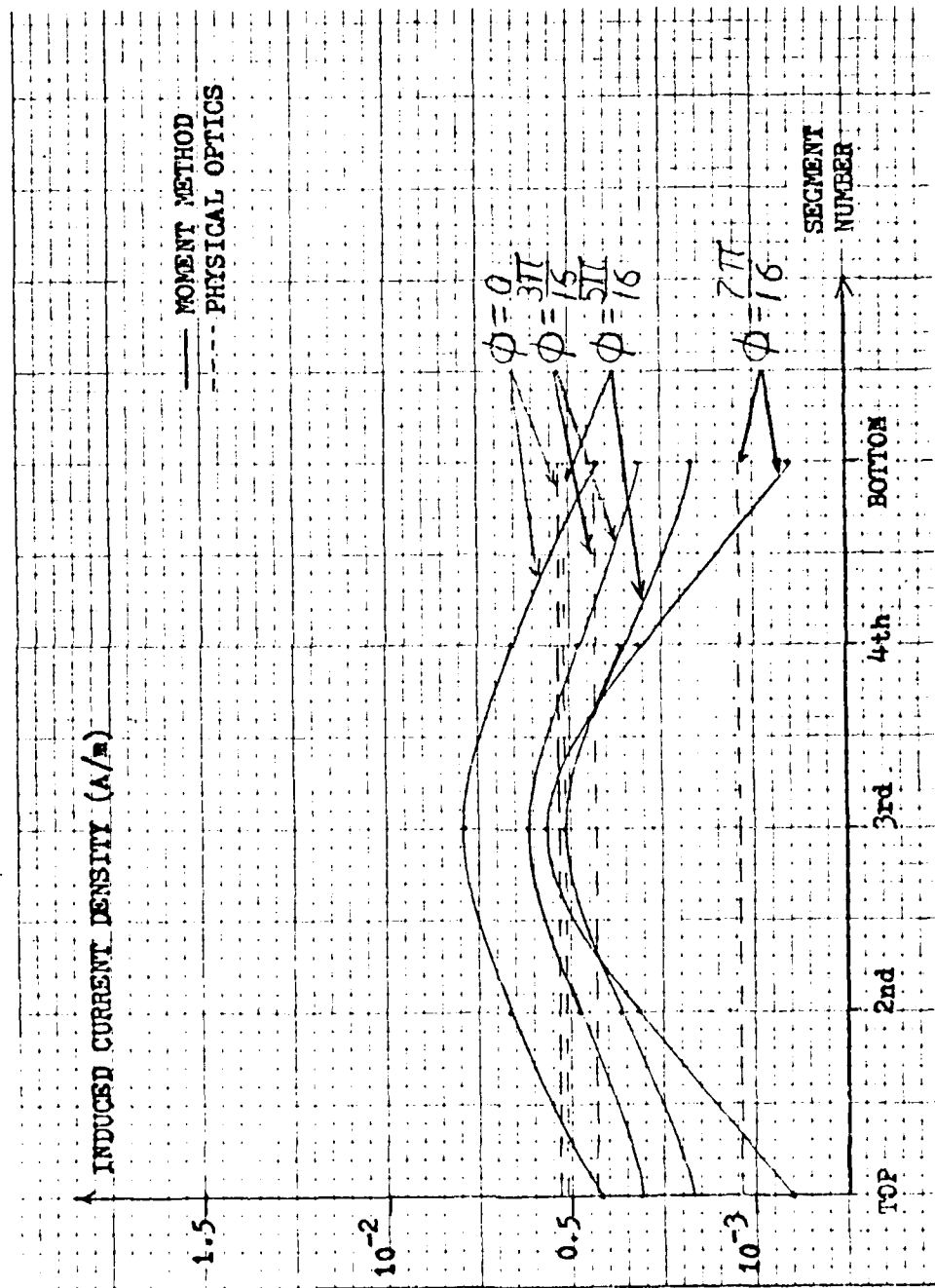


Figure 21. Current on a vertical cut of a 26 wire, 5 segment array for  $\phi$  varying,  $\theta = \pi/2$ .

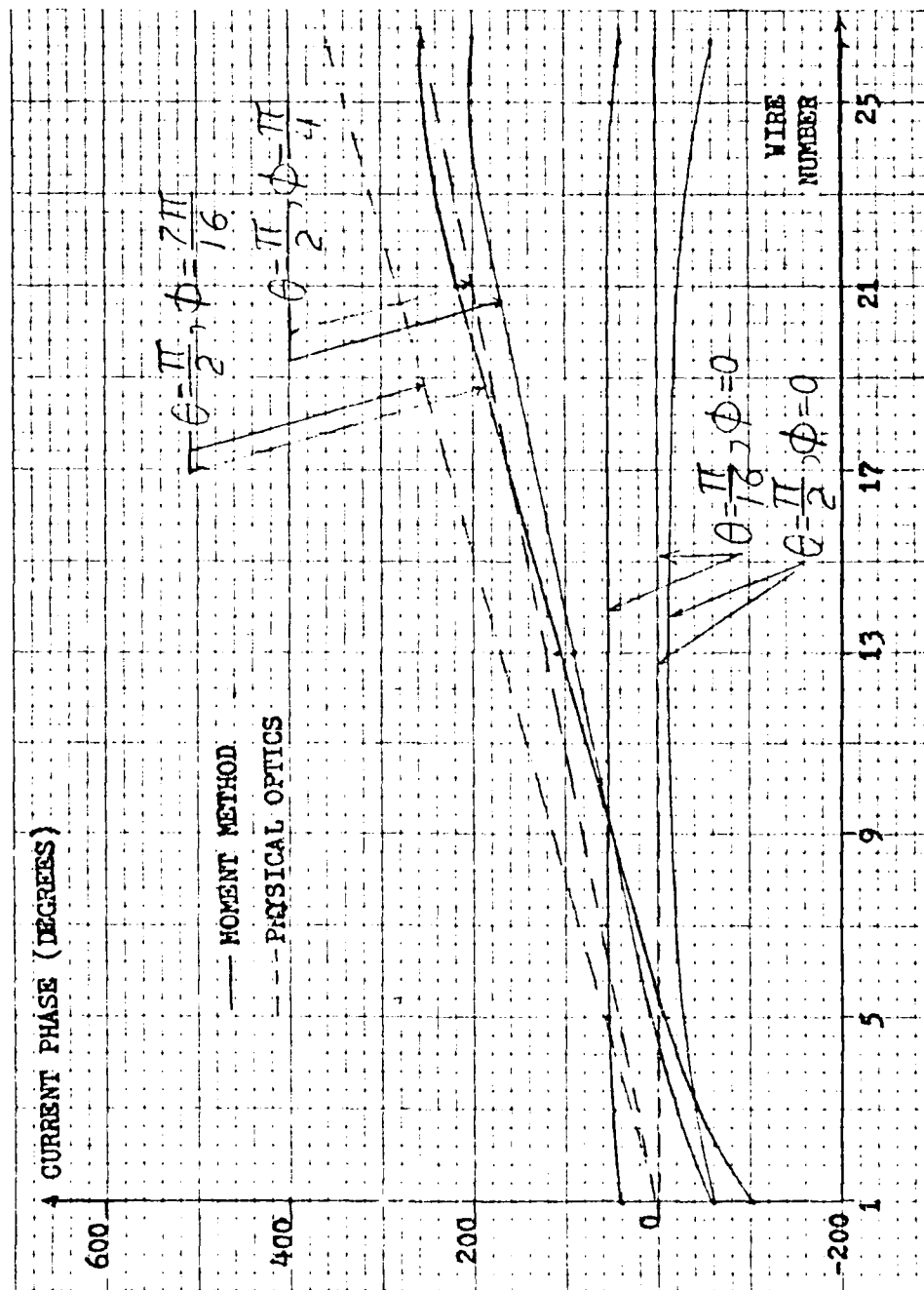


Figure 22. Horizontal cut of current phase on a 26 wire, 5 segment array for various incidence angles.

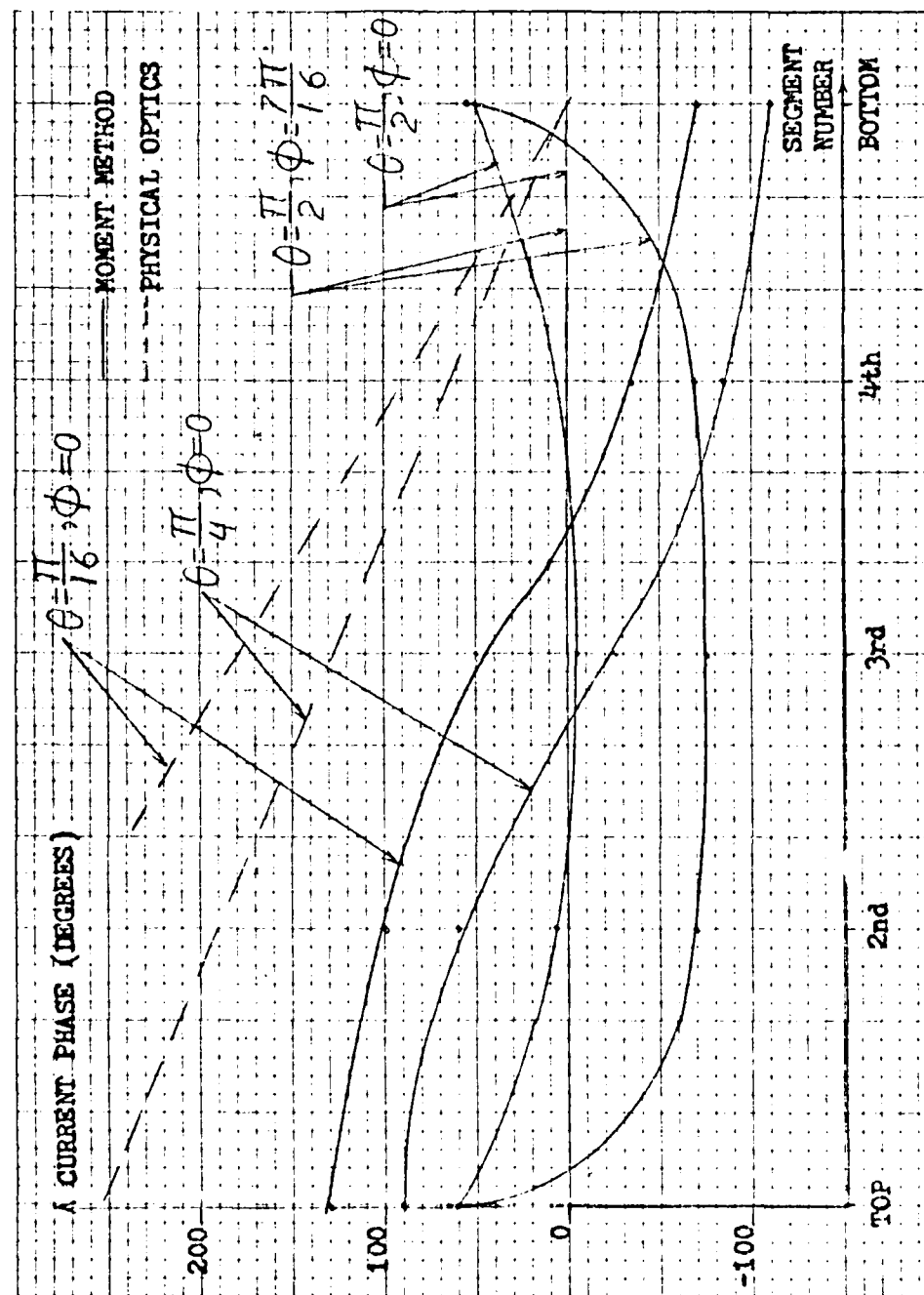


Figure 23. Vertical cut of current phase on a 26 wire, 5 segment array for various incidence angles.



seem to agree with actual physical behavior. The vertical cut of the current, Figure 21, however, is symmetric for each case. This is entirely reasonable, since a change in the  $\phi$  component of the incident plane wave would not be expected to affect the shape of the current in the  $\theta$  direction. There is only a shift in magnitude, which is probably caused by the change in the horizontal current.

The phase relationships for both cuts are shown in Figure 23 and 24. As expected, the phase in the horizontal cut is dependent upon  $\phi$ , but independent of  $\theta$ . The physical optics approximation predicts a linear phase change for each  $\phi$  as shown, which is calculated from Eq (64). The moment method technique also indicates a similar linear change, with a slight distortion near the edges as shown. The vertical cut of the phase, Figure 23, is also reasonable. As expected, there is no change in phase for  $\phi$  variations, only  $\theta$  variations. The physical optics approximation predicts a linear change, as shown. The moment method results show a similar, but not exactly linear variation, which may be caused by reflections from the ends of the wire, which will tend to induce a "standing wave" on the wire as  $\theta$  is decreased.

A second case was also studied to investigate current behavior on an array for various incidence angles. Its dimensions were chosen as  $1\lambda$  wide by  $2\lambda$  long (13 wires of 10 segments each) to determine the currents, especially in the vertical cut. Since the previous example has already established that the horizontal currents are independent of  $\theta$ , and the vertical currents are independent of  $\phi$ , these graphs are omitted.

The horizontal cut, Figure 24, indicates a definite change in the distribution as  $\phi$  is changed, as expected. Again note that the

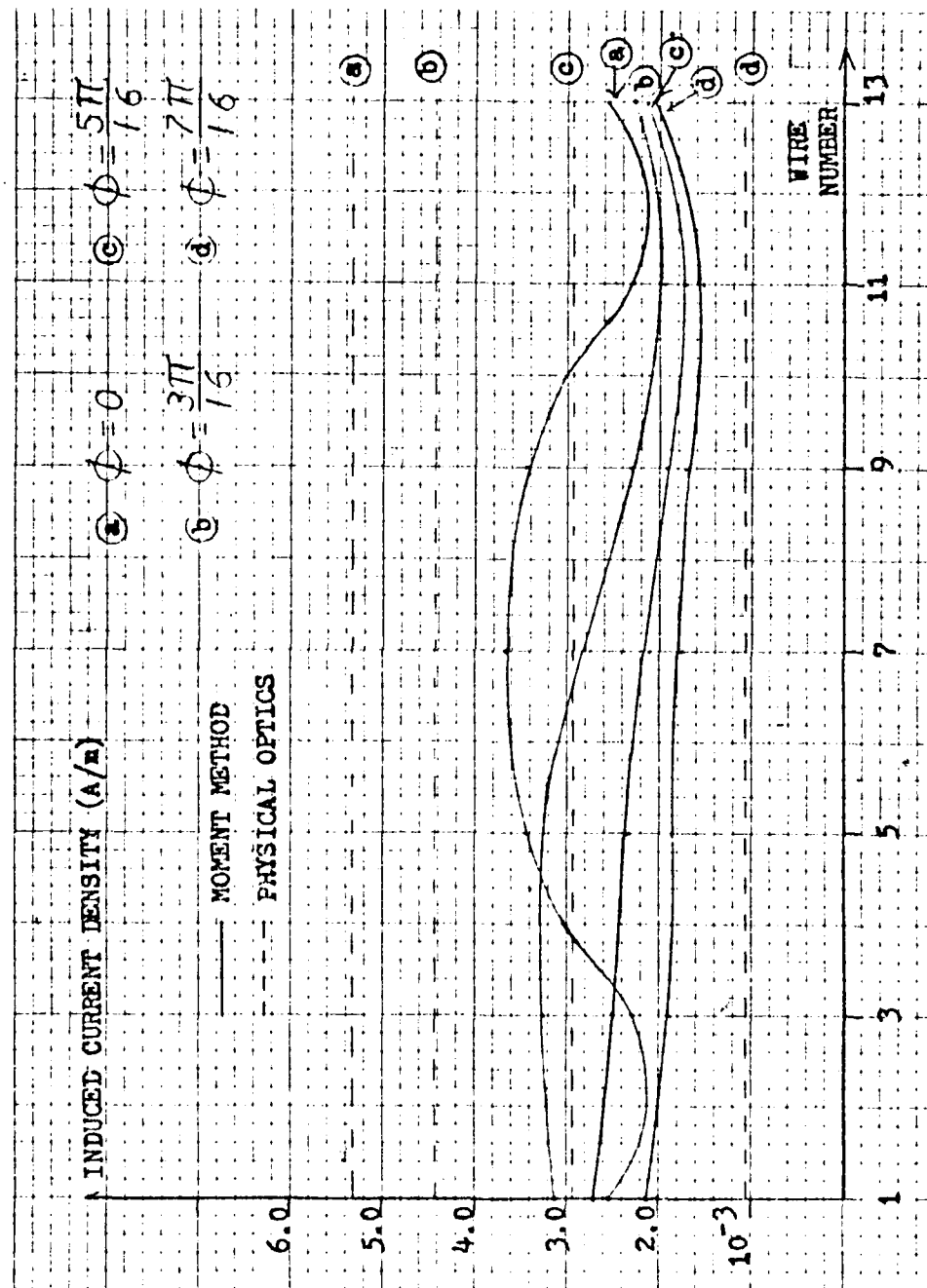


Figure 24. Current on a horizontal cut of a 13 wire, 10 segment ( $2\lambda$  long) array for  $\phi$  varying,  $\theta = \pi/2$ .

physical optics approximation reflects no change in shape, only a shift in magnitude. Also of interest is the fact that the relative changes in the horizontal cut for the moment method results are less than the corresponding results for the previous example (see Figure 19). Again, this is an indication that the center region becomes more "isolated" from current variations as the size of the array is increased.

The vertical cut for  $\theta$  variations, Figure 25, is also reasonable. The current for normal incidence illumination is symmetric, and has the two-lobed structure, as expected for a  $2\lambda$  long wire. As  $\theta$  is varied, the current becomes asymmetric, and in fact resembles a standing wave pattern. The physical optics approximation shows no change in shape for different  $\theta$ 's, only a shift in magnitude.

The phase relationships for this example are shown in Figures 26 and 27. The horizontal cut of the phase agrees well with physically expected behavior. For changes in  $\theta$ , there is no change in general shape, only a shift in magnitude, as expected. As  $\theta$  is decreased, the rate of phase change across the array tends to increase, indicating that the rate of phase change is proportional to the incidence angle. The vertical cut of the phase, Figure 27, shows similar agreement. Changes in  $\phi$  have little effect on the vertical phase, except a small shift in magnitude, as expected. As the incidence angle increasingly deviates from normal, the rate of phase change increases proportionally. Note that the physical optics approximations predicts an exactly linear phase shift, whereas the moment method predicts the same general trend, but also includes minor variations and distortions near the edges/ends.

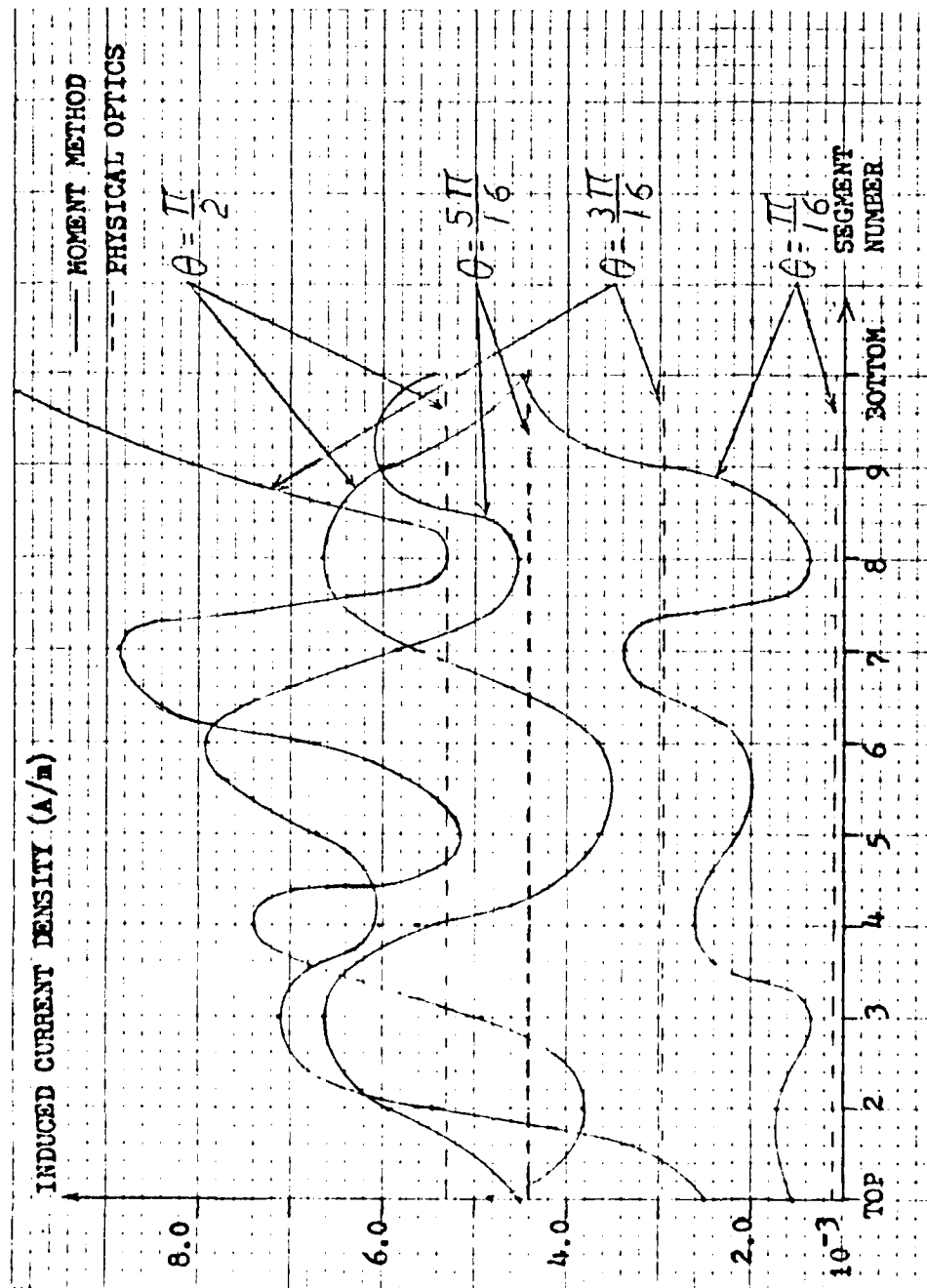


Figure 25. Current on a vertical cut of a 13 wire, 10 segment ( $2\lambda$  long) array for  $\theta$  varying,  $\phi = 0$ .

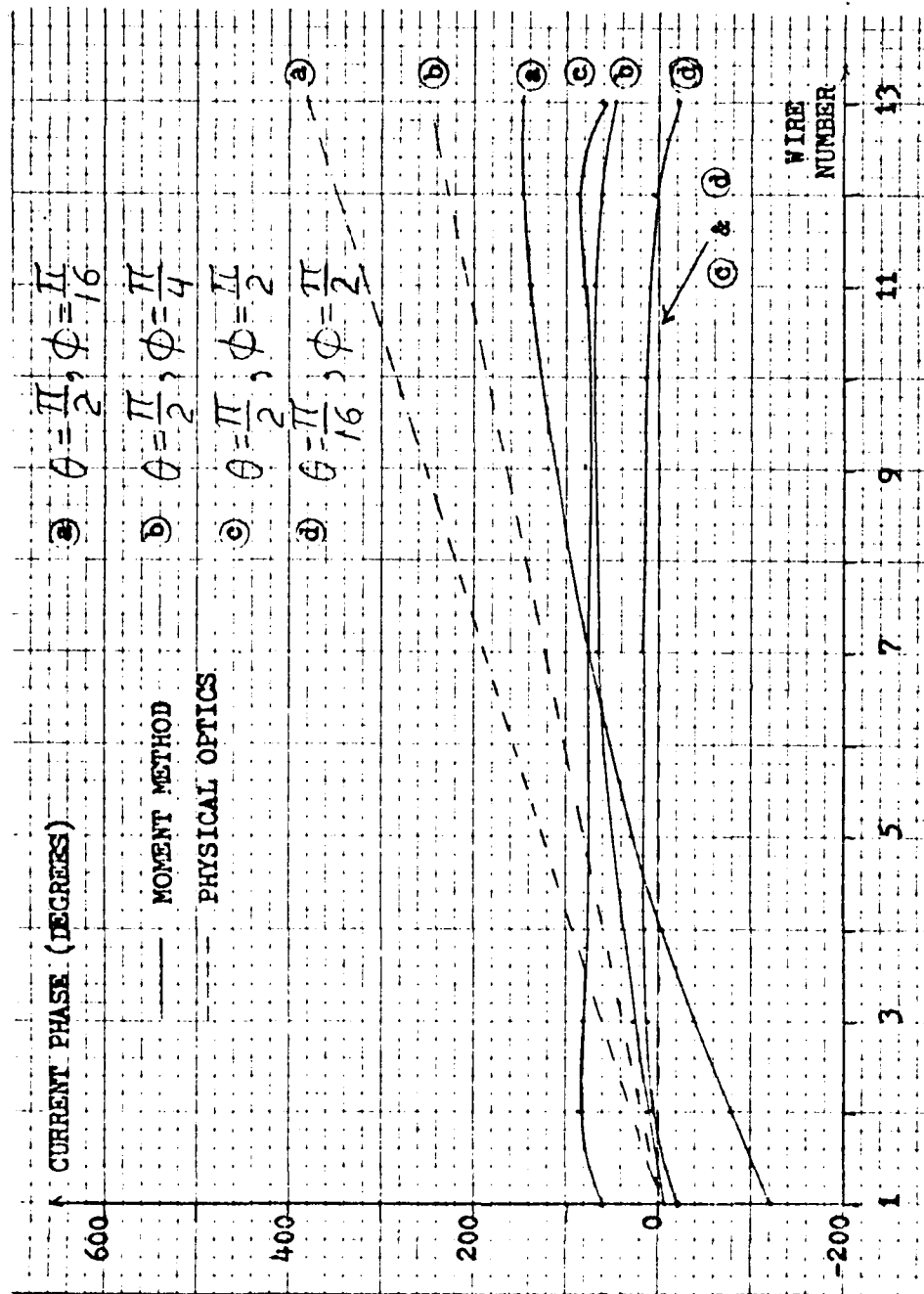


Figure 26. Horizontal cut of current phase one 13 wire, 10 segment ( $2\lambda$  long) array for various incidence angles.

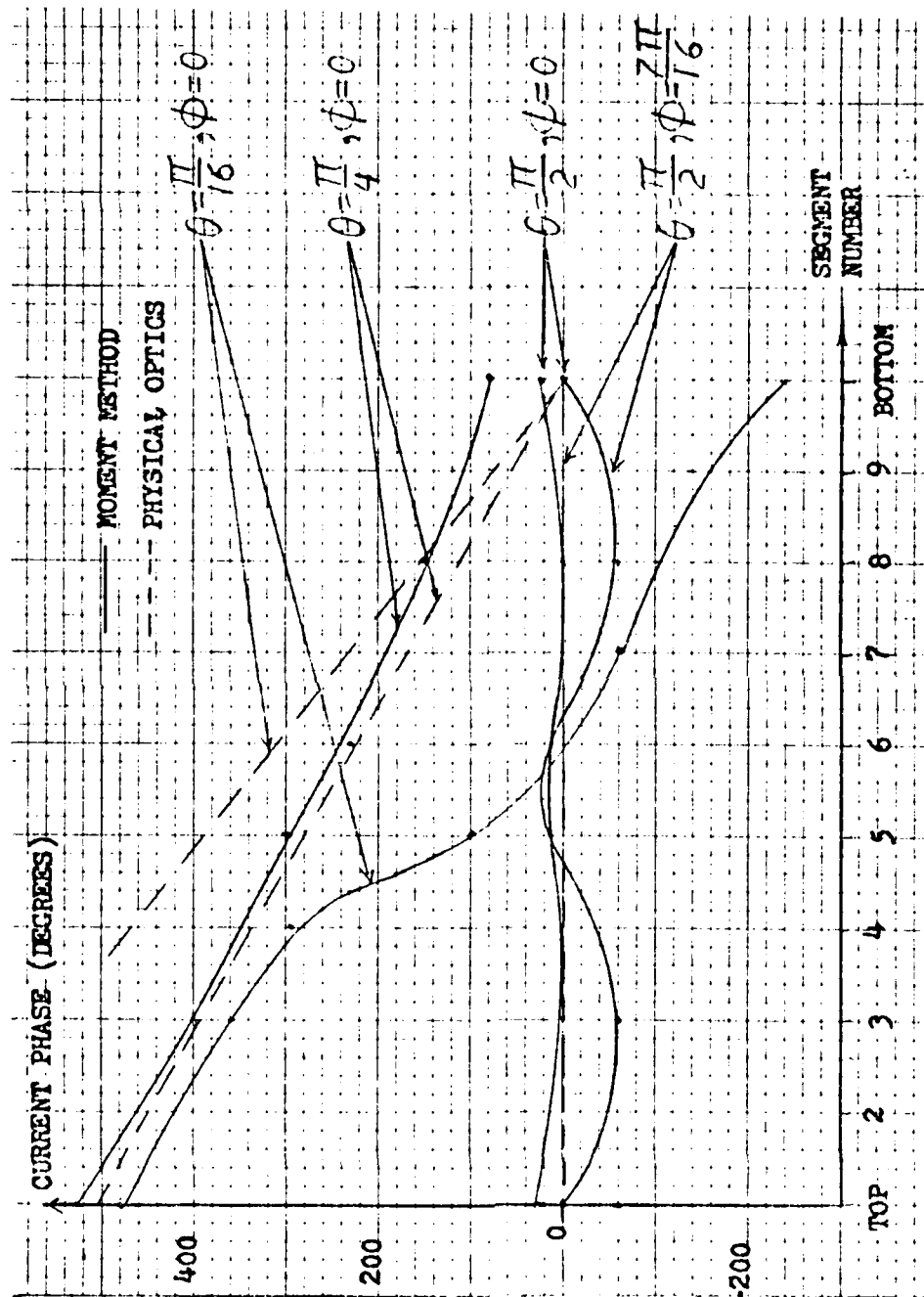


Figure 27. Vertical cut of current phase on a 13 wire, 10 segment ( $2\lambda$  long) array for various incidence angles.

### 3.5 Array $0.25\lambda$ Above a Ground Plane

The current magnitudes and phases for an 18 wire, 5 segment array  $0.25\lambda$  above a ground plane are presented in Figures 28 through 31. Again, because of the independence of  $\theta$  and horizontal currents and  $\phi$  and vertical currents, these graphs are omitted.

The horizontal cut with varying  $\phi$  is shown in Figure 28. As expected, the normal incidence case is flat and symmetric, with increasing changes as  $\phi$  is increased. The interesting point to consider is how these results differ from a same sized array not over a ground plane, as Figure 19. The physical optics approximation for the two situations (both over and not over a ground plane) are the same. This is because the array is being modelled as a completely reflecting ground plane itself, which in effect completely shields the actual ground plane behind it from the incident wave (at least for normal incidence--this is not true for all incidence angles, and this point will be elaborated upon subsequently). The moment method technique shows that the current in both situations have the same general magnitude, but that the current on the horizontal cut of the array above a ground plane increases at a greater rate across the array. This is reasonable, as one would expect the ground plane to reflect the incident wave back onto the array and increase the current density.

The vertical current cut, Figure 29, is also somewhat different than its free space counterpart, Figure 20. Again, the physical optics approximation is the same for both situations. The moment method results, on the other hand, are of the same general order of magnitude, but are different in shape for each situation. Here again, the moment

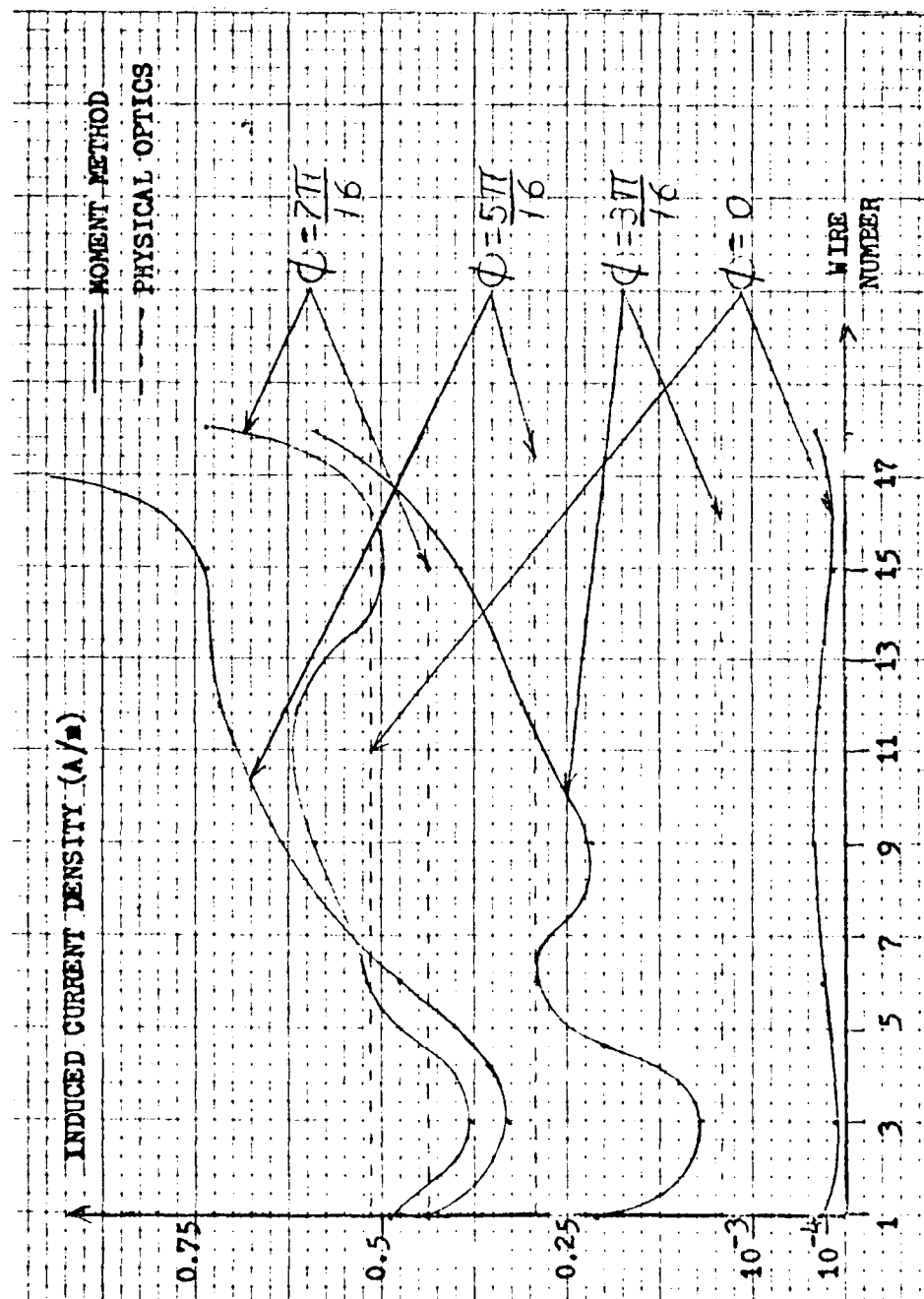


Figure 28. Horizontal cut of current density on an 18 wire, 5 segment array  $\frac{1}{2}\lambda$  above a ground plane for  $\phi$  varying,  $\theta = \pi/2$ .



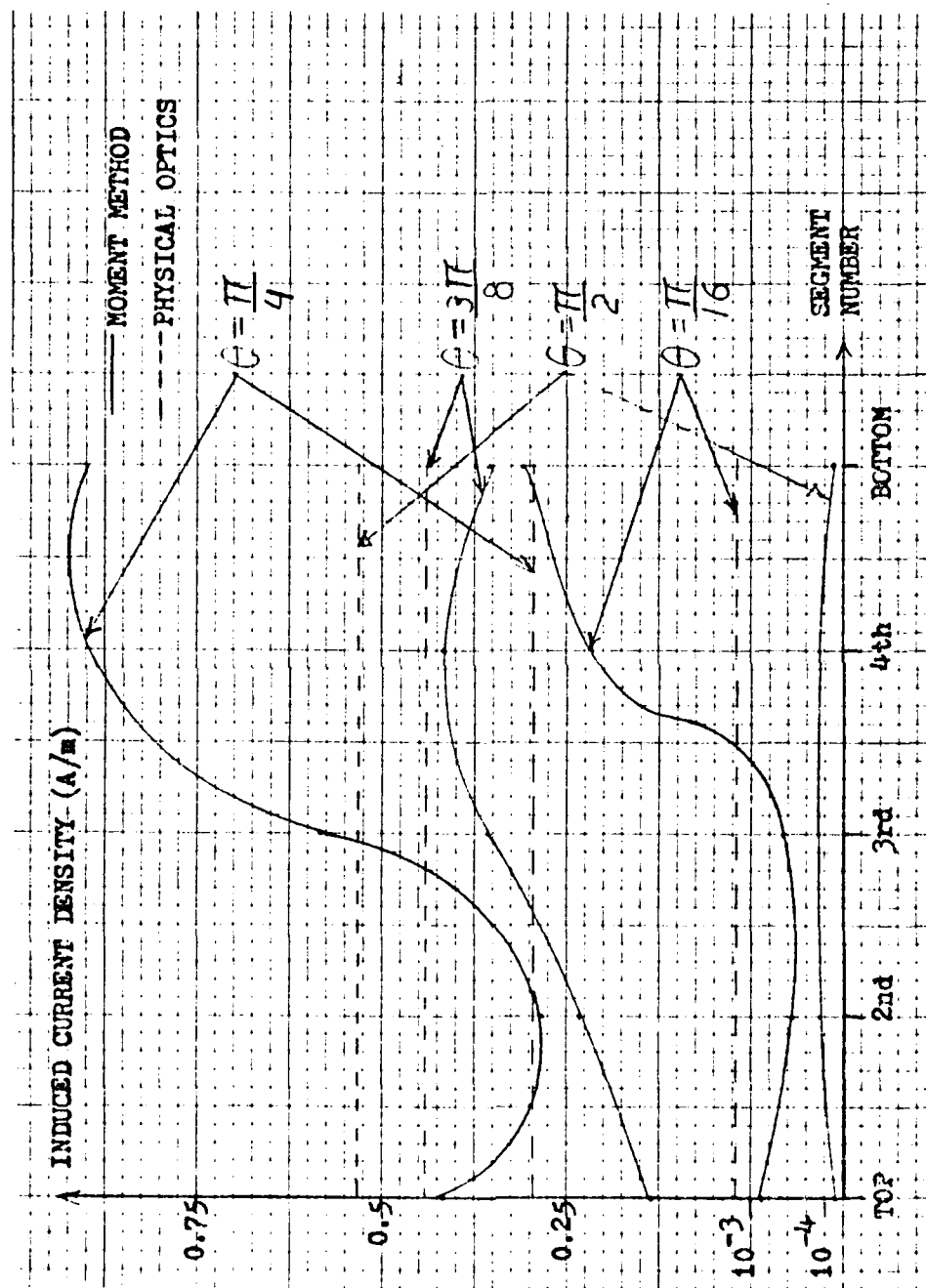


Figure 29. Vertical cut of current density on an 18 wire, 5 segment array  $\frac{1}{2}\lambda$  above a ground plane for  $\theta$  varying,  $\phi = 0$ .

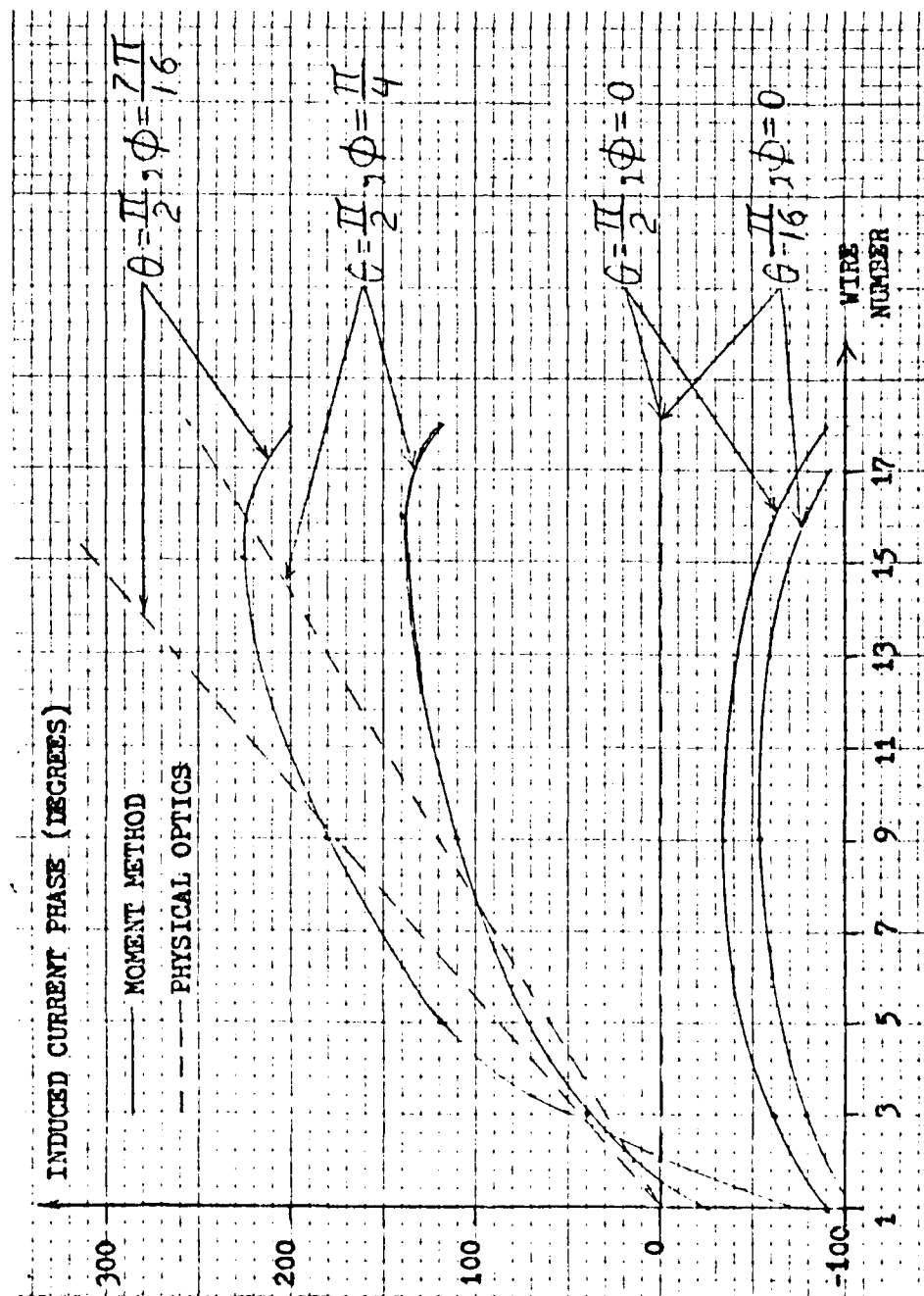


Figure 30. Horizontal cut of current phase on an 18 wire, 5 segment array  $\frac{1}{4}\lambda$  above a ground plane for various incidence angles.

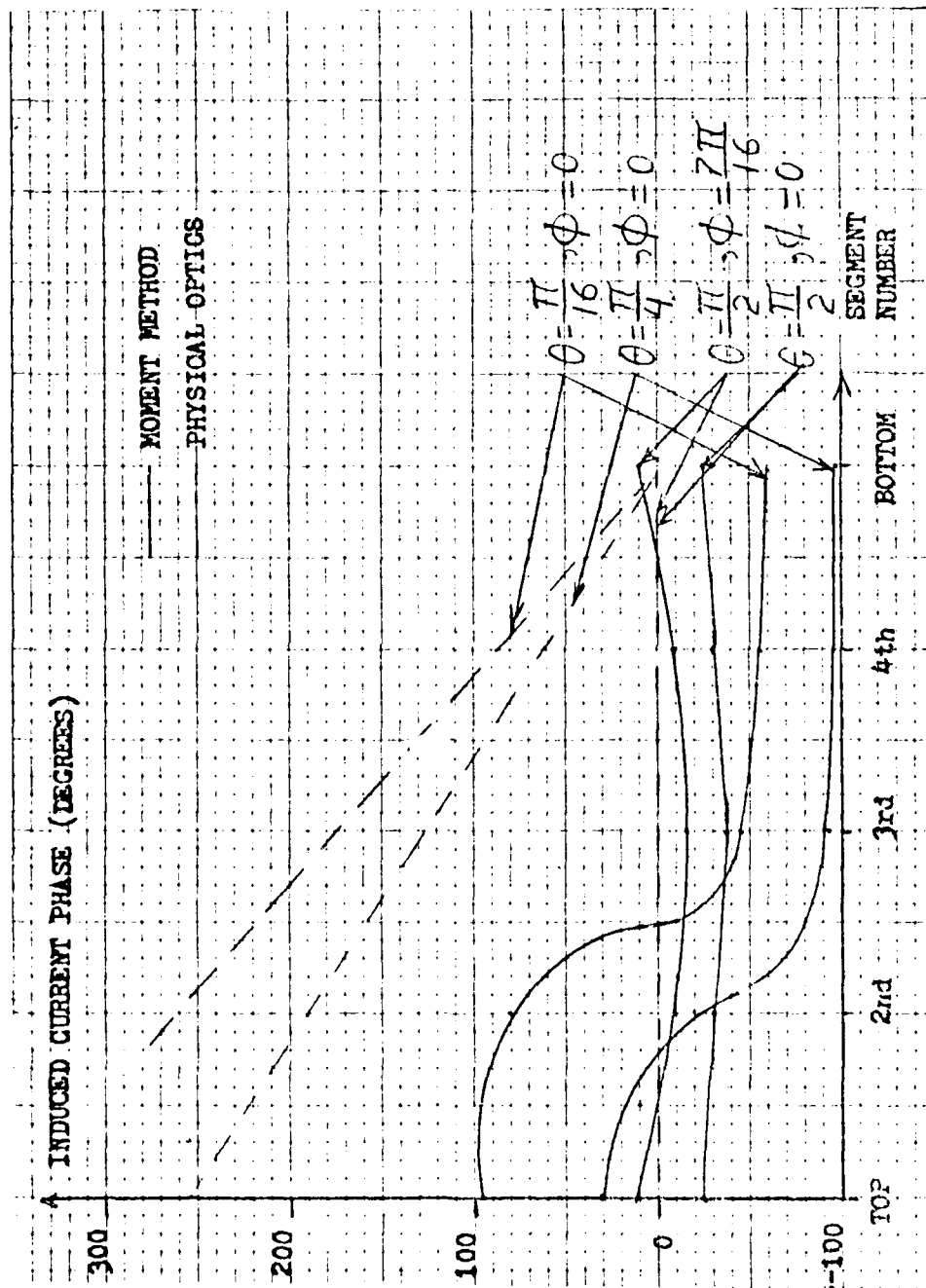


Figure 31. Vertical cut of current phase on an 18 wire, 5 segment array  $\frac{1}{2}\lambda$  above a ground plane for various incidence angles.

method results appear more accurate than the physical optics approximation, since different results would be expected for different situations.

Similar conclusions can be made concerning the horizontal and vertical phase relationships for both situations. The horizontal and vertical phases for the array over a ground plane (Figures 30 and 31) are expected to differ from the array in free space results (Figures 22 and 23). Again, there is no difference between each for the physical optics approximation. The moment method technique differ, as expected.

An important point of the geometry of the problem should be noted. As was previously stated, the physical optics approximation models the array as a conducting sheet, and therefore, the actual ground plane is completely shielded from the incident wave at normal incidence. At any oblique angle, however, part of the incident wave will pass by the edge of the array, and still illuminate the ground plane; this in turn may then be reflected back onto a different section of the array (see Figure 32). This effect is not accounted for in the results of the physical optics approximation as presented in the previous example. To properly account for this effect would drastically complicate the presently simple approximation, and would therefore defeat the whole purpose of using it. The moment method, on the other hand, has already taken this effect into account by virtue of Image Theory, with no additional modification or complexity.

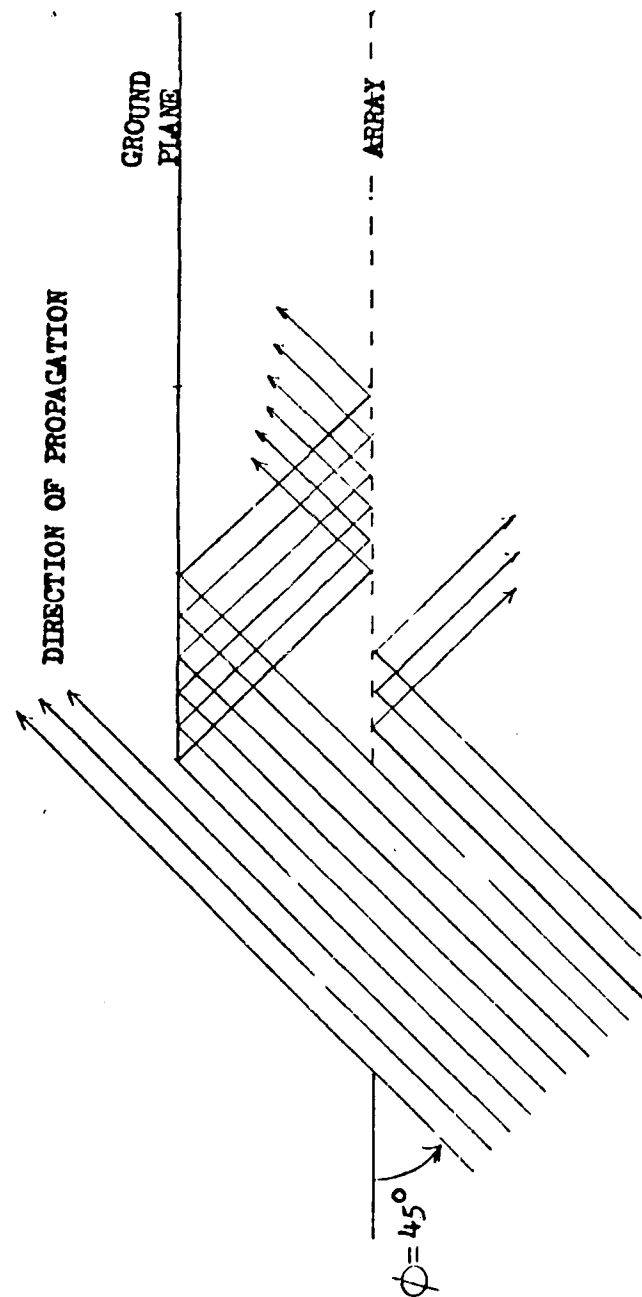


Figure 32. Top view of geometry illustrating reflection effects.

#### IV. Conclusions and Recommendations

##### 4.1 Conclusions

The objective of this thesis was to determine the induced currents on an array of wires both in free space and in front of a ground plane using the method of moments, and then to compare the results to those obtained by the modified physical optics approximation. The induced currents for the moment method were determined by developing a general algorithm (Appendix A). Results were obtained for a variety of different cases.

In general, moment method results agree well with expected physical behavior, but do not agree closely with the physical optics approximation for most cases. The moment method and physical optics approximations tend to agree in general magnitudes, but sometimes differ significantly with respect to the general shape of the current distribution. For example, consider an array illuminated by a normally incident plane wave. The physical optics approximation would indicate the current to be exactly uniform across the entire array; the moment method shows relative uniformity in the center region, with a perturbation near the edges. For this case, the moment method appears to be more accurate, since one would physically expect a deviation near the edge caused by the abrupt boundary change.

Also, the physical optics approximation shows no change in the shape of the distribution as the incidence angles are varied; it only reflects a change in magnitude. This does not appear to be physically realistic. It can be concluded that the physical optics approximation does not adequately represent "edge" effects. The physical optics

approximation also does not reflect the fact that the current must equal zero at the endpoints of each wire. It does, however, produce a reasonably close approximation to the current along the center region of the wires. From this, it can be generally concluded that the physical optics approximation may be useful for larger sized arrays, to obtain a "rough" idea of the current magnitude, but not useful to determine the shape of the distribution with any great degree of accuracy. Its greatest advantage is in its simplicity. For a large enough array, it provides a good idea of the current magnitude with minimal effort.

The moment method, on the other hand, requires considerably more effort (i.e., large matrix inversions), but appears to be far more accurate. The accuracy can be increased by increasing the number of wires and segments, but this cannot be done arbitrarily, since there will be an upper bound imposed by the available computer resources. However, reasonably accurate approximations of the currents are obtainable with a modest number of segments, as is evidenced by this thesis. Some other conclusions of the moment method technique are:

1. The accuracy of the solution tends to increase as the wire spacing is decreased, i.e., as more wires/wavelength are used. Reasonable results are obtainable for as few as five wires/wavelength, but as many as 30 will provide an obviously better result. The reader is cautioned that the wire spacing/diameter ratio may not be decreased too small, since doing so may invalidate the assumption that there is no circumferential current variation on the wires. Although this thesis made no definite determination of the lower limit of this ratio, good results

were obtained with a ratio as small as 5.55:1. The actual lower limit may in fact be substantially less than this value.

2. The accuracy of the solution will increase as the number of segments/wire increases. Although there is theoretically no upper limit, little additional accuracy is gained when the number of segments used is increased beyond 10/wavelength. However, very reasonable results are obtainable with as few as five segments/wavelength.

3. This moment method technique appears to adequately represent the various effects caused by changing the wire lengths and/or incidence angles of the illuminating plane wave. Results indicate that the current distribution develops a second lobe as expected when the wire length is increased to  $2.0\lambda$ . Also indicated was the independence of the horizontal current to changes in  $\theta$ , as well as the vertical current to changes in  $\phi$ . The moment method also indicates the distortion near the ends of the array, the trend toward zero current at the endpoints of the wire, and the different distributions of current for the array in free space as opposed to the array above a ground plane. The physical optics approximation reflects none of these.

Thus, the moment method works well in approximating the currents on arrays both in free space and near a ground plane. The physical optics approximation provides a very "rough" idea of the current magnitude at the center of the array, but does not reflect many of the important aspects of the shape of the distribution, especially near the edges/endpoints of the array. The physical optics approximation may be more useful for larger sized arrays, however, where the center region is more independent of "edge effects". For smaller arrays (on the order



of the ones in this thesis), however, the physical optics approximation does not provide a very accurate solution.

#### 4.2 Recommendations

Although very good results can be obtained with the values used in this thesis, even greater accuracy may be desired. To accomplish this, one may choose to incorporate a larger number of wires/wavelength. As previously stated, this may invalidate the assumption that there is no circumferential current variation on the wires. Therefore, a logical extension of this work could be to better determine the lower limit of the wire spacing/diameter ratio. Or, perhaps even better if possible, to exclude this assumption entirely and rework the theory to account for a possible circumferential current variation.

Secondly, the major disadvantage of the moment method is the large, time-consuming matrix inversion required. A paper was recently published (July 1982) by Kastner and Mittra (Ref 9:673-679) describing a new spectral iteration technique which analyzes a similar problem with no large matrix inversions; instead, it employs a Fourier-series approach. Possible future study may include a detailed comparison of the two techniques.

### Bibliography

1. Richmond, J. H. "Digital Computer Solutions of the Rigorous Equations for Scattering Problems," Proceedings of the I.E.E.E., 53: 796-804 (8 August 1965).
2. Mei, K. K. "On the Integral Equations of Thin Wire Antennas," I.E.E.E. Transactions on Antennas and Propagation, AP-13: 374-378 (3 May 1965).
3. Richmond, J. H. "Scattering by an Arbitrary Array of Parallel Wires," I.E.E.E. Transactions on Microwave Theory & Techniques, 13: 408-412 (4 July 1965).
4. Wait, J. R. "Reflection at Arbitrary Incidence From a Parallel Wire Grid," Applied Scientific Research, 4: 393-400 (1955).
5. Michel, Yves, Pauchard, and P. Vidal. "Diffraction of a Plane Wave by a Finite Set of Cylindrical Conductors," 8th European Microwave Conference Proceedings, published by Microwave Exhibitions and Publishers, LTD., 1978.
6. Richmond, J. H. "A Wire Grid Model for Scattering by Conducting Bodies," I.E.E.E. Transactions on Antennas and Propagation, AP-14: 782-786 (6 November 1966).
7. \_\_\_\_\_. Computer Program For Thin Wire Structures in a Homogeneous Conducting Medium. Contractor Report for NASA, # CR-2399, June 1974.
8. Stutzman, Warren L. and Gary A. Thiele. Antenna Theory and Design. Canada: John Wiley and Sons, 1981.
9. Kastner, Raphael and Raj Mittra. "A Spectral-Iteration Technique For Analyzing a Corrugated-Surface Twist Polarizer for Scanning Reflector Antennas," I.E.E.E. Transactions on Antennas and Propagation, AP-30: 673-676 (4 July 1982).
10. Schelkunoff, S. A. and H. T. Friis. Antennas--Theory and Practice. New York: John Wiley and Sons, 1952.
11. Finlayson, B. A. The Method of Weighted Residuals and Variational Principles. New York: Academic Press, 1972.

## Appendix A: Computer Program

This appendix contains the computer program. Included below is a brief description of the general development and operation of this program.

### DEVELOPMENT

Before beginning, it should be noted that a program (for a single wire case) has already been written (Ref 8:568). This program, however, is significantly different; it allows for the more general case of wires located near a ground plane. The major difference between the two programs is that this program does not inherently assume that a (block) Toeplitz matrix will be obtained. It does not exploit the fact that a Toeplitz matrix is highly symmetric (and therefore more easily inverted); in fact, it assumes the most general case that the matrix is totally asymmetric.

The program actually solves Eq (43) using Eqs (59) and (63). In order to accomplish the matrix inversion, it calls upon the International Mathematics and Statistics Library (IMSL) functions DCADRE and LEQ2C. The IMSL is a set of subroutines which should be available at most computer installations. Some minor problems developed with the use of DCADRE, however, which are worth mentioning.

DCADRE is the IMSL subroutine to evaluate a real integral, given the integrand, the limits (finite), and the maximum allowable error, AERR. The problem occurred in trying to use DCADRE to evaluate the complex integral in Eq (59) and (63). The solution used was to break the complex integral into real and imaginary parts, evaluate each

separately, and then recombine into complex form. Also, because of the repetitious nature of the integrand, several common terms were extracted and made into function subprograms, as shown below.

$$\text{INTC} = \frac{-30}{\sin(\beta * \text{DZ})} \int_{Z_{q-1}}^{Z_q} \frac{\sin \beta (Z - Z_{q-1})}{\sin(\beta * \text{DZ})} [\text{BRCKT1}] dz \quad (\text{A-1a})$$

$$\text{INTD} = \frac{-30}{\sin(\beta * \text{DZ})} \int_{Z_q}^{Z_{q+1}} \frac{\sin \beta (Z_{q+1} - Z)}{\sin(\beta * \text{DZ})} [\text{BRCKT1}] dz \quad (\text{A-1b})$$

$$\text{INTE} = \frac{-30}{\sin(\beta * \text{DZ})} \int_{Z_{q-1}}^{Z_q} \frac{\sin \beta (Z - Z_{q-1})}{\sin(\beta * \text{DZ})} [\text{BRCKT2}] dz \quad (\text{A-1c})$$

$$\text{INTF} = \frac{-30}{\sin(\beta * \text{DZ})} \int_{Z_q}^{Z_{q+1}} \frac{\sin \beta (Z_{q+1} - Z)}{\sin(\beta * \text{DZ})} [\text{BRCKT2}] dz \quad (\text{A-1d})$$

such that

$$\text{Total Integral} = (\text{INTC} + \text{IND}) + j(\text{INTE} + \text{INTF}) \quad (\text{A-2})$$

where

$$\text{BRCKT1} = \left\{ \frac{\sin(\beta * R_{q-1})}{R_{q-1}} - \frac{2 \cos(\beta * \text{DZ}) \sin(\beta * R_q)}{R_q} + \frac{\sin(\beta * R_{q+1})}{R_{q+1}} \right\} \quad (\text{A-3a})$$

$$\text{BRCKT2} = \left\{ \frac{\cos(\beta R_{q'-1})}{R_{q'-1}} - \frac{2\cos(\beta DZ)\cos(\beta R_{q'})}{R_{q'}} + \frac{\cos(\beta R_{q'+1})}{R_{q'+1}} \right\} \quad (\text{A-3b})$$

and  $R_{q'-1}$ ,  $R_{q'}$ , and  $R_{q'+1}$  are evaluated by functions RBOT, RMID, and RTOP, respectively.

#### OPERATION

The program was written in FORTRAN V. It requires the use of IMSL subroutines DCADRE and LEQ2C. Because of the matrix manipulations, it requires a larger than average amount of memory and CPU time. Although the amount will vary depending upon the system used, the user should request approximately 256K words memory and 9000 seconds (150 min.) of CPU time for a 250 element array.

The user should specify N, M, WSY, etc., according to the input format statement. The output is dependent upon the four control parameters SWEEP, PV, PZ, and TYPE.

SWEEP must be an integer value 0 or 1. 0 indicates that only an incident plane wave of normal incidence ( $\text{THETA} = \pi/2$ ,  $\text{PHI} = 0$ ) will be evaluated. 1 indicates that the incidence angle will be varied in  $\pi/16$  increments along the THETA and PHI axis from 0 to  $\pi/2$ .

PV must be an integer value 0 or 1. 0 indicates that the voltage array  $V_{q'}(q)$  is not to be printed. 1 indicates print  $V_{q'}(q)$ .

PZ must be an integer value 0, 1, or 2. 0 indicates do not print impedance array  $Z_{qq'}$ . 1 indicates to print only the first row of

$Z_{qq}$  . 2 indicates to print entire  $Z_{qq}$  array. It is recommended that option 0 or 1 be used, since 2 can produce a tremendous amount of unnecessary output.

TYPE must be an integer value 0 or 1. 0 indicates that the free space case is to be studied, i.e., no ground plane. Here,  $Q=MN$  so the DIMENSION statement is MN in magnitude. 1 indicates the ground plane case. Here,  $Q=2MN$ , so each array in the DIMENSION statement should be accordingly doubled.

NOTE: WA and WK arrays in the DIMENSION statement are work areas for the IMSL subroutines. See any IMSL Operator's Guide for further details.

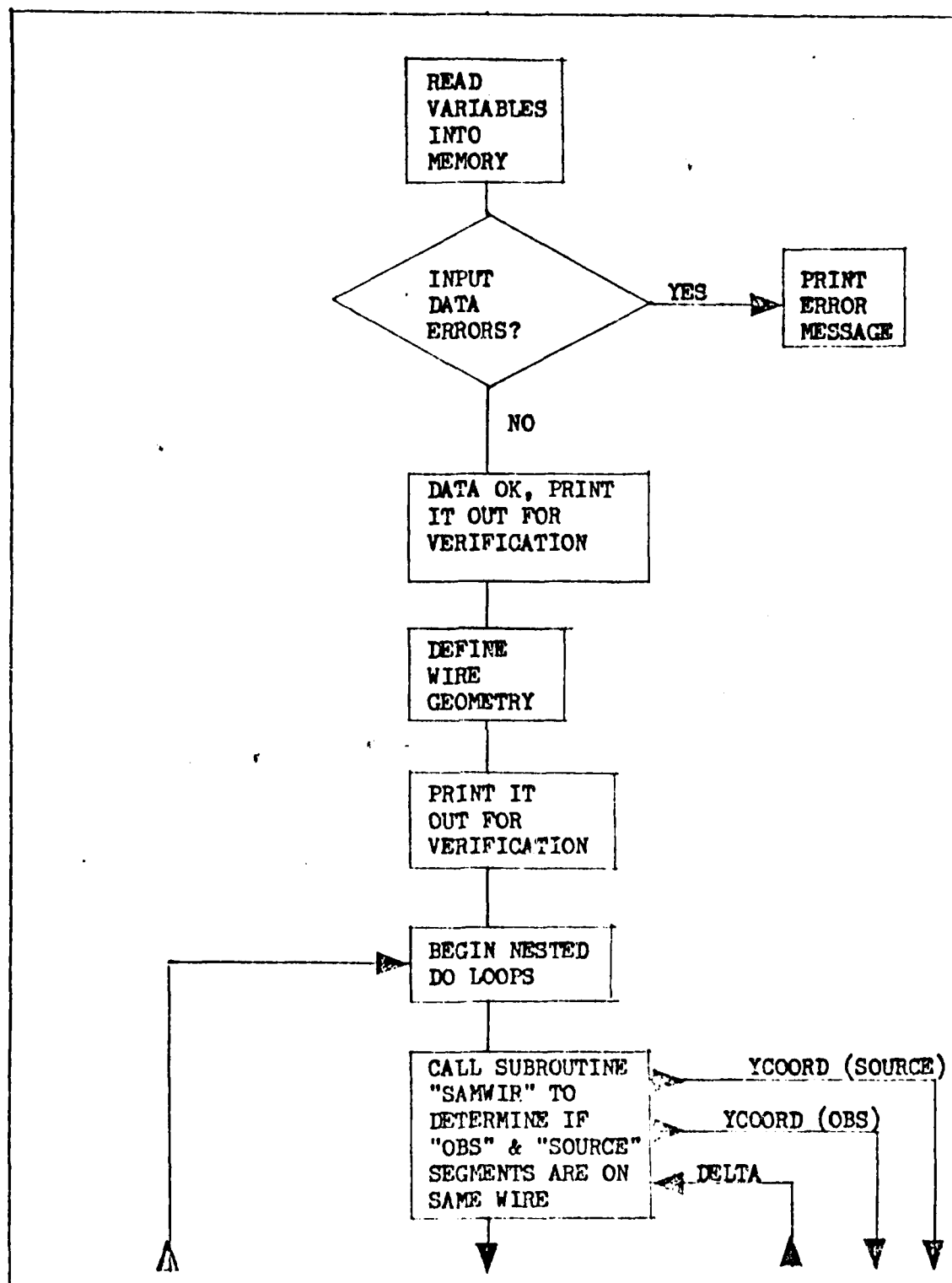


Figure A-1. Computer program flowchart.

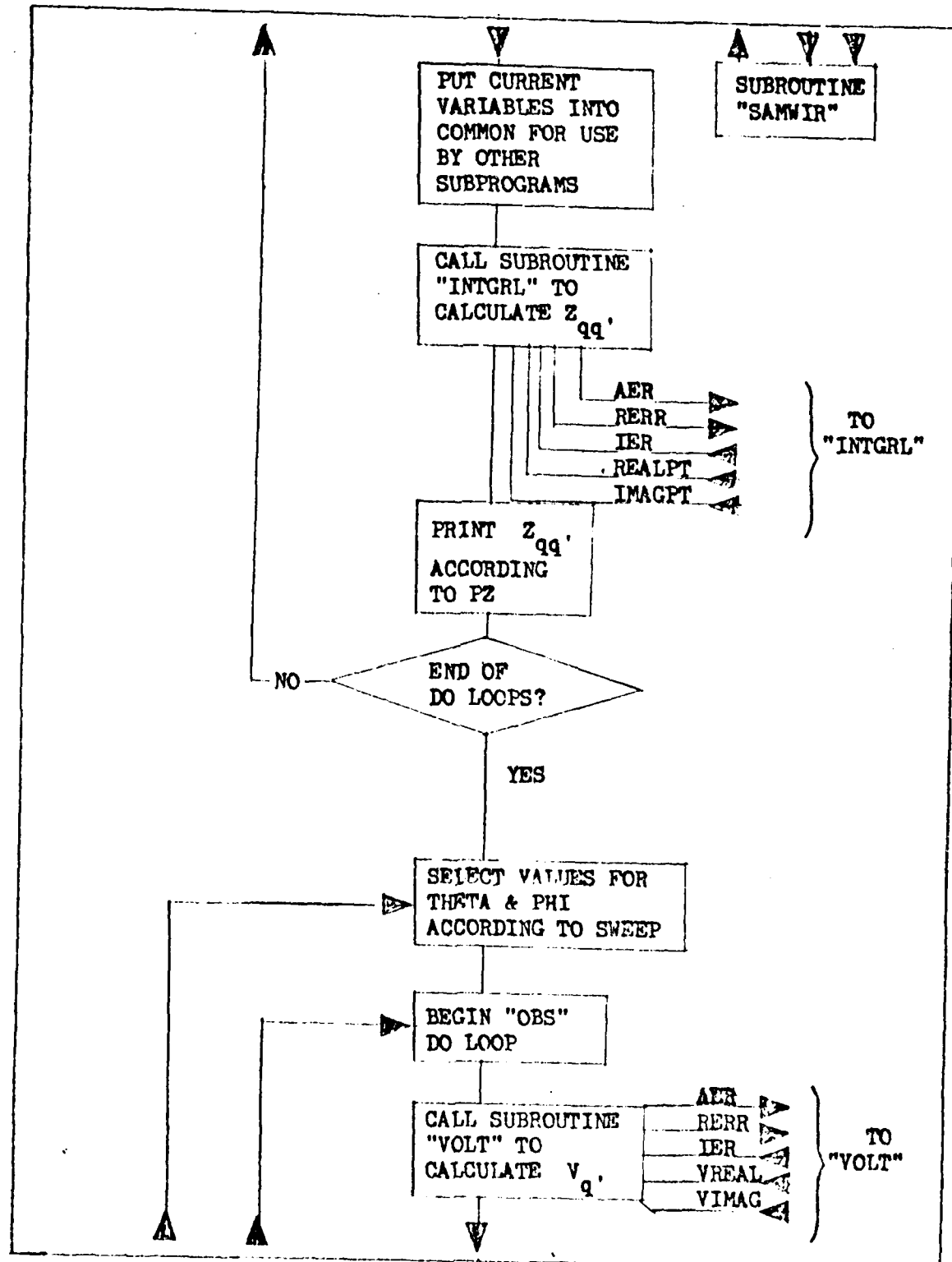


Figure A-1 (Continued)



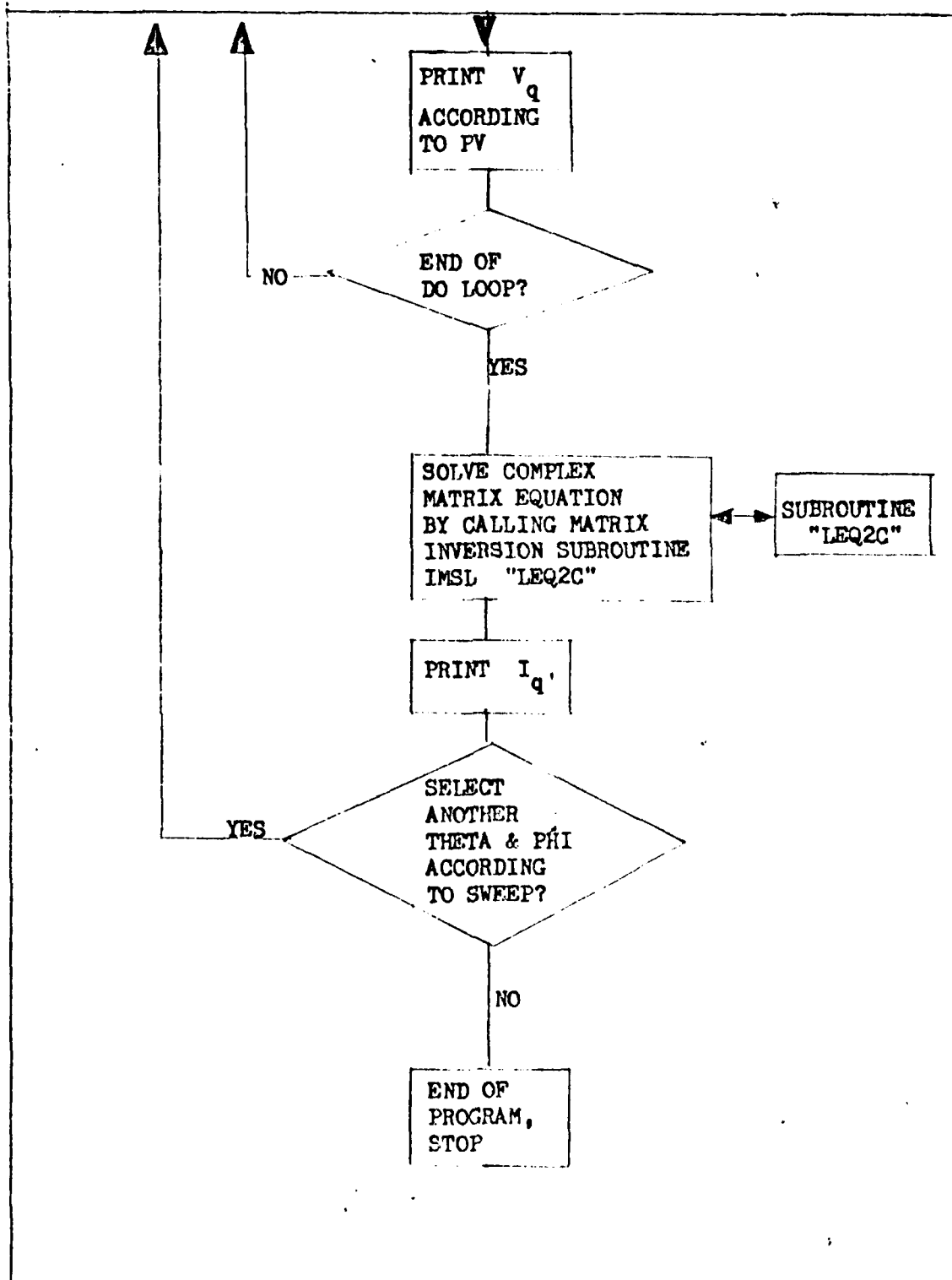


Figure A-1 (Continued)

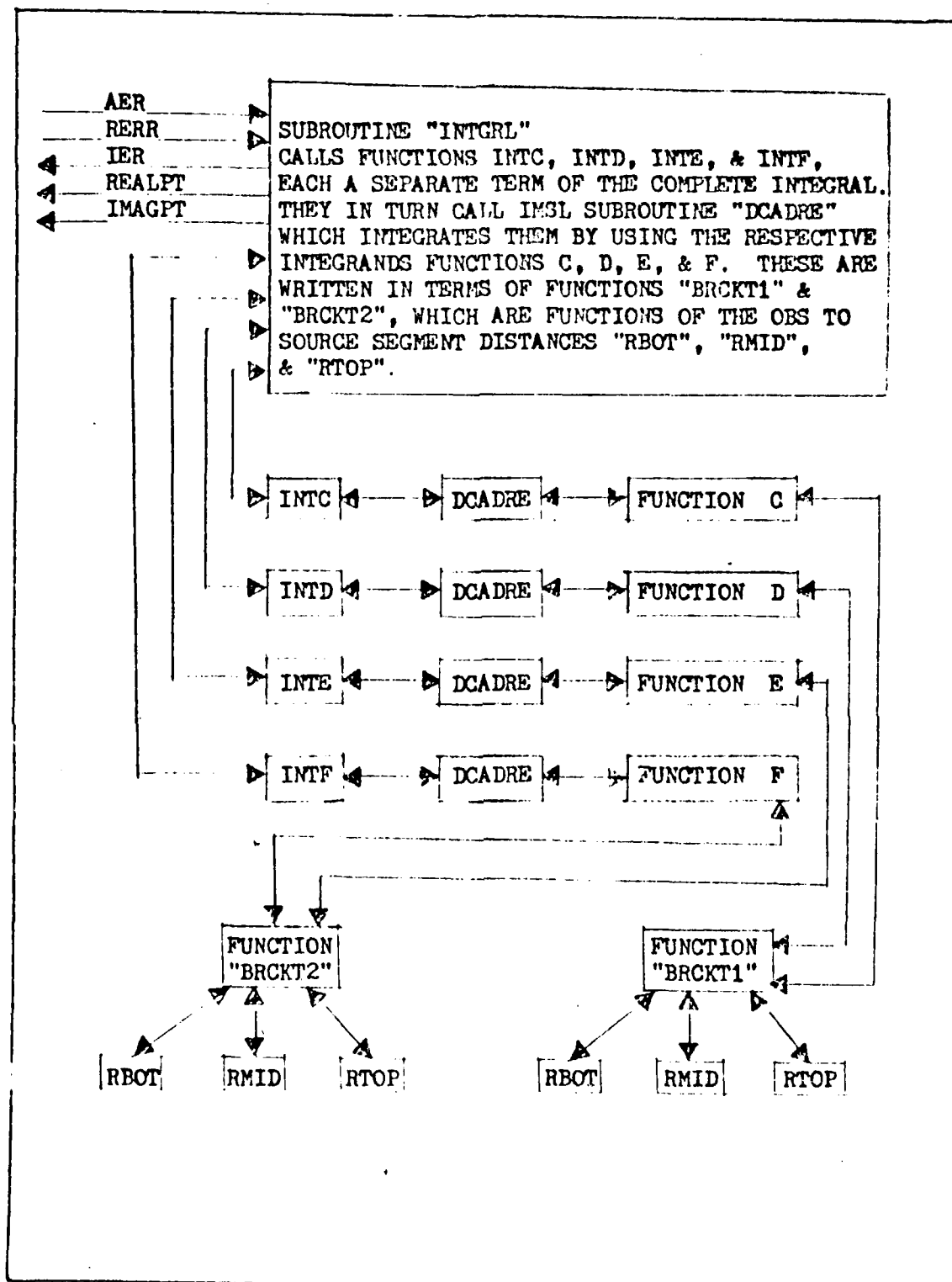


Figure A-1 (Continued)

AD-A125 646

ANALYSIS OF THE INDUCED CURRENTS ON A SECTION OF  
PARALLEL WIRES IN FRONT O. (U) AIR FORCE INST OF TECH  
WRIGHT-PATTERSON AFB OH SCHOOL OF ENGI. T W GODOWSKY  
DEC 82 AFIT/GE/EE/82D-35 F/G 9/1

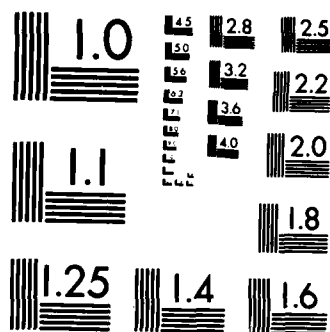
2/2

UNCLASSIFIED

NL

END

FILED  
20  
DEC



MICROCOPY RESOLUTION TEST CHART  
NATIONAL BUREAU OF STANDARDS-1963-A

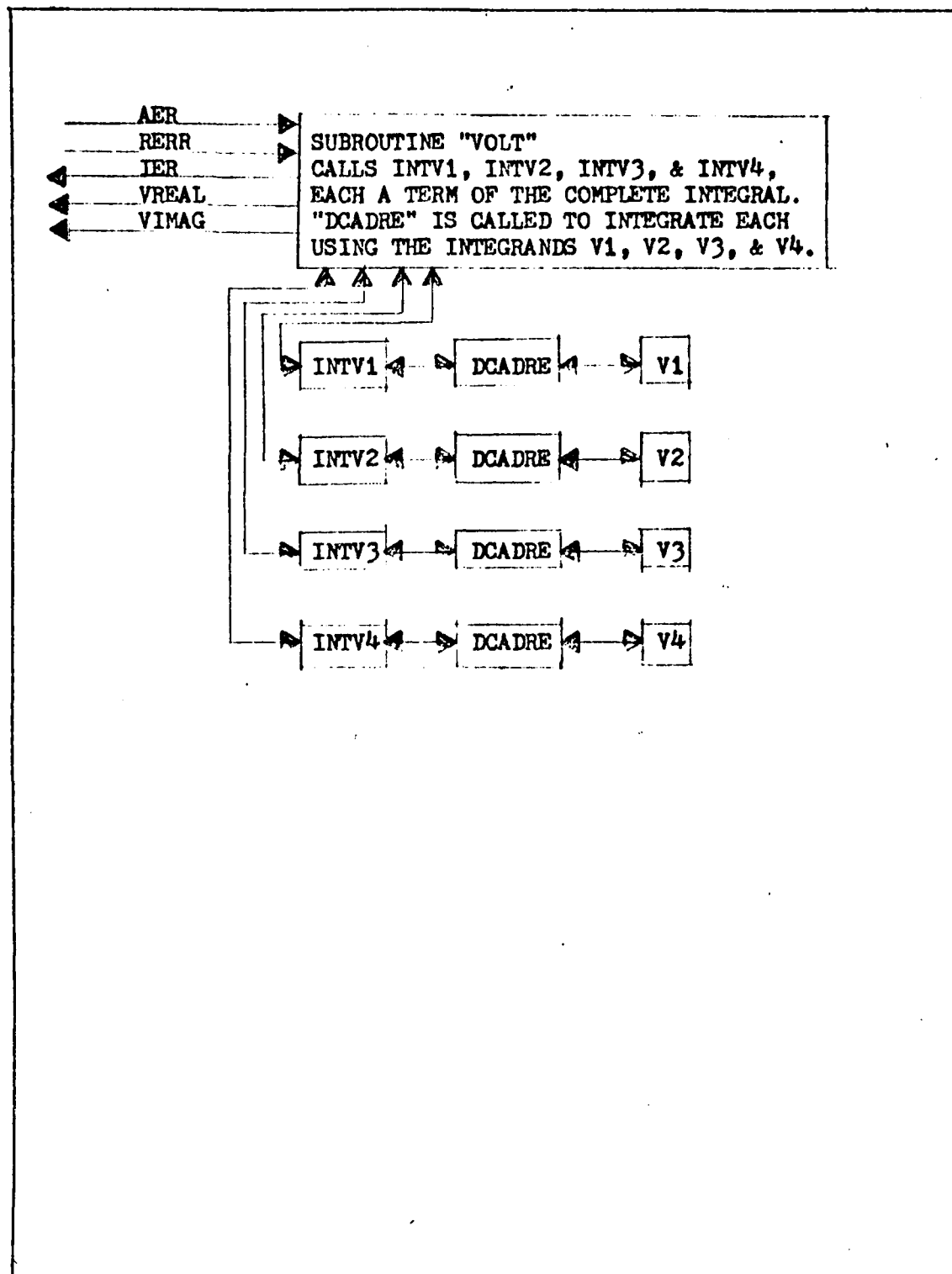


Figure A-1 (Continued)



29: C	R	IS PROPAGATION CONSTANT
30: C	THETA AND PHI DESCRIBE INCIDENT FIELD VECTOR	
31: C		
32: C	S FFF IS A CONTROL PARAMETER (INTEGER)	
33: C	S FFF = 0 -> NORMAL INCIDENCE CASE ONLY	
34: C	S FFF = 1 -> SPECTRUM THEORY, BUT IN PT/16 INCREMENTS	
35: C		
36: C		
37: C	P7 IS A CONTROL PARAMETER (INTEGER)	
38: C	P7=0 -> POINT POINT ARRAY 2	
39: C	P7=1 -> ONLY POINT 1ST ROW OF 7	
40: C	P7=2 -> POINT POINT 2 ARRAY	
41: C		
42: C	PV IS A CONTROL PARAMETER (INTEGER)	
43: C	PV = 0 -> NO POINT ARRAY V	
44: C	PV = 1 -> POINT ARRAY V	
45: C		
46: C	TYPE IS A CONTROL PARAMETER (INTEGER)	
47: C	TYPE = 0 -> 2 DIMENSIONAL TO 2 ARRAY ONLY	
48: C	TYPE = 1 -> FULL 3 DIMENSIONAL CASE	
49: C		
50: C	CHECK DATA FOR OBVIOUS ERRORS	
51: C	1: IF MORE THAN 300 ELEMENTS	
52: C	2: IF A IS GREATER THAN 1/10 OF COS	
53: C	3: IF A IS NEGATIVE	

Figure A-2 (Continued)

```

54: C
55: C
56: C
57: C
58: C
59: C
60: C
61: C
62: C
63: C
64: C
65: C
66: C
67: C
68: C
69: C
70: C
71: C
72: C
73: C
74: C
75: C
76: C
77: C
78: C

C=V* IS TOTAL NO. OF ELEMENTS
C=I*
IF (TYPE.EQ.1) I = 2**I*
IF (TYPE.EQ.0) IX = 0.0
R = (0.209845-01) * REXP
ALPHA = (300.)/REXP
IF (C.GT.300).GOTO(15,0) GO TO 25
IF (10.0).GT.(SV) GO TO 32
IF (TYPE.EQ.1).GOTO(18X.11.(2.40)) GO TO 31
IF (0.15.0) GO TO 30

DATA C TO HERE, PRINT IT OUT,C,TYPE
CONTINUE
WRITE(6,12)
FORMAT(1,3X,10(1F10.4))
WRITE (6,13)
FORMAT(3X,17NUMBER OF IPES =,13)
WRITE (6,14)
FORMAT(3X,26NUMBER SEGMENTS PER IPF =,13)
WRITE (6,15) IL
FORMAT(3X,13H, IF IPFGE =,F10.4)
WRITE (6,16) A
FORMAT(2X,13H, IPE RADII =,F10.4)

```

Figure A-2 (Continued)



70:	WRITE (6,17) PGV
80:	FORMAT(35,16) TYPE SPACING =,F10.5)
81:	WRITE(6,173) PGV
82:	FORMAT(35,16) TYPE SPACING =,F10.5)
83:	WRITE (6,171) PGV
84:	FORMAT(35,12) FREQUENCY =,F10.5,100 (PERCENT)
85:	WRITE (6,172) ALFA
86:	FORMAT(35,13) MAGNITUDE =,F10.5,7 (STARS)
87:	WRITE(6,18) PGV
88:	FORMAT(35,17) PROP CONSTANT =,F12.5)
89:	WRITE (6,19) PGV
90:	FORMAT(35,14) MAGNITUDE =,F10.5)
91:	WRITE(6,20) PGV
92:	WRITE(6,21) PGV
93:	WRITE(6,22) TYPE
94:	FORMAT(35,6) PGV =,11)
95:	FORMAT(35,5) PGV =,11)
96:	FORMAT(35,7) PGV =,11)
97:	SKIP OVER ERROR FOR SEGMENT, CONTINUE AT 40
98:	GO TO 40
99:	END OF SEGMENT
100:	
101:	
102:	
103:	

Figure A-2 (Continued)



```

129: C
130: C
131: C
132: C
133: C
134: C
135: C
136: C
137: C
138: C
139: C
140: C
141: C
142: C
143: C
144: C
145: C
146: C
147: C
148: C
149: C
150: C
151: C
152: C
153: C

      DEFINE COORDINATES OF FIRST WIRE AND LABEL PARALLEL
      SECRET IS ACCORDANT GIVE BY OF 1002.
      J IS TRANSFERRED 1 THRU 1002.
      K IS COUNT OF SECRET VALUE, 1 THRU 1002.

      INITIALIZE COUNTERS
      K = 1
      CONTINUE
      J = 1
      CONTINUE
      DO 60 I=1,N
      4P
      49
      50

      CALCULATE ENDPOINTS OF FIRST WIRE (121) FOR 1 THRU N SECRETS
      ROUN(J) = J1 - (J-1)*DZ
      ROUN(J) = J1 - (J-1)*DZ

      EQUATE CUMULATIVE INDEX K TO COUNT Y WIRE INDEX
      YCOORD(K) = 0.0
      IF((TYPE,PO,J).AND.(1.GT.("N")))) YCOORD(K) = -1. * KEY
      YCOORD(K) = (J-1) * ISY
      ROUN(J) = ROUN(J)

```

Figure A-2 (Continued)

```

154: C      RNDL(X)=RNDL(X)
155: C
156: C      I COUNTER IS RESET EACH TIME THE FOLLOWING GOES FOR EACH TIME
157: C      K COUNTER IS INCREASSED BY A EACH TIME BUT NOT RESET
158: C      TO OBTAIN CONSECUTIVE COUNTS THROUGH SEVERAL IS
159: C
160: C      K=K+1
161: C      CONTINUE
162: C
163: C      CHECK IF ON LAST(J=1) TIME
164: C      YES - OUT OF LOOP, GO TO 65
165: C      NO - INCREMENT RICE COUNT IF J, REPEAT LOOP AT 50
166: C
167: C      IF (J.GE.2) GO TO 65
168: C      J=J+1
169: C      GO TO 40
170: C
171: C      CONTINUE
172: C      IF((TYPE.EC.1).AND.(K.IE.(COUNT+1))) GO TO 40
173: C
174: C      CALCULATE AVERAGES ON ALL C SECTIONS
175: C
176: C      DO 70 J=1,2
177: C      SFG(J)=RNDL(1)-RZ
178: C      CONTINUE
179: C

```

Figure A-2 (Continued)

```

179: C      PRINT CALCULATED COORDINATES FOR
180: C      VERIFICATION OF RESULT WIRE GEOMETRY
181: C
182: C
183: C      WRITE(6,701) DZ
184: C      FORMAT(3X,5H07 = ,F10.5)
185: C      WRITE(6,702)
186: C      FORMAT(10I,3X,16H07RE COORDINATES)
187: C      DO 750 N = 1,7
188: C      WRITE(6,705) N
189: C      FORMAT(3X,7HSEQUENCE,1Z)
190: C      WRITE(6,706) FVALUE(N)
191: C      WRITE(6,707) SECTID(N)
192: C      WRITE(6,708) BOREL (N)
193: C      WRITE(6,709) YCOORD(N)
194: C      WRITE(6,710) XCOORD(N)
195: C      FORMAT(10X,10H07RE FSEQUENT,7 = ,F10.5)
196: C      FORMAT(10X,13H07RECT,7 = ,F10.5)
197: C      FORMAT(10X,16H07RE FBORE,7 = ,F10.5)
198: C      FORMAT(10X,12H07 COORDINATE,F10.5)
199: C      FORMAT(10X,12H07 COORDINATE,F10.5)
200: C      CONTINUE
201: C
202: C      CALCULATE DIFFERENCE COPY 2(0,0)
203: C      BY FIRST BO LOGS. OF INDEX IS SCORF,

```

Figure A-2 (Continued)

```

204: C OTHER IS DRS
205: C
206: C DO DO DRS=1.0
207: C DO DO SOURCE=1.0
208: C
209: C CALL SAMP1N TO DETERMINE IF SOURCE AND DRS SECTIONS
210: C ARE OF THE SAME TYPE
211: C YES - DELTA=1.0
212: C NO - DELTA=0.0
213: C
214: C CALL SAMP1P(DELTA,YCOORD(SOURCE),YCOORD(DRS),
215: C YCOORD(SOURCE),YCOORD(DRS))
216: C
217: C PUT CURRENT VARIABLES INTO COMMON AREA
218: C FOR USE BY OTHER SUBPROGRAMS
219: C DEL = DELTA
220: C XCOORD = XCOORD(DRS)
221: C YCOORD = YCOORD(DRS)
222: C XCOORD = XCOORD(DRS)
223: C SOURCE = XCOORD(SOURCE)
224: C SOURCE = YCOORD(SOURCE)
225: C XCOORD = XCOORD(SOURCE)
226: C YCOORD = YCOORD(DRS)
227: C YCOORD = YCOORD(SOURCE)
228: C XCOORD = XCOORD(DRS)

```

Figure A-2 (Continued)

```

229: C      SXCF = XSCOR(SOURCE)
230: C
231: C      SET FORCE CONTROL DATA FILES FOR USE TO SIMULATIONS
232: C
233: C      AEPF = 1.0 E-05
234: C      RFPF = 1.0 E-05
235: C      JEP = 0
236: C
237: C
238: C      CALCULATE 7(CFS, SOURCE) BASED ON VALUES TO COME.
239: C
240: C      CALL TITEL (REALP1, IMAGPT, AEPF, RFPF, JEP)
241: C      7(CFS, SOURCE) = CPLY(REALPT, IMAGPT)
242: C
243: C      DISPLAY TITELANCE DATA
244: C      IN PLOT FOR:
245: C
246: C      IF(P7.EQ.0) GO TO 71
247: C      IF((P2.EQ.1).AND.(CFS.EQ.2)) GO TO 75
248: C      IF((CFS.EQ.1).AND.(SOURCE.EQ.1)) GOTO(6,71)
249: C      ECR = 1.0E-1, 3X, 1501#FF10CF 20 (AV)
250: C      ZKAB = CORT(CAL(7(CFS, SOURCE)))*2*PI*W(7(CFS, SOURCE))**2)
251: C      /P7ASF = AIA (CAL(AR(7(CFS, SOURCE)))/REAL(7(CFS, SOURCE)))
252: C      7(FS) = 57.295779 * ZKAB*E
253: C      GOTO(6,73) CFS, SOURCE, ZKAB, 7(P7ASF, 7(FS)

```

71

Figure A-2 (Continued)

```

254: 73  FORMAT(3X,18U7(09S,50U6(F) = 7(,17,1),,13,0')) = ,
255:  C F12.5,3Y,F12.5,
256:  C 114 (A)10'S = ,F12.5,3Y, 000000000
257: 75  000110000
258: 40  00 000000
259: C
260: C  CALCULATE VOLTAGE ARRAY V(0)
261: C  BY LOOPING THRU THE SEGMENTS
262: C  AND USING CURRENT VALUES TO COMPUTE
263: C
264: IF(SHIFT.F0.0) GO TO 47
265: DO 266 ITHETA = 1,9
266: DO 266 ISHT = 1,2
267:  IF(ITHETA.F0.1) THETA = 0.1953309
268:  IF(ITHETA.F0.2) THETA = 0.3926600
269:  IF(ITHETA.F0.3) THETA = 0.5899901
270:  IF(ITHETA.F0.4) THETA = 0.7873202
271:  IF(ITHETA.F0.5) THETA = 0.9846503
272:  IF(ITHETA.F0.6) THETA = 1.1799804
273:  IF(ITHETA.F0.7) THETA = 1.3773105
274:  IF(ITHETA.F0.8) THETA = 1.5746406
275:  IF(ITHETA.F0.9) THETA = 1.7719707
276:  IF(ITHETA.F0.1) PSI = 0.0
277:  IF(ITHETA.F0.2) PSI = 0.106319
278:  IF(ITHETA.F0.3) PSI = 0.302639
279:  IF(ITHETA.F0.4) PSI = 0.598959

```

Figure A-2 (Continued)



```

279: TF(PNT,EP,5) PNT = 0.765300
280: TF(JPNT,EP,6) PNT = 0.931747
281: TF(IPNT,EP,7) PNT = 1.178097
282: TF(OPNT,EP,4) PNT = 1.370046
283: TF(IPNT,EP,2) PNT = 1.570766
284: TF(TPNT,EP,1.570766).000.(PNT, 0.0,0) GO TO 286
285: CONTINUE
286: IF(S-EP,20.0) TUPNT = 1.571794
287: IF(S-EP,20.0) PNT = 0.0
288: WRITE (6,93) TUPNT,PNT
289: FOR AT(PNT,SY,7)TUPNT =,F12.5,SY,SYOUT =,F12.5)
290: DO 100 I=1,3
291: CCM1 = CPLE(P1S)
292: CCM2 = SEC10(P1S)
293: CCM3 = CPLE(P1S)
294: CCM4 = SEC10(P1S)
295: CCM5 = SEC10(P1S)
296: CALL VOLT (VREAL,VTAG,IPR0,IPR1,IPR2)
297: VREAL = P1*SY*(TUPNT)+VREAL
298: VTAG = E*CCM1*(TUPNT)+VTAG
299: C
300: C
301: C
302: C
303: C

```

IF TYPE 1, CALCULATE VOLTAGE INCREASE  
BY TRACE FIELD. IF TYPE = 0, SKIP OVER  
THIS SECTION AND CONTINUE.

Figure A-2 (Continued)

```

304: C
305: C
306: C
307: C
308: C
309: C
310: C
311: C
312: C
313: C
314: C
315: C
316: C
317: C
318: C
319: C
320: C
321: C
322: C
323: C
324: C
325: C
326: C
327: C
328: C

```

```

TECTYPE,EO,0) GO TO 99

CALCULATE THETA, PUT FOR TRACE FIELD.

TRACE THETA = ORIGINAL THETA

PUT = 3.141592 - PUT
CALL VOLT(VREF,VREF,VREF,DEPR,DEPR,TER)

ADD VOLTAGE BY TRACE FIELD TO THAT
CAUSED BY ACTUAL FIELD.

VREF = VREF - EO * SIN(THETA) + VREF
VREF = VREF - EO * SIN(THETA) + VREF

RETURN THETA, PUT TO ORIGINAL VALUES
FOR NEXT OBS SECTORS.

PUT = 3.141592 - PUT
CONTINUE
V(ORS) = C*ELX(VREF,VREF)
VREF = SQRT(VREF**2 + VREF**2)
TECTYPE,LT,1,00-10) GO TO 65
VREF = ATAN2(VREF,VREF)

```

Figure A-2 (Continued)

```

329:      GO TO 97
330:      VPHASE = 0.0
331:      CONTINUE
332:      VDEG = 57.295779 * VPHASE
333:      IF (V.FG.O) GO TO 99
334:      WRITE (6,98) (OS,V,SGM,VPHASE,VDEG
335:      FUE, A15X.24Y(,13,3)) =,F12.573,112.5,
336:      110 DATA IS = ,E12.5,80 DEGREE)
337:      CONTINUE
338:      CONTINUE
339:      C
340:      C
341:      C
342:      C
343:      C
344:      C
345:      C
346:      C
347:      C
348:      C
349:      C
350:      C
351:      C
352:      C
353:      C
354:      C
355:      C
356:      C
357:      C
358:      C
359:      C
360:      C
361:      C
362:      C
363:      C
364:      C
365:      C
366:      C
367:      C
368:      C
369:      C
370:      C
371:      C
372:      C
373:      C
374:      C
375:      C
376:      C
377:      C
378:      C
379:      C
380:      C
381:      C
382:      C
383:      C
384:      C
385:      C
386:      C
387:      C
388:      C
389:      C
390:      C
391:      C
392:      C
393:      C
394:      C
395:      C
396:      C
397:      C
398:      C
399:      C
400:      C
401:      C
402:      C
403:      C
404:      C
405:      C
406:      C
407:      C
408:      C
409:      C
410:      C
411:      C
412:      C
413:      C
414:      C
415:      C
416:      C
417:      C
418:      C
419:      C
420:      C
421:      C
422:      C
423:      C
424:      C
425:      C
426:      C
427:      C
428:      C
429:      C
430:      C
431:      C
432:      C
433:      C
434:      C
435:      C
436:      C
437:      C
438:      C
439:      C
440:      C
441:      C
442:      C
443:      C
444:      C
445:      C
446:      C
447:      C
448:      C
449:      C
450:      C
451:      C
452:      C
453:      C
454:      C
455:      C
456:      C
457:      C
458:      C
459:      C
460:      C
461:      C
462:      C
463:      C
464:      C
465:      C
466:      C
467:      C
468:      C
469:      C
470:      C
471:      C
472:      C
473:      C
474:      C
475:      C
476:      C
477:      C
478:      C
479:      C
480:      C
481:      C
482:      C
483:      C
484:      C
485:      C
486:      C
487:      C
488:      C
489:      C
490:      C
491:      C
492:      C
493:      C
494:      C
495:      C
496:      C
497:      C
498:      C
499:      C
500:      C
501:      C
502:      C
503:      C
504:      C
505:      C
506:      C
507:      C
508:      C
509:      C
510:      C
511:      C
512:      C
513:      C
514:      C
515:      C
516:      C
517:      C
518:      C
519:      C
520:      C
521:      C
522:      C
523:      C
524:      C
525:      C
526:      C
527:      C
528:      C
529:      C
530:      C
531:      C
532:      C
533:      C
534:      C
535:      C
536:      C
537:      C
538:      C
539:      C
540:      C
541:      C
542:      C
543:      C
544:      C
545:      C
546:      C
547:      C
548:      C
549:      C
550:      C
551:      C
552:      C
553:      C
554:      C
555:      C
556:      C
557:      C
558:      C
559:      C
560:      C
561:      C
562:      C
563:      C
564:      C
565:      C
566:      C
567:      C
568:      C
569:      C
570:      C
571:      C
572:      C
573:      C
574:      C
575:      C
576:      C
577:      C
578:      C
579:      C
580:      C
581:      C
582:      C
583:      C
584:      C
585:      C
586:      C
587:      C
588:      C
589:      C
590:      C
591:      C
592:      C
593:      C
594:      C
595:      C
596:      C
597:      C
598:      C
599:      C
600:      C
601:      C
602:      C
603:      C
604:      C
605:      C
606:      C
607:      C
608:      C
609:      C
610:      C
611:      C
612:      C
613:      C
614:      C
615:      C
616:      C
617:      C
618:      C
619:      C
620:      C
621:      C
622:      C
623:      C
624:      C
625:      C
626:      C
627:      C
628:      C
629:      C
630:      C
631:      C
632:      C
633:      C
634:      C
635:      C
636:      C
637:      C
638:      C
639:      C
640:      C
641:      C
642:      C
643:      C
644:      C
645:      C
646:      C
647:      C
648:      C
649:      C
650:      C
651:      C
652:      C
653:      C
654:      C
655:      C
656:      C
657:      C
658:      C
659:      C
660:      C
661:      C
662:      C
663:      C
664:      C
665:      C
666:      C
667:      C
668:      C
669:      C
670:      C
671:      C
672:      C
673:      C
674:      C
675:      C
676:      C
677:      C
678:      C
679:      C
680:      C
681:      C
682:      C
683:      C
684:      C
685:      C
686:      C
687:      C
688:      C
689:      C
690:      C
691:      C
692:      C
693:      C
694:      C
695:      C
696:      C
697:      C
698:      C
699:      C
700:      C
701:      C
702:      C
703:      C
704:      C
705:      C
706:      C
707:      C
708:      C
709:      C
710:      C
711:      C
712:      C
713:      C
714:      C
715:      C
716:      C
717:      C
718:      C
719:      C
720:      C
721:      C
722:      C
723:      C
724:      C
725:      C
726:      C
727:      C
728:      C
729:      C
730:      C
731:      C
732:      C
733:      C
734:      C
735:      C
736:      C
737:      C
738:      C
739:      C
740:      C
741:      C
742:      C
743:      C
744:      C
745:      C
746:      C
747:      C
748:      C
749:      C
750:      C
751:      C
752:      C
753:      C
754:      C
755:      C
756:      C
757:      C
758:      C
759:      C
760:      C
761:      C
762:      C
763:      C
764:      C
765:      C
766:      C
767:      C
768:      C
769:      C
770:      C
771:      C
772:      C
773:      C
774:      C
775:      C
776:      C
777:      C
778:      C
779:      C
780:      C
781:      C
782:      C
783:      C
784:      C
785:      C
786:      C
787:      C
788:      C
789:      C
790:      C
791:      C
792:      C
793:      C
794:      C
795:      C
796:      C
797:      C
798:      C
799:      C
800:      C
801:      C
802:      C
803:      C
804:      C
805:      C
806:      C
807:      C
808:      C
809:      C
810:      C
811:      C
812:      C
813:      C
814:      C
815:      C
816:      C
817:      C
818:      C
819:      C
820:      C
821:      C
822:      C
823:      C
824:      C
825:      C
826:      C
827:      C
828:      C
829:      C
830:      C
831:      C
832:      C
833:      C
834:      C
835:      C
836:      C
837:      C
838:      C
839:      C
840:      C
841:      C
842:      C
843:      C
844:      C
845:      C
846:      C
847:      C
848:      C
849:      C
850:      C
851:      C
852:      C
853:      C
854:      C
855:      C
856:      C
857:      C
858:      C
859:      C
860:      C
861:      C
862:      C
863:      C
864:      C
865:      C
866:      C
867:      C
868:      C
869:      C
870:      C
871:      C
872:      C
873:      C
874:      C
875:      C
876:      C
877:      C
878:      C
879:      C
880:      C
881:      C
882:      C
883:      C
884:      C
885:      C
886:      C
887:      C
888:      C
889:      C
890:      C
891:      C
892:      C
893:      C
894:      C
895:      C
896:      C
897:      C
898:      C
899:      C
900:      C
901:      C
902:      C
903:      C
904:      C
905:      C
906:      C
907:      C
908:      C
909:      C
910:      C
911:      C
912:      C
913:      C
914:      C
915:      C
916:      C
917:      C
918:      C
919:      C
920:      C
921:      C
922:      C
923:      C
924:      C
925:      C
926:      C
927:      C
928:      C
929:      C
930:      C
931:      C
932:      C
933:      C
934:      C
935:      C
936:      C
937:      C
938:      C
939:      C
940:      C
941:      C
942:      C
943:      C
944:      C
945:      C
946:      C
947:      C
948:      C
949:      C
950:      C
951:      C
952:      C
953:      C
954:      C
955:      C
956:      C
957:      C
958:      C
959:      C
960:      C
961:      C
962:      C
963:      C
964:      C
965:      C
966:      C
967:      C
968:      C
969:      C
970:      C
971:      C
972:      C
973:      C
974:      C
975:      C
976:      C
977:      C
978:      C
979:      C
980:      C
981:      C
982:      C
983:      C
984:      C
985:      C
986:      C
987:      C
988:      C
989:      C
990:      C
991:      C
992:      C
993:      C
994:      C
995:      C
996:      C
997:      C
998:      C
999:      C
1000:      C

```

Figure A-2 (Continued)





```

406:      FUNCTION E(G)
407:      COMMON,CCOML,CCOMH,CCOML,SCOML,SCOMH,SCOMH,
408:      CYCOM,SYCOM,P,BZ,BFL,A,ASY,IMETA,PHI
409:      EXTERNAL ECKT1
410:      SZ=ST(P*27)
411:      F=(-30*ST*(P*(CCOMH-6))*ECKT1(G)/SZ**2)
412:      RETURN
413:      END

414:      FUNCTION E(G)
415:      COMMON,CCOML,CCOMH,CCOMH,SCOML,SCOMH,SCOMH,
416:      CYCOM,SYCOM,P,BZ,BFL,A,ASY,IMETA,PHI
417:      EXTERNAL ECKT2
418:      SZ=ST(P*27)
419:      F=(-30*ST*(P*(CCOML)))*ECKT2(G)/SZ**2)
420:      RETURN
421:      END

422:      FUNCTION F(G)
423:      COMMON,CCOML,CCOMH,CCOMH,SCOML,SCOMH,SCOMH,
424:      CYCOM,SYCOM,P,BZ,BFL,A,ASY,IMETA,PHI
425:      EXTERNAL ECKT2
426:      SZ=ST(P*27)
427:      F=(-30*ST*(P*(CCOMH-6))*ECKT2(G)/SZ**2)
428:      RETURN
429:      END

```

Figure A-2 (Continued)



```

454: FUNCTION WROT(G)
455: C=CORR, SCORL, SCORH, SCORL, SCORH, SCORL,
456: C=CORR, SCORL, SCORH, SCORL, SCORH, SCORL, SCORH,
457: C=CORR, SCORL, SCORH, SCORL, SCORH, SCORL, SCORH,
458: C=CORR, SCORL, SCORH, SCORL, SCORH, SCORL, SCORH,
459: C=CORR, SCORL, SCORH, SCORL, SCORH, SCORL, SCORH,
460: C=CORR, SCORL, SCORH, SCORL, SCORH, SCORL, SCORH,
461: C=CORR, SCORL, SCORH, SCORL, SCORH, SCORL, SCORH,
462: C=CORR, SCORL, SCORH, SCORL, SCORH, SCORL, SCORH,
463: C=CORR, SCORL, SCORH, SCORL, SCORH, SCORL, SCORH,
464: C=CORR, SCORL, SCORH, SCORL, SCORH, SCORL, SCORH,
465: C=CORR, SCORL, SCORH, SCORL, SCORH, SCORL, SCORH,
466: C=CORR, SCORL, SCORH, SCORL, SCORH, SCORL, SCORH,
467: C=CORR, SCORL, SCORH, SCORL, SCORH, SCORL, SCORH,
468: C=CORR, SCORL, SCORH, SCORL, SCORH, SCORL, SCORH,
469: C=CORR, SCORL, SCORH, SCORL, SCORH, SCORL, SCORH,
470: C=CORR, SCORL, SCORH, SCORL, SCORH, SCORL, SCORH,
471: C=CORR, SCORL, SCORH, SCORL, SCORH, SCORL, SCORH,
472: C=CORR, SCORL, SCORH, SCORL, SCORH, SCORL, SCORH,
473: C=CORR, SCORL, SCORH, SCORL, SCORH, SCORL, SCORH,
474: C=CORR, SCORL, SCORH, SCORL, SCORH, SCORL, SCORH,
475: C=CORR, SCORL, SCORH, SCORL, SCORH, SCORL, SCORH,
476: C=CORR, SCORL, SCORH, SCORL, SCORH, SCORL, SCORH,
477: C=CORR, SCORL, SCORH, SCORL, SCORH, SCORL, SCORH,

```

Figure A-2 (Continued)





```

508: FUNCTION V1(H)
509:   CO = CO*(COOHI,OCOHI,OCOHI,OCOHI,SCOHI,SCOHI,SCOHI,
510:   COYCOHI,SYCOHI,P,Z,PCL,A,SY,THETA,OUT
511:   C *XCOHI,SYCOHI
512:   V1 = (CPI*(C*(C-OCOHI))/ST*(C*(Z))) *
513:   COS(P*(ST*(THETA)+SIN(OUT)*V(COHI+COS(THETA)
514:   C +XCOHI*ST*(THETA)+COS(OUT)))
515:   RETURN
516:   END

517: FUNCTION V2(H)
518:   CO = CO*(COOHI,OCOHI,OCOHI,OCOHI,SCOHI,SCOHI,SCOHI,
519:   COYCOHI,SYCOHI,P,Z,PCL,A,SY,THETA,OUT
520:   C *XCOHI,SYCOHI
521:   V2 = (ST*(C*(OCOHI-H))/ST*(C*(Z))) *
522:   COS(P*(ST*(THETA)+SIN(OUT)*V(COHI+COS(THETA)
523:   C +XCOHI*ST*(THETA)+COS(OUT)))
524:   RETURN
525:   END

```

Figure A-2 (Continued)

```

526:      FUNCTION V3(X)
527:      COMMON /CCOM/ ,CCOM1,CCOM2,SCOM1,SCOM2,SCOM3,
528:      CYCOM1,CYCOM2,P,P7,PFL,A,SY,THETA,PIJ
529:      C ,XCOM ,XCOM1
530:      V3 = (SIN(P*(X-CCOM1)))/SIN(P*(X+07)) +
531:      SIN(P*(PI-PI-PI-PI)*SIN(P*PI))*XCOM1 + COS(THETA)
532:      C XCOM1*SIN(THETA)*COS(P*PI))
533:      RETURN
534:      END

535:      FUNCTION V4(X)
536:      COMMON /CCOM/ ,CCOM1,CCOM2,SCOM1,SCOM2,SCOM3,
537:      CYCOM1,CYCOM2,P,P7,PFL,A,SY,THETA,PIJ
538:      C ,XCOM ,XCOM1
539:      V4 = (SIN(P*(X-CCOM1+PI)))/SIN(P*(X+17)) +
540:      SIN(P*(PI-PI-PI-PI)*SIN(P*PI))*XCOM1 + COS(THETA)
541:      C XCOM1*SIN(THETA)*COS(P*PI))
542:      RETURN
543:      END

```

Figure A-2 (Continued)

## VITA

Thomas W. Godowsky was born on 13 August 1959 in Wilkes-Barre, Pennsylvania. He graduated from Wyoming Valley West High School, Kingston PA, in 1977. He began undergraduate studies at Wilkes College, Wilkes-Barre PA, and was awarded an Air Force R.O.T.C. Full Scholarship. While a Senior, he was the Chairman of the Student Branch of the I.E.E.E. at Wilkes College, and was named the Outstanding Senior Engineering Student for 1981 by the Society of American Military Engineers. He graduated from Wilkes College in 1981 with a B.S.E.E., and accepted a commission in the Air Force. Lieutenant Godowsky was then assigned to begin graduate studies at the School of Engineering, Air Force Institute of Technology, WPAFB, in June, 1981.

Permanent address: 449 Moss St.  
Plymouth PA 18651

UNCLASSIFIED

SECURITY CLASSIFICATION OF THIS PAGE (When Data Entered)

REPORT DOCUMENTATION PAGE		READ INSTRUCTIONS BEFORE COMPLETING FORM
1. REPORT NUMBER AFIT/GE/EE/82D-35	2. GOVT ACCESSION NO. <b>A125 646</b>	3. RECIPIENT'S CATALOG NUMBER
4. TITLE (and Subtitle) ANALYSIS OF THE INDUCED CURRENTS ON A SECTION OF PARALLEL WIRES IN FRONT OF A GROUND PLANE		5. TYPE OF REPORT & PERIOD COVERED MS THESIS MAR-DEC 1982
7. AUTHOR(s) Thomas W. Godowsky, B.S.E.E. 2Lt. USAF		6. PERFORMING ORG. REPORT NUMBER
9. PERFORMING ORGANIZATION NAME AND ADDRESS Air Force Institute of Technology (AFIT/EN) Wright-Patterson AFB, Ohio 45433		8. CONTRACT OR GRANT NUMBER(s)
11. CONTROLLING OFFICE NAME AND ADDRESS		10. PROGRAM ELEMENT, PROJECT, TASK AREA & WORK UNIT NUMBERS
12. REPORT DATE December 1982		13. NUMBER OF PAGES 118
14. MONITORING AGENCY NAME & ADDRESS (if different from Controlling Office)		15. SECURITY CLASS. (of this report) UNCLASSIFIED
15a. DECLASSIFICATION/DOWNGRADING SCHEDULE		
16. DISTRIBUTION STATEMENT (of this Report)  APPROVED FOR PUBLIC RELEASE; DISTRIBUTION UNLIMITED.		
17. DISTRIBUTION STATEMENT (of the abstract entered in Block 20, if different from Report)		
18. SUPPLEMENTARY NOTES  Approved for Public Release: LNW AFH 190-17. <i>Lynn E. Godowsky</i> Lynn E. Godowsky Dean for Research and Professional Development Air Force Institute of Technology (ATC) Wright-Patterson AFB, OH 45433		
19. KEY WORDS (Continue on reverse side if necessary and identify by block number) Electromagnetic fields Electromagnetic scattering Induced currents Method of moments		
20. ABSTRACT (Continue on reverse side if necessary and identify by block number) This investigation determines the induced currents on a finite sized array of parallel wires when illuminated by a plane wave with varying incidence angles by the method of moments. The arrays considered are of various spacings, lengths, and widths, ranging from 5 to 36 wires per wavelength, and one to two wavelengths in length. The effects of a ground plane on the induced currents and the induced fields are also studied. (over)		

UNCLASSIFIED

SECURITY CLASSIFICATION OF THIS PAGE (When Data Entered)

The analysis is accomplished by the method of moments using piecewise sinusoidal expansion functions and Galerkin's method. An algorithm is developed to accomplish the integration and matrix inversion. It was written general enough for the user to specify: number of wires, number of segments, wire length, wire diameter, wire spacing, spacing above the ground plane, frequency, and magnitude of the incident electric field. The results illustrate the various effects that changing the wire spacing, wire lengths, number of segments, and incidence angle have upon the induced current. The results of this investigation indicate that the moment method is accurate enough to produce very reasonable approximations to the induced current for most applications.

UNCLASSIFIED

SECURITY CLASSIFICATION OF THIS PAGE (When Data Entered)

4-8  
DT